

Johannes Gutenberg University Mainz (JGU)
Faculty of Natural Sciences
Institute for Geography

Alfred Wegener Institute, Helmholtz Centre for Polar and Marine Research (AWI)
Research Unit Potsdam
Geosciences Department
Polar Terrestrial Environmental Systems

Reconstruction of central Siberian fire history using lake sediments

A unique charcoal record spanning the last 2000 years

MASTER'S THESIS

First Advisor: Prof. Dr. Andreas Vött, JGU

Second Advisor: Dr. Elisabeth Dietze, AWI

Ramesh Glückler, B.Sc. Geography
M.Sc. Climate and Environmental Changes, 5th semester
Student number: 2738415
Address: Leipziger Str. 52, 14473 Potsdam, Germany
E-Mail: rglueckl@students.uni-mainz.de
To be handed in until June 5th, 2020

Table of contents

I. List of figures	2
II. List of tables	3
III. Abbreviations	3
IV. Acknowledgements.....	4
V. Abstract	5
1. Introduction	7
1.1. Motivation	7
1.2. Fires in the boreal zone	8
1.3. Charcoal as a fire proxy	13
2. Location	17
3. Methods.....	18
3.1. Field work and core sampling.....	19
3.2. Age dating.....	20
3.3. Macroscopic charcoal.....	22
3.4. Pollen samples and microscopic charcoal	26
3.5. TOC and C/N	28
3.6. Micro-XRF	29
3.7. Statistical methods	29
4. Results	33
4.1. Chronology	33
4.2. Charcoal-based fire history	37
4.3. Reconstructed vegetation	47
4.4. Impacts on soil geochemistry.....	51
5. Discussion	53
5.1. Approach to age-depth modelling	53
5.2. Significance of the charcoal record	56
5.3. Impact on the environment	67
6. Conclusion.....	71
VI. References.....	73
VII. Appendix	82
Erklärung	90

I. List of figures

Figure 1: Basic processes and workflow when using macroscopic charcoal as a fire proxy.....	13
Figure 2: Map indicating the location of Lake Khamra in Russia and the position of sediment core drilling in the lake.....	17
Figure 3: Charcoal morphotype classification scheme based on classes of particle appearances	24
Figure 4: Images of various macroscopic charcoal morphotypes found at Lake Khamra.	25
Figure 5: A: Exemplary age-depth model adjusting only the topmost ¹⁴ C age, c. 90 % of all 5000 iterations were removed due to age-reversals. B: Final age-depth model adjusting all ¹⁴ C ages	36
Figure 6: Macroscopic charcoal concentration in of counted samples from Lake Khamra's sediment core EN18232-3.....	37
Figure 7: Charcoal accumulation rate (CHAR) of the continuous sequence of counted samples	38
Figure 8: CHAR with LOWESS smoothing and identified fire events	40
Figure 9: Signal-to-noise index (SNI) with cut-off value of SNI = 3 and the charcoal record's peak component with threshold of 0.492	42
Figure 10: Comparison of contributions of the macroscopic charcoal size classes' concentration to the sum of all particles	43
Figure 11: Correlations between macroscopic charcoal morphotypes and size classes (based on 247 samples)	44
Figure 12: Principal component analysis (PCA) of charcoal morphotypes and size classes (vectors) ..	45
Figure 13: Comparison of macroscopic with microscopic charcoal concentration	46
Figure 14: Pollen and non-pollen palynomorph record.....	47
Figure 15: Correlations of macroscopic charcoal classes and pollen types (based on 18 samples)	49
Figure 16: Correlations of macroscopic charcoal classes and grouped pollen types.....	50
Figure 17: Correlations of grouped macroscopic morphotypes and pollen classes	50
Figure 18: SEA for titanium using all identified fire events.....	51
Figure 19: SEA for titanium using the reduced version of identified fire events.....	52

II. List of tables

Table 1: Radiocarbon age dating results of bulk sediment samples.....	33
Table 2: Pb/Cs dating results of parallel short core EN18232-4	34
Table 3: Radiocarbon age dating results of macrofossil samples	35
Table 4: Fire return interval (FRI) length for the macroscopic charcoal record.....	41
Table 5: Reconstructed charring temperature from charcoal reflectance measurements	46

III. Abbreviations

aDNA: Ancient deoxyribonucleic acid
AWI: Alfred Wegener Institute
(B)CE: (Before the) Common Era
BP: Before Present (referring to 1950 CE)
CHAR: Charcoal accumulation rate
C/N: Carbon to nitrogen ratio
FRI: Fire return interval
GCD: Global Charcoal Database
GFZ: German Research Center for Geosciences
IPCC: Intergovernmental Panel on Climate Change

LOWESS: Locally weighted scatterplot smoothing
MAC: Macroscopic charcoal
MIC: Microscopic charcoal
MICADAS: Mini Carbon Dating System
PCA: Principal component analysis
SEA: Superposed epoch analysis
TIC: Total inorganic carbon
TN: Total nitrogen
TOC: Total organic carbon
XRF: X-ray fluorescence

IV. Acknowledgements

I wish to show my sincere gratitude to the supervisors of this thesis.

Prof. Dr. Andreas Vött from the Johannes Gutenberg University in Mainz was eager to provide professional feedback and always had an open door for me to ask for his well-founded advice.

The realization of this thesis was only made possible thanks to the persistent guidance of Dr. Elisabeth Dietze from the Alfred Wegener Institute in Potsdam and her scientific experience, which strongly encouraged me to dive deeper into the geoscientific reconstruction of fire history.

Furthermore, I would like to recognize that my participation at AWI Potsdam only came into being thanks to the great opportunity of an internship organized and supervised by Dr. Stefan Kruse.

It was a valuable experience and I am very happy that I was able to come back for more.

Finally, I wish to thank Prof. Dr. Ulrike Herzschuh and the whole team of scientists in the Polar Terrestrial Environmental Systems section at AWI Potsdam for providing such a welcoming, open-minded and constructive research environment. This thesis benefitted greatly from all our interdisciplinary and (mostly) technical discussions during and beyond lunchtime.

V. Abstract

English:

Wildfires are an important ecological disturbance with the power to shape ecosystems and considered a dominant driver of change in the world's boreal zone. The vast forests of the boreal account for roughly a quarter of all global biomass and house enormous amounts of carbon above and below ground. These forests are also subject to change. Increased tree mortality, altered species composition, permafrost degradation and the transition towards acting as a net carbon source are some of the consequences thought to be linked to an increase in global temperatures. Fire plays an important role in all those aspects, yet for most of Siberia, long-term fire regimes remain poorly understood. This thesis attempts to start filling a pronounced gap in the global distribution of fire history reconstructions based on sedimentary charcoal. From a sediment core of Lake Khamra (SW Yakutia, Russia), a continuously sampled, high-resolution record of macroscopic charcoal particles was created, spanning the last c. 2000 years. The mean fire return interval ranges between c. 70 - 80 years. Fire activity decreases after a maximum around c. 750 CE. Despite a slight increase in fire frequency within recent centuries, charcoal accumulation since the 20th century is among the lowest of the record. Larger charcoal particles seem to indicate fires directly at the lake's shore. No clear fire impact on XRF-derived soil geochemistry was found. However, different charcoal morphotypes show promising contrasting patterns when correlated with the reconstructed vegetation. This thesis highlights both the challenges and the great potential of fire reconstructions in the Siberian boreal forest.

Deutsch / German:

Waldbrände sind ein wichtiger ökologischer Faktor mit dem Potential ganze Ökosysteme zu formen und gelten als ein maßgeblicher Antrieb von Veränderungen in der borealen Zone. Die weitläufigen Wälder des Boreals machen ungefähr ein Viertel der gesamten globalen Biomasse aus und beherbergen riesige Mengen Kohlenstoff über wie auch im Boden. Eine höhere Sterblichkeit von Bäumen, veränderte Vegetationszusammensetzung, degradierender Permafrost und ein Übergang hin zur Funktion als Quelle von Kohlenstoff sind nur einige der Folgen, die dort mit einem Anstieg der globalen Temperaturen einhergehen könnten. In all diesen Aspekten spielen Feuerereignisse eine wichtige Rolle, aber dennoch ist das Wissen über das langfristige Waldbrandverhalten in Sibirien sehr beschränkt. Diese Arbeit will damit beginnen eine deutliche Lücke in der globalen Verteilung von Feuerrekonstruktionen mittels sedimentärer Holzkohle zu füllen. Mit einem Sedimentkern des Lake Khamra (SW Jakutien, Russland) wurde eine kontinuierlich beprobte, hoch aufgelöste Aufzeichnung der makroskopischen Holzkohleakkumulation der letzten c. 2000 Jahre erstellt. Die mittlere Feuerwiederholungsrate liegt bei c. 70 - 80 Jahren. Nach einem Maximum um c. 750 CE nimmt die Feueraktivität kontinuierlich ab. Trotz eines geringen Anstiegs der Frequenz von Feuerereignissen in den letzten Jahrhunderten gehört die Akkumulationsrate von Holzkohle im 20. Jahrhundert zu den geringsten der gesamten Aufzeichnung. Größere Holzkohlepartikel scheinen Feuerereignisse direkt am Ufer des Sees widerzuspiegeln. Feuerereignisse zeigen keine klare Auswirkung auf die mit XRF-Scan festgestellte Geochemie des Bodens. Korrelationen der verschiedenen Holzkohle-Morphotypen mit der rekonstruierten Vegetation zeigen jedoch vielversprechende, gegensätzliche Muster. Diese Arbeit betont sowohl die Herausforderungen wie auch das große Potential von Feuerrekonstruktionen im sibirischen borealen Nadelwald.

1. Introduction

This thesis follows the common structure of articles found in geoscience journals. Following a brief background of the thesis, a general introduction to the boreal forest and wildfires as an important ecological disturbance is given. After presenting the location of research at Lake Khamra in SW Yakutia, Russia, both practical and statistical methods applied are described. The results segment lays out the new findings regarding the history of fire activity and potential impacts on the surrounding environment. These findings are evaluated in more detail in the discussion segment, where a comparison with other scientific literature and a deeper look into potential sources of uncertainty are used to assess their significance. Finally, the conclusion will summarize the key outcome of this thesis and end on a brief outlook towards a possible longer-term goal for fire reconstructions in Siberia's boreal forest.

1.1. Motivation

Wildfires have been a prominent topic coming up in all sorts of media reports around the globe during the last years. The notion that an increase in average global temperatures might lead to a higher fire activity seems widely acknowledged. And although fire is an essential part of many – if not most – terrestrial ecosystems, an extrapolation into the future is complicated by a high spatial and temporal variability in fire regimes. However, the common saying “In order to foresee the future, one first must understand the past” points out a possible way to improve forecasting efforts. An evaluation of past fire activity could shed light onto the complex relationships between fire, vegetation, soil and climate. This thesis is about the reconstruction of past fire activity in the boreal forest of Siberia. Paleoecological, geoscientific methods will be used in an attempt to gain information about fire activity during the last two millenniums in this vast and important ecosystem, where to this day comparable data is rare.

Composition of this thesis and the accompanying research project on the reconstructed fire history at Lake Khamra (SW Yakutia, Russia), was carried out at the Alfred Wegener Institute, Helmholtz Centre for Polar and Marine Research (AWI), at its research unit in Potsdam, Germany. As part of Germany's largest scientific organisation, the Helmholtz Association, the AWI conducts research within the polar to subpolar regions of the earth comprising a variety of divisions from biosciences (e.g. coastal ecology, ecological chemistry, marine biogeosciences), climate sciences (e.g. polar meteorology, physical oceanography, climate dynamics) and geosciences (e.g. marine geology, glaciology, permafrost research). Besides its main location in Bremerhaven and the site in Potsdam, offices of AWI are located in Oldenburg as well as on the islands of Helgoland and Sylt. The project of this thesis was conducted

specifically within the division of geosciences, section Polar Terrestrial Environmental Systems, headed by Prof. Dr. Ulrike Herzschuh, in the High-latitude Vegetation Change working group.

This thesis aims at achieving two interconnected goals:

- **Primary: Reconstruct fire history in SW Yakutia** - Creating a charcoal record from a sediment core of Lake Khamra spanning the late Holocene and assessing the fire signal within charcoal particle counts of varying size classes and appearances
- **Secondary: Evaluate potential fire impacts on vegetation and soil biogeochemistry** - Comparing the reconstructed fire history to (a) sedimentary pollen and non-pollen palynomorph data, (b) μ XRF data for elements that were previously found to react to fire events and (c) the C/N ratio of the sediment

1.2. Fires in the boreal zone

This segment serves as an introduction to the Siberian boreal forest and factors like its climate, vegetation and ecological processes, including the formation and effects of wildfires in more general terms. It highlights research on biogeochemical impacts of wildfires and the various ways in which climate change might also lead to changes in the boreal forest, potentially driving them towards environmental tipping points of a global scale.

The boreal forest

The boreal forest or taiga consists of large, circumpolar areas of coniferous trees exclusively on the northern hemisphere of the Earth, due to a lack of comparable land mass and continental climate on the southern hemisphere. It is mainly located between c. 50 - 70 °N within Russia, Canada and Alaska, but also to lesser extent in northern parts of Fennoscandia and Japan. The boreal forest is a record holder: It accounts for roughly a third of all global forested areas, spanning c. 10 million km² (KLINK 2008). The vast forests make up for c. 25 % of all global biomass and act as an enormous carbon storage, with the boreal zone containing about half of the world's forest carbon (CONARD et al. 2002) and about a third of all global terrestrial carbon (KUULUVAINEN and GAUTHIER 2018). Estimates vary in magnitude but usually agree that most of that carbon is stored within the soils below the forest (WALKER et al. 2019). In general, boreal forests are characterized by a short growing season and low annual mean temperatures, showing drastic amplitudes with increasing climatic continentality. Lowest arctic temperatures were measured in the town of Oymyakon (southern Yakutia, Siberia), reaching

almost - 70 °C. Low temperatures are not in general problematic for tree growth, as long as the growing season is long enough to ensure a conifer's robust needle development (KREEB 1983).

In Siberia, there's a gradient of predominant tree species between West and East. While in western Siberia, the evergreen *Picea obovata* (spruce) is most prominent, beginning from central Siberia it is being replaced by *Larix sibirica* and *Larix gmelinii* (larch). *Larix* are the only summergreen conifers, shedding their needles during winter season. In this cold environment, their deciduous nature gives the *Larix* species an advantage over their evergreen competitors: Reducing transpiration to a minimum in turn reduces the risk of frost desiccation. Additionally, shallow-rooting species of *Picea* and *Larix* have an advantage in permafrost regions with limited active layer depth. Together with *Abies* (fir) and *Pinus* (pine), these four groups account for most of the trees found in the boreal forest. Depending on local environmental factors and especially when moving towards the southern boundary of the boreal, broad-leaved trees can also be found, some more prevalent being *Betula* (birch), *Populus* (aspen), *Alnus* (alder) and *Salix* (willow) (KLINK 2008).

Due to the in many places rather extreme and therefore limiting climatic conditions, the boreal zone is not regarded as a hotspot of biodiversity. Tree populations mostly belong to only one or two different species at a time. This uniform appearance makes boreal forests attractive for forestry and logging: a large share of all wood for paper production originates from here. In Siberia, long distances lacking infrastructural development result in logging mainly taking place near towns, streets or along rivers. In contrast to logging in the tropics, deforested areas in the boreal zone experience a rather quick initial resettlement of vegetation, although tree growth can take up to multiple centuries depending on the location (KLINK 2008).

Fires of the boreal zone

Wildfires are a naturally occurring phenomenon, although obviously, fires can also be started by humans, be it deliberately or not. Fires can serve as an important ecological disturbance, shaping whole ecosystems to the point of the emergence of fire-adapted and even fire-dependent systems. They are labelled as "[...] a major evolutionary force" by some (CONEDERA et al. 2009: 435). Fire events in boreal forests cause a tree succession, e.g. with a burned down *Picea* population experiencing at first broad-leaved trees leading the resettlement, directly followed by *Pinus*. In Canada's boreal forest, *Pinus banksiana* is also labelled the "fire tree" for its preference of quickly settling on recently cleared locations receiving lots of direct sunlight (KREEB 1983). Different vegetation compositions are also linked to an accompanying common type of wildfire and a specific fire succession appearance (DAVIDENKO 2003). In Yakutia, *Larix*, *Pinus* and *Betula* can act as pioneering trees on recently burned areas (CHERSOV et al. 2010).

For North America there is evidence that the trigger behind most fires in the boreal forest is indeed a natural one: Ignition by lightning accounted for "[...] more than 55 % of the interannual variability in burned area, and was correlated with temperature and precipitation, which are projected to increase [...]" (VERAVERBEKE et al. 2017: 529). According to the authors of this study, lightning frequency is projected to rise due to an increase in convective storm activity with climate change. Whether or not this proves true for the boreal forest of Siberia as well has yet to be answered in more detail, however, key factors driving fire frequency and intensity besides lightning strikes are also on the rise in Siberia, mainly due to rising air temperatures creating an increase in fire weather severity (SEIDL et al. 2017). For the purpose of reconstructing the fire regime of the past, no distinction between natural and anthropogenic fires is made in this thesis. However, finding means to differentiate between the two might greatly advance the understanding of fire regimes throughout time.

There is the assumption that only about 15 % of fires in Russia are caused by lightning, the major natural cause, while most other fires are started by humans (DAVIDENKO 2003). However, it is unclear whether this information is only regarding officially recognized fires, which likely tend to be those closer to human settlements and thus more likely to be started by humans. CHERSOV et al. (2010) describe that in Yakutia 50 % of fires are started by thunderstorms in the dry months of July - August, with less than half of all fires being started by humans. While the Canadian boreal forest experiences more high-intensity crown fires, the Siberian counterpart is characterized by "low to moderate intensity surface fires of moderate frequency" (DE GROOT et al. 2013: 35). From a fire regime perspective, North America's and Eurasia's boreal forests behave quite differently, highlighting limitations of transferring research results from one to the other.

The complete suppression of fires by fire management institutions has been suspected to not be beneficial in the boreal zone, in fact, even detrimental regarding fire damages. This is because without any occurrence of fires, fuel load within the forest gradually increases. If then a severe fire season (warm and dry weather) does set off wildfires exceeding suppression thresholds, they can dramatically increase in severity. During recent decades, fire management in many of these regions therefore started to allow low severity surface fires to take place in areas where no harmful societal or economic damages can arise (DAVIDENKO 2003). In Russia, the Aerial Forest Protection Service (Russian: Авиалесоохрана, Avialesookhrana) monitors and fights wildfires across the boreal as the oldest airborne firefighting unit in the world. Their capacity is now lower than few decades ago due to cuts of governmental funding, but it includes hundreds of aircrafts and helicopters spread across hundreds of bases in the country. Their arsenal furthermore consists of "smokejumpers" (a term that originated in the United States), specially prepared firefighters jumping off planes in parachutes to reach fires in difficult terrains (HODGES n.d.). This highlights how even though Siberia's boreal forest stretches across

an enormous area and population density is generally low, humans are to some degree actively involved in shaping the fire activity.

Fire impact on soil biogeochemistry

Other effects of fires can be traced in soil biogeochemistry. Terrestrial nutrients “[...] ultimately constrain ecosystem productivity and could serve as either a positive or negative feedback among changes in climate, forests, and fire regimes” (LEYS et al. 2016: 1). Forest carbon storage and nitrogen availability can be directly affected by wildfires, with nitrogen being a limiting factor for net primary productivity and therefore for the total amount of carbon stored within a forest’s biomass (DUNETTE et al. 2014). Two studies using lake sediments are of special importance for this thesis, with the goal of testing their methodology in slightly altered ways at the boreal research location in SW Yakutia. For this segment, the focus is on providing an overview of potential fire impacts on soil biogeochemistry. An introduction to the method of linking soil geochemistry with reconstructed fire events follows in 3.7.

First, DUNETTE et al. (2014) compared the macroscopic charcoal record (see 1.3) of a lake within a sub-alpine forest in the Rocky Mountains with measurements of carbon and nitrogen concentrations. They found that after identified high-severity wildfires, there is a significant decrease in carbon and nitrogen concentrations and sediment organic matter. They attribute this to fire-caused forest floor destruction and erosion. Their study also shows how this forest was able to deal with decades-long decreased nitrogen availability numerous times throughout the past c. 4250 years, mainly because the fire return interval (FRI) between high-severity fire events was longer than the recovery time of soil nutrients, thus never fully depleting the storages. This might change with shorter FRIs (or higher severity of fires) as predicted for increasing global temperatures (DUNETTE et al. 2014).

The second study by LEYS et al. (2016) focusses on a similar method to compare the same but expanded macroscopic charcoal record with XRF (X-ray fluorescence) measurements of key nutrient elements. Their reconstruction shows how following high-severity fires, element concentrations of titanium (Ti), calcium (Ca), potassium (K), aluminium (Al) and phosphorus (P) in the lake significantly increase for up to c. 30 years, likely due to increased post-fire weathering and erosion within the catchment leading to an increased deposition. On the contrary, sulphur (S) concentrations decrease, likely because of a lower volatilization temperature, while silicon (Si) showed no reaction (LEYS et al. 2016). Results concerning the application of similar methods to Lake Khamra are presented and discussed later in this thesis (see 4.2 and 5.2).

Climate change in the boreal

The Arctic is experiencing stronger warming than the rest of the planet. This is due to the polar amplification effect, a feedback loop of a warming-caused decrease of ice-covered area, thereby increasing absorption of solar radiation by lowering the surface albedo, in turn leading to warming temperatures (ice-albedo-feedback, LENTON 2012). Besides this decrease in Arctic sea ice and the Greenland ice sheet, other feedback loops could potentially affect the climate, like thawing permafrost soils releasing greenhouse gases or changes in the Atlantic ocean's circulation patterns. It is thought that there exist certain thresholds (e.g. a specific magnitude of global warming) upon which these feedback loops are started and/or accelerated and difficult to stop, labelled tipping points. LENTON et al. (2019) argue that the time to prevent a cascade of global tipping points from happening might already have run out, but a quick response in reducing greenhouse gas emissions and therefore the magnitude of projected global warming might still reduce the expected damage.

Due to global warming, the vast boreal zone is subject to change. Not only is there an expected increase in fire severity and frequency but changing climate will also favour the resettlement of different species after fires. This change in species composition might alter large parts of especially the larch-dominated eastern Siberian boreal forest, being a heritage of sorts from the last glacial eras (HERZSCHUH et al. 2016). The boreal forest is projected to move north into current day tundra, where it will benefit permafrost thawing and an increase in albedo (KRUSE et al. 2016), while in the South, boreal conifers are gradually exchanged by temperate species (SEIDL et al. 2017). Because of the warming climate, tree mortality from drought, fire, pests and disease is likely to increase (LENTON 2012), which in turn might lead to the emergence of larger areas of open woodlands more susceptible to fire, creating a positive feedback loop (IPCC 2018). There's also evidence that some intermediary stages of tree cover are not stable and therefore tend to rapidly change towards a more stable state, indicating non-linear shifts in tree population density (SCHEFFER et al. 2012). Fires are regarded as one of the main drivers of ecological changes in the boreal forest and with increasing frequency and intensity, they might start burning more "legacy carbon" that has been accumulated in the top layers of soil by previous, lower intensity fires, therefore increasing net carbon emissions into the atmosphere (WALKER et al. 2019). Because of this multitude of interconnected processes, it seems difficult to pinpoint an individual tipping point for the whole boreal biome. However, these accumulated changes within the world's largest forests lead LENTON et al. (2019) to including them as a climatic tipping point of global significance. Notably, wildfires are an essential element in most of these processes, further highlighting the need of a thorough understanding of fire activity in the boreal.

1.3. Charcoal as a fire proxy

Charcoal is produced by the partial burning of biomass. Charred fragments are subsequently detached, spread across the surroundings of a fire through the air, water streams and on the ground. Charcoal particles reaching a lake will eventually be submerged and deposited on the lake floor, potentially experiencing some mixing processes before settling in the sediment, where they can be preserved over long time spans due to their chemical inertness (CONEDERA et al. 2009, WHITLOCK and LARSEN 2001). An evaluation of fossil charcoal particles found in lacustrine sediment cores can serve as a proxy for changing fire activity throughout time. Commonly, a higher accumulation of charcoal is linked to higher fire activity (e.g. BARHOUMI et al. 2019, CONEDERA et al. 2009, WHITLOCK and LARSEN 2001) and has been shown to correlate well with the local total burned area (LEYS et al. 2015). Besides their abundance, additional sources of information from charcoal particles include their size, appearance or surface reflectance. A basic scheme of charcoal taphonomy and the workflow to reconstruct fires can be seen in *figure 1*.

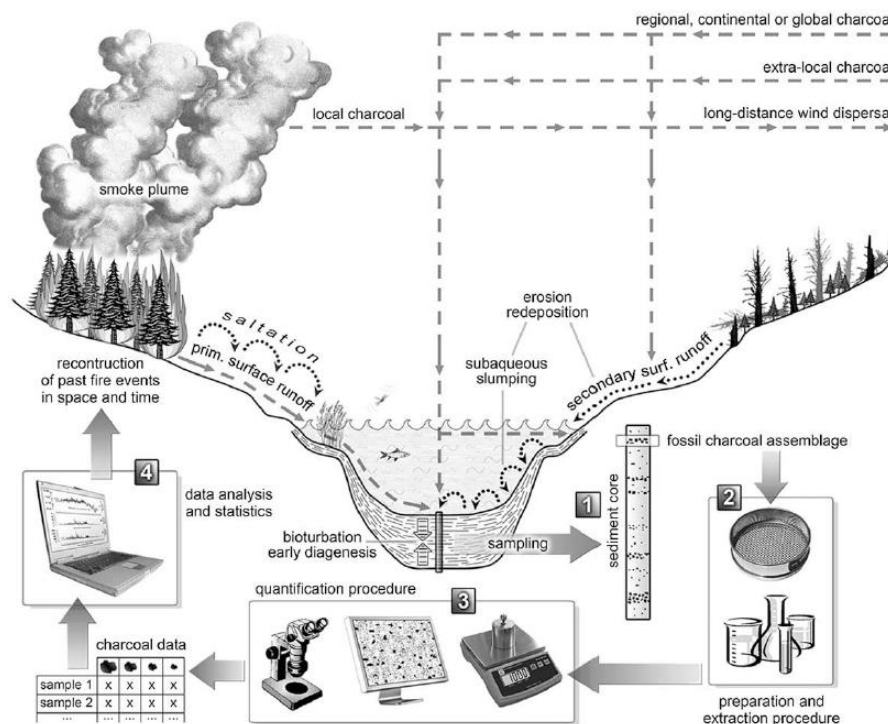


Figure 1: Basic processes and workflow when using macroscopic charcoal as a fire proxy (CONEDERA et al. 2009: 444)

Although this method and its relationship between charcoal abundance and fire activity might seem to be of limited complexity at first, diving deeper into the variety of factors influencing charcoal particle appearance and distribution reveals a more depth to this proxy than what might have been suspected beforehand. And although using charcoal as a fire proxy is a well-established method being conceived about 80 years ago (IVERSEN 1941, who was first to use microscopic charcoal on pollen slides to deduce

fire activity), a more wide-spread and systematic approach seems to have first started only some decades later. After microscopic charcoal (e.g. SWAIN 1973), macroscopic charcoal was analyzed in thin-sections of annually laminated (varved) lake sediment (e.g. RHODES and DAVIS 1995). During the last two decades, preparation of macroscopic charcoal by wet-sieving the sediment seems to have become the most popular method, likely because it is comparably quick and inexpensive (WHITLOCK and LARSEN 2001). Here, the choice of mesh size acts as a threshold of sorts and is based on the assumption that larger particles originate from fires closer to the archive. The variety of approaches to the charcoal method does not stop with the preparation method, however. There are also various ways of counting macroscopic charcoal particles, including a point-count method to approximate particle surface (TOLONEN 1986), measurements of the two longest axes of a particle (MACDONALD et al. 1991), digital image analysis (e.g. HALSALL et al. 2018) or a count of the absolute amount of particles per sample (e.g. DUNNETTE et al. 2014, BRUNELLE and ANDERSON 2003, MOONEY and RADFORD 2001). A compromising approach is counting the absolute number of particles per sample but sorting these counts to different size classes in order to see differences between the distribution of smaller and larger particles (CONEDERA et al. 2009).

As a general rule of thumb, WHITLOCK and Larsen (2001) noted that for lakes set in temperate forests, fire events were often identified when samples showed 50 counts of charcoal particles or more. However, this obviously must be considered as a generalization that should not be used to infer fire events from any charcoal record. In order to deduce fire events from a macroscopic charcoal record, statistical methods were created that are presented, applied and discussed in this thesis (see 3.7, 4.2 and 5.2). In studies using charcoal as a fire proxy, there usually is a separation of a “background” component, which is assumed to represent long-term variations of charcoal input to the lake, changes in particle taphonomy or limits of analytical precision, and a “peak” component representing predominantly local charcoal accumulation during fire events (KELLY et al. 2011, HIGUERA et al. 2009, WHITLOCK and LARSEN 2001). By subtracting the background component from the charcoal record, it is effectively detrended, resulting in the peak component. The peak component is then again divided into signal and noise components with the help of a threshold value. Peaks in charcoal accumulation rate (CHAR) rising above the threshold value (the signal) are labelled “fire peaks” in this thesis and are thought to represent fire events. The term fire events can be misleading however, as it does not necessarily refer to individual wildfires: the temporal resolution of those fire peaks is limited by the deposition time of every charcoal sediment sample and might therefore include more than just one wildfire. The terminology of “fire event” was introduced to better differentiate the interpretation of charcoal “fire peaks” from strictly resembling individual fires (WHITLOCK and LARSEN 2001).

An essential part of this fire reconstruction method is the approximation of charcoal source area, to estimate a spatial extent of fires that added to the charcoal record. In contrast to using e.g. fire scars

on trees as a fire proxy, where it is evident a fire took place right at the location of research, charcoal from within sediment cores might have been produced in close proximity to the lake's shore, within its catchment (local) or beyond (extra-local to regional). It is usually thought that smaller charcoal particles are transported further from their location of origin than larger ones, mainly because they may be lifted up into the air easier – supported by convection from the fire itself – and stay airborne for longer periods of time. This led to the common interpretation of larger particles being a proxy for a local source of fire, whereas small particles are supposed to have their sources on extra-local and regional scales (WHITLOCK and LARSEN 2001). Some studies even claimed potential continental to global sources of the smaller among microscopic charcoal particles (CLARK 1988). There is no definitive radius of charcoal origin around a research location, since this might vary depending on weather, geomorphology, type of fire and vegetation burning (CONEDERA et al. 2009). This probably explains why studies came to different conclusions in the past when estimating charcoal source area. However, calibration studies using unambiguously located and dated fires were able to approximate a range of distances to the lake archives (HIGUERA et al. 2007, TINNER et al. 2006, PISARIC 2002). After reviewing previous research, CONEDERA et al. (2009) summarize a likely origin of macroscopic charcoal (defined by the authors as > 100 - 200 μm length) from local fires within few hundred meters. Smaller particles (microscopic charcoal) on the other hand are thought to originate from within 20 - 100 km from the lake archive. However, the authors also note how stronger convection of higher intensity fires was able to spread even some centimeter-scale particles for multiple kilometers (CONEDERA et al. 2009, after TINNER et al. 2006 and PISARIC 2002). OHLSON and TRYTERUD (2000) analyzed the spread of charcoal particles from experimental fires in the boreal forest of Scandinavia. Large charcoal (> 500 μm) abundance was 56 times higher within the burnt area. There it accounted for c. 80 % of all particles, with this share dropping to below 5 % in up to 100 m distance to the fire.

In another approach to get additional information out of fossil charcoal particles, the appearance of individual particles was categorized as morphotype classes and used to obtain information about a fire's fuel material, since different forms of vegetation (i.e. grass, wooden branches, leaves) produce different shapes and structures of charred material when burned (MUSTAPHI and PISARIC 2014, LEYS et al. 2015). Other interpretations of morphotype classes include charcoal taphonomy processes and a differentiation between primary and secondary input to a lake (ENACHE and CUMMING 2007, 2006).

A newer method of obtaining information from sedimentary charcoal particles involves the measurement of reflected light of a particle under an adequately equipped microscope. In wood burning experiments and field studies it has been shown that the amount of light reflected from polished charcoal surfaces increases with higher charring temperatures (SCOTT and GLASSPOOL 2005). This is likely due to the molecular level of charcoal being more aromatic and thus more orderly structured at higher temperatures of formation (HUDSPITH et al. 2015, SCOTT 2010). HUDSPITH et al. (2015) were among the first

to apply the relationship between charring temperature and reflectance to a Holocene charcoal record and reconstruct minimum fire temperatures, which could then be compared to the changing prevalent vegetation at different points in time.

In contrast to macroscopic charcoal, microscopic charcoal is often counted on pollen slides and therefore often includes particle sizes of up to a maximum of 100 - 150 μm , depending on mesh size of sieves used. It likely originates from a way larger source area than larger particles, thought to be similar to the source area of pollen grains. Due to intrinsic and analytical limitations, individual fire events cannot be identified using microscopic charcoal records. Therefore, they are mostly used for a more general interpretation of larger-scale fire activity within a given region (CONEDERA et al. 2009). WHITLOCK and LARSEN (2001: 82) summarize the limitations of microscopic charcoal with three key points: “(1) *samples in most Holocene studies are spaced centimeters apart in a core, and gaps of decades to centuries exist in the record; (2) charcoal particles are broken during pollen preparation, thus creating an artificially high abundance of microscopic particles (< 100 μm [sic]); and (3) the exact source of area of microscopic charcoal is generally vague [...]*”. This emphasizes that microscopic and macroscopic charcoal particles serve as proxies of different scales and attributes of fire activity.

The Global Paleofire Working Group unites scientists from an interdisciplinary background and is responsible for the Global Charcoal Database (GCD, POWER et al. 2011) and statistical tools to access its information (e.g. the R package “paleofire”, BLARQUEZ et al. 2014). The GCD incorporates data from charcoal records (macro- and microscopic) all over the planet and provides a pool of previous work on fire reconstruction. This allows for a more efficient synthesis of larger-scale fire history (e.g. MARLON et al. 2013, 2008), but it also highlights regions where data is still very sparse. For this reason, MARLON et al. (2016: 3237) highlight the need of “[f]illing the gaps [...]”, which besides the continent of Africa and the tropics predominantly exist in tundra regions and the boreal forest of Eurasia. In fact, in all of Russia only a handful of macroscopic charcoal records exists in the GCD, with only one of those suitable for the reconstruction of fire events and return intervals (located in the Ural region about 3000 km distant from Lake Khamra, see BARHOUMI et al. 2019). Some publications featuring macroscopic charcoal are not included in the GCD (e.g. EICHLER et al. 2011), however, it seems as though none of them aim at or meet the prerequisites for deducing fire events either (a discussion of reasons is presented in 5.2). This scarcity of data stresses the need for obtaining continuous, high-resolution charcoal records from the Siberian boreal forest, which is part of the motivation for this thesis.

2. Location

Lake Khamra (Russian: Озеро Хамра) is located at 59.99 °N, 112.98 °E in SW Yakutia (Sakha Republic, Lensky District; see *figure 2*), c. 30 km northwest of the Lena river, where a small village exists (Krestovski Leso-oetsjastok, Russian: Крестовский Лесоэтсъясток) and c. 40 km north of a small town named Peledui (Russian: Пеледуй). The lake lies at an elevation of c. 340 m above sea level. It covers an area of c. 4.6 km² and reaches a maximum water depth of c. 22 m. According to a detailed cryolithological map showing the extent of permafrost and different types of vegetation in Yakutia by FEDOROV et al. (2018), Lake Khamra lies within the landscape zone of the “middle taiga” featuring discontinuous and sporadic permafrost, which is classified by an average of c. 160 days/year with > 0 °C temperatures and a mean annual temperature of - 5.5 to - 9 °C, corresponding to a mean January temperature of - 30 to - 40 °C and a mean July temperature of c. 18 °C. Covering an area of 27.5 %, the middle taiga is the most prevalent of the described landscape zones and also has the highest amount of biomass per area. It “[...] includes larch, pine, pine-larch, and pine-larch with cedar and spruce forests. [It is] characterized by low shrub and low shrubby/lichen/moss covers” (FEDOROV et al. 2018: 7). The terrain type around the lake is categorized as low and middle terraces, with cryogenic textures and ice appearing massive, lenticular and layered, featuring Holocene ice wedges in the lower terrace sections. Volumetric ice content lies between 20 - 40 % and basic cryogenic processes include frost cracking, thermokarst, heaving and thermosuffusion, which can create collapsing sinkholes. In the middle taiga, larch forests develop the “[...] lowest soil temperatures of up to from - 1 to - 1.5 °C and active layer thickness up to 2 - 3 m” (FEDOROV et al. 2018: 12).

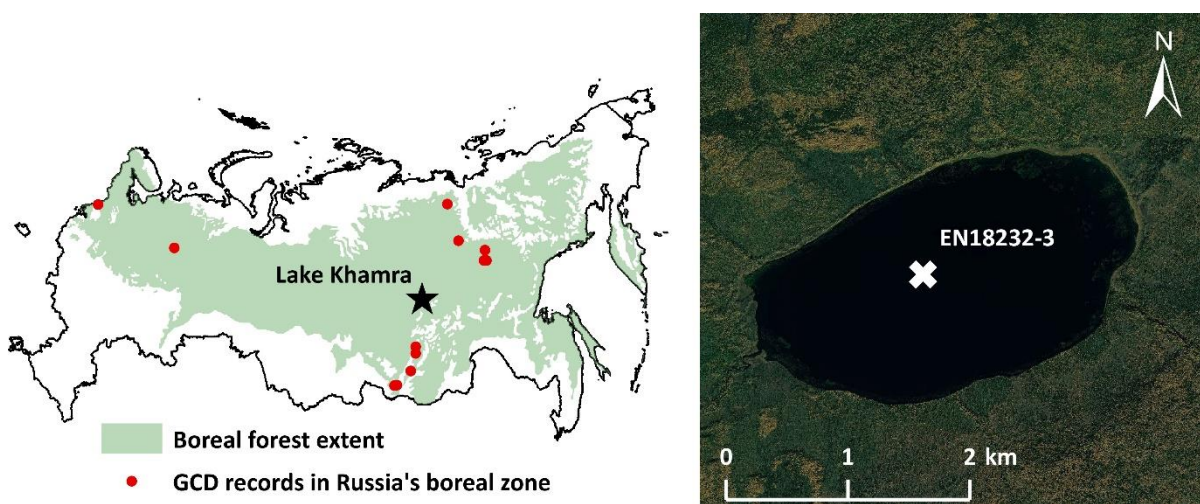


Figure 2: Map indicating the location of Lake Khamra in Russia and the position of sediment core drilling in the lake. Red dots represent all charcoal records in the Global Charcoal Database within Russia's boreal forest. World Imagery map: Esri (2020), Boreal forest extent: Olson et al. (2001), GCD records: Power et al. (2011)

Judging very generally from categories proposed by FEDOROV et al. (2018), Lake Khamra lies in a region that does meet prerequisites for thermokarst development, e.g. a soil volumetric ice content of 30 % or higher for some parts. Ice content above that amount was found to be typical for the development of thermokarst lakes (GROSSE et al. 2013), where local warming or disturbance by a fire leads to thawing soil ice content, landscape subsidence and a following collection of water within the newly formed depression (referred to as “*alas*” in Siberia). The high heat capacity of water in turn leads to accelerated thawing of ice and a gradual increase in thermokarst lake area and depth of unfrozen soil below (referred to as “*talik*”). With mechanical and thermo erosion, these thawing processes also tend to undercut the shoreline and gradually incorporate resulting loose material into the lake sediment (BOUCHARD et al. 2016). With thermokarst lakes being a widespread phenomenon in Yakutia and their inception and development being defined by different processes than lakes which form in other landscape depressions or based on impermeable soil and rock layers, it is important to note that Lake Khamra is not considered to be of thermokarst origin. Lake Khamra’s appearance does not match some key thermokarst lake attributes like steep slopes (KATAMURA et al. 2009a, 2009b) or the usually shallow water depth of less than 10 m (BOUCHARD et al. 2016, WEST and PLUG 2008). Additionally, ice wedges thought to signal the existence of closeby thermokarst (SÉJOURNÉ et al. 2015, KATAMURA et al. 2009b) were not found around the lake, likely due to a deeper active layer because of the sporadic/discontinuous nature of the permafrost and generally denser vegetation at c. 60 °N. This lack of ice wedges might also be evidence for the area around Lake Khamra to lie at the lower end of the soil volumetric ice content range of 20 - 40 % as proposed by FEDOROV et al. (2018), which would in turn make the appearance of large-scale thermokarst landforms less likely. Even though no thermokarst origin is considered for Lake Khamra, there is still evidence for the introduction of older, maybe previously frozen, organic carbon into the lake’s sediment, as will be discussed later in this thesis (see 5.1). However, ruling out thermokarst origin enables the exclusion of description and discussion of thermokarst lake processes in more detail, which tend to be a strong and often to some degree unknown influence on reconstructions in these types of archives (BOUCHARD et al. 2016).

3. Methods

In the following segment practical and statistical methods used within this thesis are described in more detail, from field work at Lake Khamra and the subsampling process of the sediment core to sample preparation and age dating. A well-established method of reconstructing fire history using sedimentary fossil charcoal particles is presented, which constitutes the foundation of this thesis. Additionally,

some newer approaches of charcoal analysis are introduced. For the statistical analyses, the mentioning of R or any of its base functions always refers to the R Core Team (2020).

3.1. Field work and core sampling

Field work at Lake Khamra was part of an expedition to Chukotka and Central Yakutia from June 29th to August 21st, 2018. According to the expedition report (KRUSE et al. 2019), this undertaking was part of an European Research Council (ERC) consolidation grant named GlacialLegacy, addressing the reasons behind the existence of larch-dominated, summergreen boreal forest in NE Asia and how its composition might rather irreversibly change in the future (HERZSCHUH et al. 2016). First, the expedition visited sites along a tundra-taiga-transition zone in NE Siberia (Chukotka), where tundra vegetation gives way to increasingly dense populations of summergreen *Larix* trees. After that, the transition zone from summergreen larch-dominated to evergreen boreal forest was visited in Yakutia, including the area of Lake Khamra. During the expedition a wide array of methods was used to obtain valuable data, like vegetation surveys, collection of plant and soil material, analysis of soil layers and measurements of temperature and humidity in soil sensors and climate stations furthermore providing radiation and wind data. From several Arctic lakes, sediment cores were obtained, including three from Lake Khamra: EN18232-3 (main core), EN18232-4 (parallel short core) and EN18233-1, drilled with a Russian corer near the southwest inflow into the lake (not used for analysis so far).

Sediment core EN18232-3 (previously known as EN18232 Long 3, precise location 59.99091 °N, 112.98373 °E), the sediment core this thesis is mainly based upon, was retrieved on August 14th, 2018. An UWITEC modified hammer-action corer was used at the estimated deepest point of the lake based on point measurements of its bathymetry. The core has a total length of 242 cm divided in three segments (0 - 42, 42 - 142 and 142 - 242 cm). All segments could be recovered without loss of sediment. They were sealed off and thoroughly labelled. A short core (EN18232-4) with a total length of 43 cm was obtained from the same location, as a parallel sample to the main core EN18232-3. It was subsampled in the field to 0.5 cm thick slices, which were safely stored in whirlpacks. All sediment material was placed in insulated thermoboxes before being transported back to AWI Potsdam, where they were stored for further work in a cooling chamber at 4 °C.

Work on the sediment core EN18232-3 began in October 2018. The core segments were moved to the German Research Center for Geosciences (GFZ), where they were opened and subsampled in a climate chamber at 4 °C. Work was done under sterile conditions to prevent contamination of the sediment, which was also scheduled for the analysis of sedimentary ancient DNA (aDNA; High-latitude Biodiversity working group of the Polar Terrestrial Environmental Systems section at AWI Potsdam). The core

liner was cut open lengthwise and the core material cut in two halves using standard AWI procedures, with effort given to not disturb any of the sediment material. One half of the opened core was covered in clean plastic foil and sealed in a vacuumed bag to be stored as archive material at AWI's cooling chamber, whereas the other half was prepared for subsampling work. Sediment appeared to be very homogenous in both its dark brown colour and grain size composition, without notable signs of layering and a soft consistency, likely due to increased water content. The sampling scheme for the EN18232-3 core comprised the extraction of a 2 ml pollen/charcoal sample, a 1.5 ml diatom sample and a 3 ml aDNA sample from the middle of every 2 cm increment. Before extraction, every increment had the top few millimetres of sediment removed to get rid of possible contamination or disturbance during the opening process.

For the extraction of sediment material, sterile syringes were used that have been manually cut open beforehand. Additionally, after the extraction of those samples, some of the remaining sediment to each side of the increment was taken out using clean knives. These additional samples served as sources of macroscopic charcoal, since an uninterrupted, continuous record of this proxy is essential not to miss out on individual peaks within its timeseries (see 1.3). However, due to the extraction process, these samples did not have a corresponding volume, which had to be accounted for later in the process (see 3.3 and 3.5). In the end every 2 cm increment consisted of 3 samples lengthwise (charcoal - pollen/charcoal - charcoal), thus creating a continuous sequence. The remaining sediment material of each increment was taken out of the core liner, having the outer layers touching the core liner removed (again, to account for disturbance during the liner's movement into the sediment). The remaining sediment material was stored for any further analysis if needed, except for one increment every 20 cm, where it was used for bulk radiocarbon age dating.

3.2. Age dating

Establishing a robust chronology is fundamental to reconstructing fire history from sediment core proxies. According to recommendations by WHITLOCK and LARSEN (2001), both radiocarbon (^{14}C) and lead-caesium ($^{210}\text{Pb}/^{137}\text{Cs}$, hereafter Pb/Cs) age determination methods were applied to Lake Khamra's cores EN18232-3 and EN18232-4, respectively.

^{14}C age dating

Bulk sediment samples for ^{14}C dating were extracted at 20 cm intervals along the core. Seven samples were prepared for the process by freeze-drying the sediment and homogenizing it in a planetary mill.

Measurement of total organic carbon (TOC) and total nitrogen (TN) was also done for those samples (using the method described in 3.5). With the exception of one ca. 2 cm long piece of wood at c. 85.5 cm depth, no larger plant macrofossils were found within the sediment core. However, some additional macrofossils of very small size like seeds or fine organic structures were collected from sieved sediment samples (thus only featuring the depth range of their respective samples instead of an exact value). Due to their small size and fractured appearance, it was not possible to confidently exclude aquatic origin in all cases. Together with the homogenized bulk sediment samples (n = 7) and the collected macrofossils (n = 15) all available information was sent to AWI's MICADAS laboratory in Bremerhaven, responsible for the ^{14}C dating procedure according to standard AWI protocols.

Pb/Cs age dating

Pb/Cs age dating was carried out using the parallel short sediment core EN18232-4, which has been subsampled in the field for that purpose (as described in 3.1). Since lead-210 (^{210}Pb) deposition from the atmosphere is considered to be constant, varying activity reliably resembles changes in sediment accumulation rate. Caesium-137 (^{137}Cs) on the other hand was distributed in the atmosphere by nuclear events of global scale, namely the accident at the Chernobyl power plant in 1986 and a peak in nuclear bomb tests during rising tensions of the Cold War in 1963. Other products of radioactive decay can be used to robustly confirm these marked events in a sediment core (BOLLHÖFER et al. 1994). However, in sediments ^{210}Pb is also the product of background radioactive decay of radium-226 (^{226}Ra). Because of the short half-life of ^{210}Pb (c. 22 years), the magnitude of measured atmospheric input to sediment is decreasing with depth, eventually reaching an equilibrium with the "background production" derived from ^{226}Ra . This equilibrium usually lies at an age of c. 120 years, equivalent to about five times the half-life of ^{210}Pb , and marks the maximum time span that can be dated with this method (SWARZENKI 2014).

The bulk sediment samples (n = 19) were sent to the Liverpool University Environmental Radioactivity Laboratory. The report notes provided by Prof. Dr. Peter Appleby and Dr. Gayane Piliposian (personal correspondence) state that "[...] [they] were analysed for ^{210}Pb , ^{226}Ra , ^{137}Cs and americium-241 (^{241}Am) by direct gamma assay, using Ortec HPGe GWL series well-type coaxial low background intrinsic germanium detectors (APPLEBY et al. 1986). ^{210}Pb was determined via its gamma emissions at 46.5 keV, and ^{226}Ra by the 295 keV and 352 keV gamma rays emitted by its daughter radionuclide ^{214}Pb , following 3 weeks storage in sealed containers to allow radioactive equilibration. ^{137}Cs and ^{241}Am were measured by their emissions at 662 keV and 59.5 keV respectively. The absolute efficiencies of the detectors were determined using calibrated sources and sediment samples of known activity. Corrections were made for the effect of self-absorption of low energy gamma-rays within the sample (APPLEBY et al. 1992)."

3.3. Macroscopic charcoal

In general, all methods used for preparation and counting macroscopic charcoal particles were based on common choices in the literature in order to increase comparability to other records.

Preparation of macroscopic charcoal

As described in 3.1, the subsampling scheme for the EN18232-3 core involved two charcoal samples per increment, separated by a pollen sample. Keeping in mind the importance of a continuous fire history record, that made it necessary to extract macroscopic charcoal from the pollen samples without influencing either the charcoal or the pollen within the sediment matrix. The standard procedure for the pollen preparation involves a lot of centrifuging and uses the ultrasonic bath, both of which might severely damage the more fragile charcoal particles and therefore influence overall results. For this reason, a method was developed that is based on the previous work as stated before, but also allowed for a safe subsequent preparation of pollen slides by removing macroscopic charcoal before any centrifuging is necessary while collecting all smaller fractions in the process.

The following process was applied to all used samples ($n = 322$, charcoal and pollen samples) of the EN18232-3 core. First, the sediment sample was weighed and put in 50 ml falcon tubes. Simultaneously, *Lycopodium* tablets (containing a known quantity of spores used as marker grains) were dissolved in 10 % hydrochloric acid (HCl) and then added to the sediment in the sample tube. This way, the ratio of pollen grains to *Lycopodium* marker grains is controlled for even throughout the charcoal preparation process. Next, the sample was wet-sieved at 150 μm mesh-width (a common choice recommended for the separation of macro- and microscopic charcoal, see DIETZE et al. 2019, HAWTHORNE et al. 2018, MOONEY and RADFORD 2011, CONEDERA et al. 2009), using gentle squirts of a standard lab water bottle to disaggregate any lumps. The soft sediment with high organic content dissolved without the need of using a disaggregating agent like sodium hexametaphosphate ($(\text{NaPO}_3)_6$; see MOONEY and RADFORD 2001; WHITLOCK and LARSEN 2001, HAWTHORNE et al. 2018, BRUNELLE and ANDERSON 2003, DUNNETTE et al. 2014) potassium hydroxide (KOH; see KATAMURA et al. 2009a) or sodium pyrophosphate ($\text{Na}_4\text{P}_2\text{O}_7$; see MACDONALD et al. 1991), so sieving was done without any exposure to such chemical agents. The suspension of smaller fractions (containing, among others, the pollen grains) was collected beneath the sieve and transferred to a new falcon tube by multiple steps of filling the tube, centrifuging and decanting the water from the sediment residuum. The result of this process is a sediment sample containing only $< 150 \mu\text{m}$ sediment particles like pollen grains, non-pollen palynomorphs, microscopic charcoal and *Lycopodium* marker grains, ready for further preparation with standard laboratory procedures to create a pollen slide. The $> 150 \mu\text{m}$ fraction remaining in the sieve was rinsed together with

a gentle stream of tap water before being transferred to 50 ml falcon tubes as well. After letting samples rest to accumulate at the tube's bottom, excess water was carefully decanted. To aid charcoal particle counting and minimize error from erroneously including dark organic particles, the charcoal samples were then bleached by adding c. 15 ml of household bleach (< 5 % sodium hypochlorite, NaClO) and left to soak overnight (see HALSALL et al. 2018, HAWTHORNE et al. 2018, DUNNETTE et al. 2014, MOONEY and RADFORD 2011). After carefully decanting the bleach, charcoal samples were ready to count (a more detailed preparation protocol can be found in appendix H).

In addition to the careful way of decanting the water/bleach from the sample material, during both of those steps, random tests were done for some of the samples in preparation to control for any lost charcoal particles. This was done by collecting the decanted liquid from multiple samples and merging any suspended particles by repeated steps of centrifuging. The resulting test samples were then examined using a stereomicroscope. Testing this potential loss of charcoal for a total of 46 samples, only one particle < 150 µm was found. This suggests that a loss of particles during the two decanting steps is a rare occasion that should not influence overall results.

Counting macroscopic charcoal particles

Finished samples were transferred to a petri dish for counting charcoal particles. The counting procedure was guided by recommendations from previous research (see 1.3). Only particles that appeared opaque, with visible charred structures and mostly jet-black in colour were included (see HAWTHORNE et al. 2018, BRUNELLE and ANDERSON 2003). The petri dish was fitted with a c. 1 cm² grid of black lines on its bottom to aid orientation during the process. It was placed under a reflected-light stereomicroscope and viewed at 10 - 40x magnification. The whole gridded area of the petri dish was systematically observed to make sure every charcoal particle was included and no double-counts occurred.

In addition to counting total charcoal particle abundance, particles were categorized into size classes ranging between > 150 µm, 300 - 500 µm and > 500 µm measured along a particle's longest axis (see DIETZE et al. 2019). For size reference, preparatory needles with known diameters/tip size of 300 and 500 µm were used that could be placed next to a charcoal particle. They also proved to be beneficial for cases in which charcoal origin of a particle was uncertain. By carefully moving a particle or applying small amounts of pressure with the needles, the flexibility could be tested. Charcoal fragments are described as fragile and non-bendable (WHITLOCK and LARSEN 2001). Particles were also categorized based on their basic morphology (see *figure 3*) by adapting the classification scheme developed by ENACHE and CUMMING (2007, 2006), however, extending it with additional morphotypes. Partially charred (Type Z), highly irregular (Type X) and fibrous, elongated particles (Type E) were not involved

in the author's original morphotype scheme and otherwise difficult to sort into existing classes. Categorization of a particle's size and its morphotype was independent from one another.

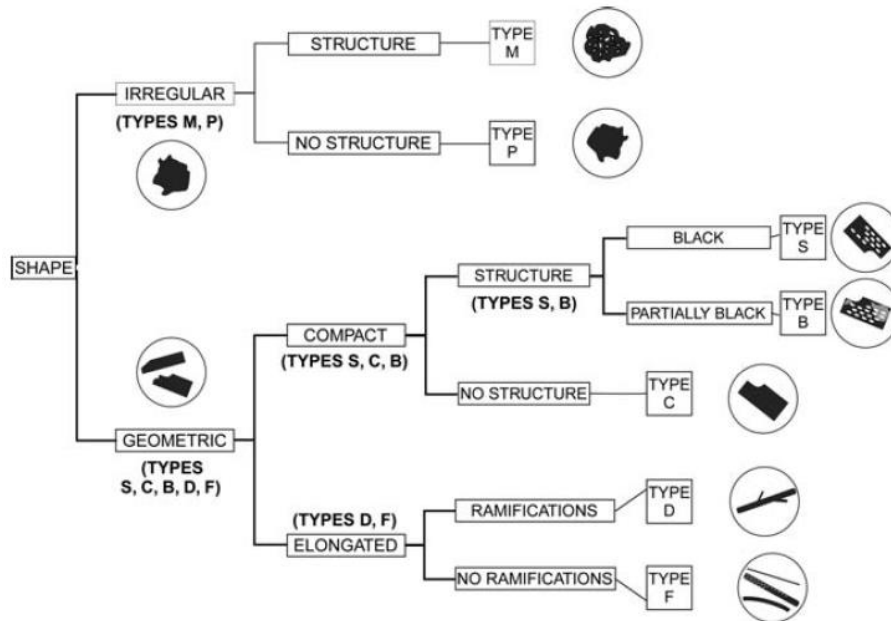


Figure 3: Charcoal morphotype classification scheme based on classes of common particle appearances (ENACHE and CUMMING 2007: 352)

Morphotypes of irregular shapes are differentiated by the visibility of charred structures (Type M) or a lack thereof (Type P). Type M tends to be fragile and easy to break. Its appearance can vary from flat, planar and grid-like particles or more dense, bulky ones. If no charred structures are visible, a particle of that appearance is classified as Type P. ENACHE and CUMMING (2007) mention that Type P was excluded in their statistical analysis because it was quite rare in their samples. Compact, geometric morphotypes are differentiated in a similar manner. A particle with clear angles and a mostly geometric shape (or a likely remnant of that), showing charred structures is classified as Type S. They can appear both dense/bulky (see figure 4) and flattened. Their charred structures often resemble parallel bands. If a particle of this sort displays brown colours (typically near the edges) in addition to the opaque black, it is classified as Type B. Particles that are all brown were not counted. A Type S particle without a visible charred structure is classified as Type C. Besides the irregular and compact geometric morphotypes, there are elongated (geometric) particles. Type F particles are generally long, thin and easy to break. They might be straight or slightly bended. A particle of this sort displaying ramifications, reminiscent of little branching twigs, is classified as Type D. Charcoal particles found at Lake Khamra displayed a great variety of shapes (see examples in figure 4) and therefore, the scheme by ENACHE and CUMMING (2007) was extended with previously mentioned Type E, X and Z. Type E belongs to the elongated particles, but instead if a unified strand like Type F, it consists of multiple interconnected fibres. Type X are highly irregular particles that often resemble curled-up strands or have an appearance like

perforated, molten glass. Type Z on the other hand does not add to the total sum of charcoal particles, as it was introduced to specifically quantify particles/structures that were only slightly charred. Usually brown, thin strands of charred material are still held together by bleached plant cells.

Counting was recorded on paper and by selecting samples without any particular order. Once counting was done for a batch of samples, the results were digitalized for further analysis and visualization.

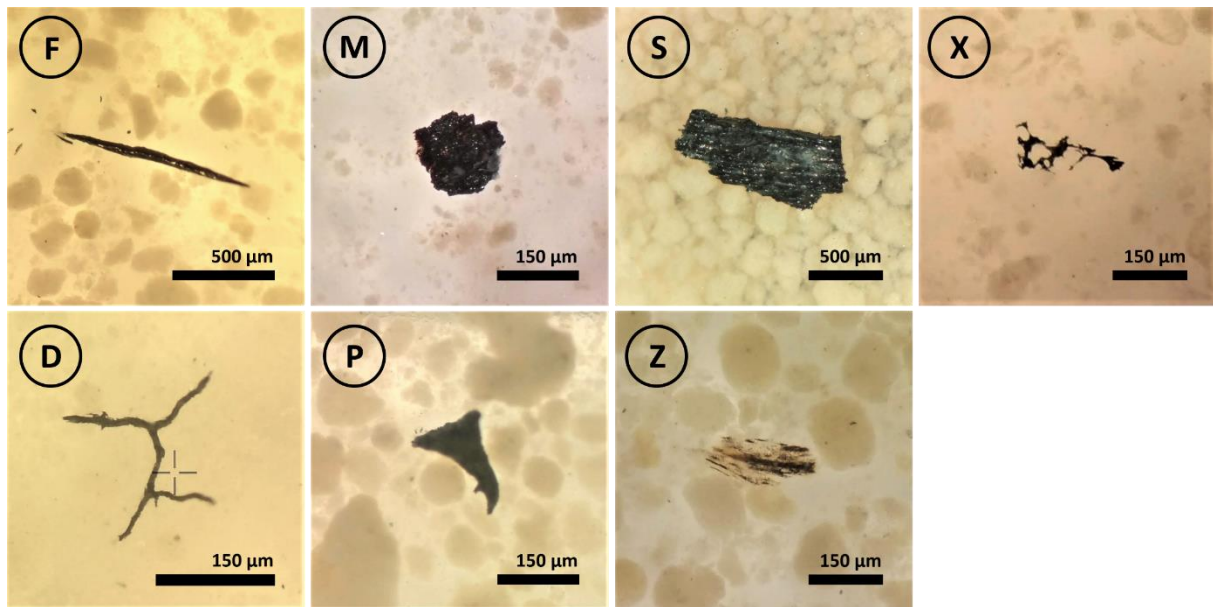


Figure 4: Images of various macroscopic charcoal morphotypes found at Lake Khamra. Letters indicate the classification according to the extended scheme by ENACHE and CUMMING (2007, 2006)

Obtaining volumes of charcoal samples

During core sampling, pollen samples of every increment were extracted using a syringe that was cut open. This was done in order to extract sediment material of a known volume (here: 2 ml). However, since there seemed to be slight inaccuracies with this form of sediment extraction, a second method of obtaining volumes for each sample was implemented in order to get as precise of a value as possible within these circumstances. During the preparation of TOC samples, a tool for the extraction of cubes with 1 cm³ in volume was used and therefore, together with the sample weights, more precise wet sediment densities for all of the 120 increments along the core could be obtained. The result shows great agreement with average volume values of the previous syringe method but is thought to be more accurate for every individual sample.

As mentioned before, the charcoal sediment samples had to be extracted from the core without a method of volume estimation. However, volumetric data is required to obtain accurate charcoal concentrations and influxes. To solve this problem, densities measured with the method stated above

were interpolated using a cubic spline in order to account for the contiguous charcoal sediment samples within all of the directly measured increments. Using the interpolated densities and the individual sample weights, the missing volume of each charcoal sediment sample could be calculated. The validity of this calculation method is backed up additionally by the lack of strong variance within the core's measured sediment densities.

Charcoal reflectance test

Thanks to correspondence of Dr. Elisabeth Dietze, there was the opportunity to test charcoal reflectance measurement on some samples ($n = 11$) of the Lake Khamra charcoal record. They were sent to the University of Exeter in May 2019 to be analysed by Dr. Alicja Bonk (University of Gdansk, Institute of Geography), who kindly provided a report describing the basic method and results. For reflectance measurement, particles are embedded on resin blocks and then polished using a diamond liquid to create smooth surfaces that can then be viewed with a reflected light microscope. Of all 11 samples sent, only 6 could be measured under the microscope for various reasons. First, particles usually used for this application are larger than what was found in these samples – apparently, no such reflectance analysis was yet done on fossil charcoal particles from lakes in Yakutia. Studies are mostly located within the temperate zone, with different fuel types and fire regimes potentially producing different (i.e. larger) charcoal particles depending on the individual situation. Other problems involved losing particles in the process of transferring them from their bleach solution to blocks of resin, or the loss of particles during the polishing of the resin blocks. Usually, 100 random point measurements of reflectance are made per sample. Due to the smaller size of our particles, only an average of 20 random point measurements could be done with no conclusive evidence from the literature about how many are deemed necessary to obtain significant results. Of the 6 measured samples, one did not yield valid results due to a contamination with minerals, leaving 5 samples that had their charring temperature calculated using the measured reflectance and a calibration curve (Dr. Alicja Bonk, personal correspondence).

3.4. Pollen samples and microscopic charcoal

Preparation of pollen samples ($n = 60$) was done according to established AWI protocols, with the only difference being that because of the extraction of macroscopic charcoal beforehand, pollen samples were already infused with *Lycopodium* marker grains. Pollen preparation aims at concentrating pollen and non-pollen palynomorphs while reducing the abundance of other particles (e.g. silicates, see CHAMBERS et al. 2011). Preparation of the smaller sediment fractions, collected after extraction of the > 150

µm fraction (as stated in 3.3), therefore begins with adding hot potassium hydroxide (KOH) to each sample and letting the solution boil for 10 mins. After sieving the samples, they were treated with c. 18 ml hydrofluoric acid (HF) and left to stand in the fume hood overnight. After centrifuging and decanting the HF, two additional treatments with hot HF followed, about 1.5 hours each. Following removal of HF from the samples, acetolysis was performed using acetic acid (CH₃COOH) and after that a mixture of acetic anhydride (C₄H₆O₃) and sulfuric acid (H₂SO₄). Finally, samples were fine-sieved in the ultrasonic bath and suspended in glycerol (C₃H₈O₃). Removal of liquids between steps was always done by centrifuging and decanting the samples.

The finished pollen samples were then ready to be put on glass slides for microscopy. Counting of pollen types, spores and non-pollen palynomorphs was done by Dr. Andrei Andreev (AWI Potsdam, High-latitude Vegetation Change working group) for a selection of pollen samples across the whole depth of the sediment core (n = 24). Using the known total quantity of exotic marker grains added (the *Lycopodium* spores; L_{added}) and their counts per sample ($L_{counted}$), the amount of counted pollen ($P_{counted}$) and the sample volume (V_{sample}), the pollen concentration (P_{conc}) can be calculated (STOCKMARR 1971):

$$P_{conc} = \frac{L_{added}}{L_{counted}} \times \frac{P_{counted}}{V_{sample}}$$

From the concentrations of all counted grains, percentages were calculated and used for further analysis of links between the charcoal record and vegetation history (see 4.3). The pollen and non-pollen palynomorph based reconstructed vegetation was visualized using the R function `strat.plot` (package “rioja”, JUGGINS 2017).

Microscopic charcoal quantities were obtained for every pollen sample that had its pollen spectrum analysed (n = 24), resulting in a lower-resolution overview of changes in smaller charcoal particle concentrations across the whole core. Slides for microscopic charcoal were created using the same technique that was applied to the creation of pollen slides (stirring the glycerol-suspended sample material for c. 30 seconds and then placing a small droplet of the suspension on a glass slide using a pipette). Slides were inspected using a transmitted-light microscope at 400x magnification.

Counting was started in one of the edges of the charcoal slide area and then continued by moving the slide in straight lines. Every black, opaque particle was counted and was classified within the morphotype scheme of ENACHE and CUMMING (2007, 2006). Although this scheme was developed for macroscopic charcoal and microscopic particles are likely to be damaged and therefore artificially altered in their appearance by the pollen preparation method, this was done more for explorative reasons and to see how microscopic morphotypes compare to their macroscopic counterparts. *Lycopodium* marker grains were counted additionally to the charcoal particles to gain the ability of calculating charcoal

concentrations, similarly to the method of calculating pollen concentrations shown above. In accordance to literature on minimum count sums for reliable results, for every sample between 300 - 400 total items were counted, including both microscopic charcoal particles and *Lycopodium* marker grains (FINSINGER and TINNER 2005).

3.5. TOC and C/N

Unfortunately, due to a malfunction of laboratory equipment and subsequent time needed to organize a replacement, no TOC and C/N measurements of the samples could be obtained. This means that no evaluation of these parameters can be done within this thesis. However, the preparation process will still be briefly described, since the samples were already prepared to the point of being ready to be measured as soon as the equipment is repaired or renewed. Also, during sample preparation for these methods, an estimate of sediment bulk density was obtained that was then used for the volume calculation of charcoal samples.

For TOC and C/N analysis, some of the remaining sediment material from each of the 120 increments along the whole core was used. Sediment was transferred to 50 ml falcon tubes using a volumetric tool for the extraction of cubes of 1 cm³. This ensured an additional and more precise method of density calculation for all samples (see 3.3). After centrifuging and decanting excess water from the tubes, the samples were freeze-dried for about 36 hours before being ground up and homogenized in a rotary mill (6 min at 360 rpm). After those steps, dry weight and water content of the sediment material could be calculated. From the homogenized, dry sediment of each of the 120 samples, c. 5 mg were transferred to a small vessel made of aluminium foil to estimate C and N content. The vessels were also filled with some tungsten oxide (WO₃) to aid combustion. The safely enclosed samples were then sorted into a plastic tray. Before and after every batch of samples, standards were included to reveal any potential offsets in measurements. Those would have been conducted with a vario EL III (elementar Analysensysteme GmbH) elemental analyser. For estimation of TOC content, c. 100 mg of each of the 120 samples were transferred to steel crucibles to measure the amount of C that is lost during ignition with a varioMax C (elementar Analysensysteme GmbH). This would have allowed for estimating the share of TOC and TIC.

Measurement of TOC and C/N from all 120 samples could be resumed as soon as the equipment allows, adding the ability to apply statistical methods of this thesis to soil biochemistry (according to DUNNETTE et al. 2014).

3.6. Micro-XRF

Micro-XRF measurement (hereafter termed XRF) of the sediment core's archive half was done by Stuart Vyse (AWI Potsdam, Arctic Lake System Dynamics working group) at AWI Bremerhaven using an Avaatech automated XRF scanner. Scanning was done in steps of 0.5 cm across all three core segments. According to the results of LEYS et al. (2016), only specific elements were used in this thesis to analyse any potentially fire-related impact on their abundance in the lake's sediment: Ti, Ca, K, Al, P, S and Si. Aside from assessing the timeseries of these XRF elements and applying the superposed epoch analysis using reconstructed fire events, no in-depth analysis of XRF data will be featured in this thesis, since that was considered to be beyond the scope of this project.

3.7. Statistical methods

This segment describes the main statistical approaches used in this thesis, which mainly consist of an evaluation of the fire signal within the macroscopic charcoal record to identify fire events. Besides that, correlation tests, principal component analysis and the superposed epoch analysis are introduced.

Macroscopic charcoal

For every sample, counts of the three size classes were added up for a total sum of charcoal particles. With the interpolated sediment densities obtained during TOC and C/N sample preparation and the weight of every charcoal sample, a volume could be calculated (see 3.3). This enabled the charcoal counts sum to be expressed as a concentration ($\#/cm^3$). Charcoal accumulation rate (CHAR, $\#/cm^2/yr$) can then be calculated by multiplying the sedimentation rate (cm/yr) obtained from the age-depth model with the charcoal concentration. To achieve a separation of background and peak component within the charcoal record and to further label the signal within the peak component to identify fire events, this thesis uses an R script published by DIETZE et al. (2019). The script is based on previous literature that makes up the well-established analytical tool "CharAnalysis" (HIGUERA et al. 2009), basically translating its original Matlab code into R. CharAnalysis works in the previously described common way of deconstructing a charcoal record (see 1.3) and was used in many previous studies (e.g. MAGNE et al. 2020, BARHOUMI et al. 2019, LEYS et al. 2016, LEYS et al. 2015, DUNNETTE et al. 2014). To clarify what is being addressed, this essential procedure will be referred to as "CharAnalysis" in this thesis, even though it is only indirectly based on the similarly named analytical tool and was applied in the form of the R script by DIETZE et al. (2019).

First, the macroscopic charcoal record was interpolated to equally spaced time intervals of 6 years, corresponding to median temporal resolution among samples, using the `pretreatment` function of the R package “paleofire” (BLARQUEZ et al. 2014). The background component was determined by computing a LOWESS at the window width of 1/5 of the total length of the record ($w = 409.2$ years), which was found to be a value leading to a more efficient signal-to-noise ratio (4.2; see BARHOUMI et al. 2019). This allows for the establishment of the peak-component by subtracting the LOWESS from the timeseries. With a Gaussian mixture model two distribution curves were fitted into the peak component to define a threshold ($t = 0.492$) at the 99th percentile of the noise distribution (DIETZE et al. 2019). Subsequently, all peak component values exceeding the threshold are identified as signal or “fire peaks”. Fire events identified using this method were marked in the CHAR timeseries and visually checked for the creation of an alternative, “reduced fire” version. For this alternative version, if two or more fire events were identified on a single peak (which was also considered when a peak more closely resembled the shape of a plateau), the younger fire events and/or fire peaks that did not intersect with the actual peak of a distribution were manually excluded from the list (see HIGUERA et al. 2009). This reduced fire version was later also used as an additional data source for the superposed epoch analysis with XRF data (see 4.4).

A signal-to-noise index (SNI) was calculated in R using a method established by KELLY et al. (2011). It aids interpretation by visualizing the degree of separation between the signal and noise within the charcoal record’s peak component, therefore giving some more evidence about the reliability of fire peak identification. After testing different window widths, SNI calculation input was based on the results of the CharAnalysis fire peak detection, using the same window width (1/5 of record length, i.e. $w = 409.2$ years) and threshold for signal identification ($t = 0.492$). This ensures that the SNI result is fully applicable to the results of the CharAnalysis method (KELLY et al. 2011).

Fire frequency per 100 years was calculated using the number of identified fire events (FE) over the complete time span of the core (Age_{max}):

$$Fire\ frequency = \left(\frac{n(FE)}{Age_{max}} \right) * 100$$

Fire return intervals (FRIs) were determined by calculating the time span between every neighbouring pair of identified fire events, resulting in both the maximum and minimum time span between fire events, as well as a mean FRI for the whole time series.

$$FRI = Age(FE_{n+1}) - Age(FE_n)$$

$$FRI_{mean} = \frac{FRI_1 + FRI_2 + \dots + FRI_n}{n(FRI)}$$

For specific time intervals, localized mean FRIs were calculated by dividing the length of the interval by the number of identified fire events.

Correlations

Correlations were calculated between the different charcoal particle types (size classes, morphotypes) and between charcoal particles and selected pollen types and classes. Morphotype and pollen type concentrations were translated into percentages and then centred log-ratio (CLR) transformed (R package “compositions”, VAN DEN BOOGAART et al. 2020) to account for their compositional nature, with total charcoal concentrations or influxes being log-transformed instead (R package “SparkR”, VENKATARAMAN et al. 2020). Only pollen types accounting for more than 10 % of the total pollen sum were examined. Due to a lack of overlapping information for both pollen counts and morphotypes, respective correlations could only be applied to 18 of the 24 counted pollen samples. Pollen classes were formed for pollen counts of arboreal (AP, including *Abies*, *Alnus*, *Betula*, *Larix*, *Picea*, *Pinus*, *Juniperus*, *Populus* and *Salix*) and non-arboreal types (NAP, including all other pollen types from terrestrial plants, i.e. herbs), the ratio of AP:NAP, evergreen and summergreen trees as well as conifers and broad-leafed trees (the difference between the last two class pairs being the inclusion of *Larix* with summergreen trees or conifers, respectively). Values of zero were instead labelled “NA” and not included in the analysis, since they would otherwise misleadingly be used for correlations by the script and render the result not interpretable. The correlation method chosen was Kendall’s tau. Both Kendall’s tau and Spearman’s rho are used to assess monotonic associations (in contrast to Pearson’s, which only measures the degree of linear association) and provided very similar results for present data. However, Kendall’s tends to produce narrower confidence intervals (PUTH et al. 2015). With present data, Spearman’s tended to produce more significant correlations in pairs with fewer samples. Therefore, Kendall’s was suspected to be more robust and preferred. All p -values for correlations were calculated and significant correlation coefficients ($p < 0.05$) marked in each correlation matrix. Calculation of coefficients and p -values was done in R using the function `corr.test` (package “psych”, REVELLE 2019), while for plotting the function `corrplot` (package “corrplot”, WEI and SIMKO 2017) was used.

Additionally, for every correlation matrix a rough scatterplot matrix of the same variables was produced using a custom R script with a loop of the R base function `plot`. This was done as an extra measure to quickly compare scatterplots and correlation results, in order to more meaningfully estimate the validity of correlation coefficients and not solely rely on resulting p -values (see WASSERSTEIN et al. 2019).

Principal component analysis

Principal component analysis (PCA) was done for the different macroscopic charcoal morphotypes and size classes. Data on morphotypes exists continuously for all samples between 54 - 207 cm and non-continuously in all pollen samples from 207 - 239 cm of core depth (n = 247). All morphotypes except Type Z (“slightly charred”) were included, with the latter not adding to charcoal particle counts. Percentages were calculated from concentrations, before being square root transformed in R using the `sqrt` base function. The PCA was subsequently created using the `prcomp` base function. The result was plotted using the `plot` base function, colouring the different sample points with a continuous colour scheme from the R package “viridis” (GARNIER 2018).

Superposed epoch analysis

A superposed epoch analysis (SEA) was used to look in more detail for associations between identified fire events from the macroscopic charcoal record and specific elements of the XRF data. SEA was applied to the XRF elements chosen according to LEYS et al. (2016), as outlined in 3.6, using the identified fire peaks from the CharAnalysis method in their original form, as well as their “reduced fire” version. SEA works by extracting a fixed time interval from an element’s timeseries before and after every identified fire event (termed “lag” in the resulting graph), and then compiling all those extracted signal intervals and overlapping them, showing what could be summarised as an averaged response of an element’s abundance to identified fire events. Before application of the SEA, the XRF data for individual elements was CLR transformed, or additive log ratio (ALR) transformed in case ratios of elements were used (R package “compositions”, VAN DEN BOOGAART et al. 2020), again to account for their compositional nature. For each transformed element or element ratio, overarching trends were removed by subtracting a LOWESS (window width of 1/5 of total record length) from the timeseries, similar to the way a peak component was created for the charcoal record and according to methods from the literature (LEYS et al. 2016, DUNETTE et al. 2014). This is done in order to keep longer-term trends in an XRF signal from influencing or even overshadowing the SEA result, which is focused rather on short-term individual event response. SEA was performed in R using a slightly modified custom script obtained from publicly accessible resources of the University of Oregon (GAVIN 2018).

4. Results

In the following segment, the results of all applied methods will be presented. Comments and reasoning will be included if they are deemed to be important for the correct understanding of the result and will not take away from the subsequent discussion and interpretation segment.

4.1. Chronology

Radiocarbon dates of the bulk sediment samples (see *table 1*) and the collected macrofossils (see *table 3*) were received from AWI's MICADAS lab in early 2019. Note that all decisions in handling the age-depth model as laid out in this section will be explained and evaluated in more detail in the discussion part of this thesis (see 5.1). The reasoning presented there will be important to judge this thesis' approach regarding the creation of the age-depth model most likely to represent the actual sedimentation processes of Lake Khamra.

Table 1: Radiocarbon age dating results of bulk sediment samples (AWI MICADAS)

Sample ID	Depth top [cm]	Depth bottom [cm]	Age [¹⁴ C yrs BP]	±
EN18232-3_1cm	0	1	1,415	27
EN18232-3_37-35cm	35	37	1,738	28
EN18232-3_79-77cm	77	79	2,542	33
EN18232-3_119-117cm	117	119	2,679	28
EN18232-3_159-157cm	157	159	3,130	32
EN18232-3_199-197cm	197	199	3,564	32
EN18232-3_237-239cm	237	239	3,551	28

When looking at the age results, particularly the topmost sample stands out showing an age of 1415 ± 27 ¹⁴C years BP, with the lowest sample of the core at 3551 ± 28 ¹⁴C years BP. Also, two neighboring sample pairs received similar ages, although their difference in depth is 40 cm (EN18232-3_79-77cm and EN18232-3_119-117cm, as well as the two deepest samples).

Since these radiocarbon results were obtained using bulk sediment samples and Lake Khamra is located in a zone of discontinuous, sporadic permafrost – basically well-preserved, old carbon (e.g. from frozen soil rich in organic material) – any input of previously frozen material to the lake is likely to also deposit carbon older than that of its recent surroundings. The Pb/Cs age dating method was therefore an important addition to judge the validity of and possible influences on the radiocarbon dates, as

recommended by WHITLOCK and LARSEN (2001). As mentioned before (see 3.2), ages documented by Pb/Cs dating were not obtained directly from the main sediment core of this thesis (EN18232-3), but from the parallel short core EN18232-4. However, the reason for obtaining that short core was to apply the resulting ages to the main core. Since parallel core drilling took place accordingly, it is assumed that these age dating results do apply to the main core as well (see *table 2*).

Table 2: Pb/Cs dating results of parallel short core EN18232-4

Depth [cm]	Year [CE]	Age [yrs]	±
0	2018	0	0
0.75	2014	4	0
1.75	2008	10	1
2.75	2002	16	1
3.75	1996	22	2
4.75	1989	29	2
5.75	1983	35	3
6.75	1976	42	4
7.75	1970	48	4
8.75	1963	55	5
9.75	1956	62	5
10.75	1949	69	5
11.75	1942	76	5
12.75	1934	84	6
13.75	1927	91	7
14.75	1919	99	8
16.5	1905	113	10
18.5	1889	129	13
20.5	1872	146	16
22.5	1855	163	19

Since the Pb/Cs dating method is not affected by the presence of old carbon, their younger and more expected ages – especially considering their recent surface age – present further evidence for the presence of old carbon in the lake influencing radiocarbon ages. This is likely to lead at least the topmost radiocarbon bulk sediment sample to show an older age than what is accounted for by the sedimentation rate of the lake.

Of the 15 plant macrofossil samples originally sent to MICADAS for radiocarbon dating, only 9 were big enough in size to be applicable by the method. The radiocarbon dates of the macrofossils do not match the results from bulk sediment or Pb/Cs dating for the most part and do not all date back in chronological order with increasing depth. Confronted with these results and considering (1) the unclear origin of many of the macrofossil samples and (2) the indicated presence of old carbon input to the lake, they were deemed too unreliable and thus not used for computing the age-depth model. However, their age dating results will also be featured in the discussion (see 5.1).

Table 3: Radiocarbon age dating results of macrofossil samples (AWI MICADAS)

Sample ID	Depth top [cm]	Depth bottom [cm]	Age [¹⁴ C yrs BP]	±
EN18232-3_20-21cm	20	21	958	108
EN18232-3_22-21cm	21	22	9,902	97
EN18232-3_25-26cm	25	26	2,132	75
EN18232-3_31-29cm	29	31	785	72
EN18232-3_31-30cm	30	31	435	76
EN18232-3_50-49cm	49	50	2,080	80
EN18232-3_51-49cm	49	51	2,079	102
EN18232-3_85.5cm	85.5		1,244	29
EN18232-3_99-97cm	97	99	1,997	76

Because the best explanation for the radiocarbon age offset in this specific case is an input of old carbon from the lake’s surroundings – an age offset that is backed up by the results of the Pb/Cs ages showing a recent age in surface samples – the topmost radiocarbon date was adjusted by subtracting its ¹⁴C age with an added 68 years (since BP refers to 1950 CE), effectively setting its age to the year of core extraction (2018 CE). However, under the assumption of a constant magnitude of old carbon input to the lake throughout time, the age offset of the topmost radiocarbon sample was subtracted from all other radiocarbon samples as well. This crucial step was justified in part by the homogenous appearance of the sediment core, which does not show any traces of the otherwise sudden changes in sedimentation rate resulting from using unadjusted radiocarbon ages (see the exemplary age-depth model in *figure 5A*), and by the lacking likelihood of old carbon being only recently incorporated into the lake’s sediment, but never before that. As mentioned before, an in-depth discussion of this adjustment of radiocarbon ages can be found in 5.1.

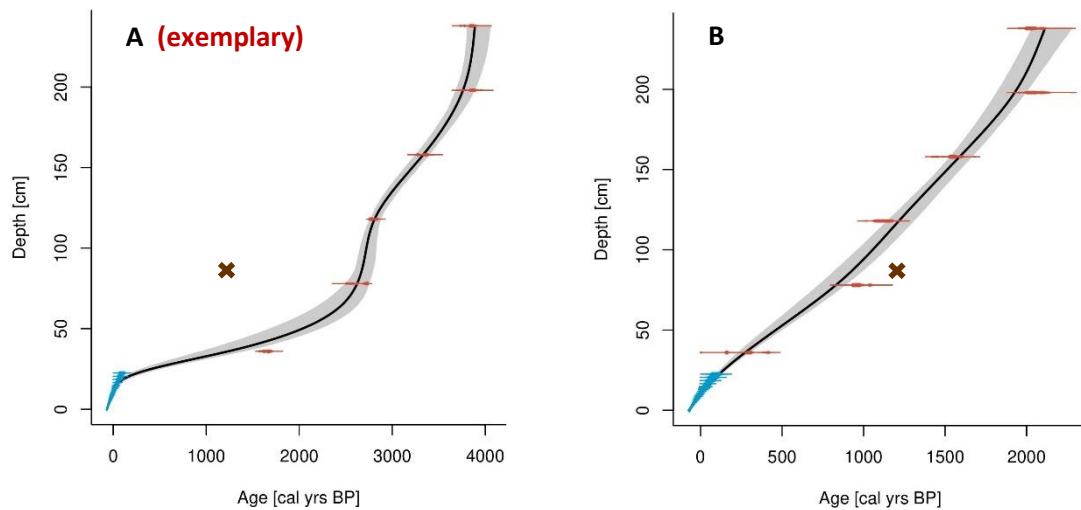


Figure 5: **A:** Exemplary age-depth model adjusting only the topmost ^{14}C age, c. 90 % of all 5000 iterations were removed due to age-reversals. **B:** Final age-depth model adjusting all ^{14}C ages. Blue: Pb/Cs, red: bulk ^{14}C , brown: wood macrofossil Computed with CLAM ver. 2.3.2 (BLAAUW 2010)

The final age-depth-model (see *figure 5B*) was calculated in R using CLAM (version 2.3.2, BLAAUW 2010). Calibration of ^{14}C ages was achieved using the IntCal13 calibration curve (REIMER et al. 2013). According to recommendations for homogenous sediment types (WHITLOCK and LARSEN 2001), a smooth spline with a high smoothing factor of 0.85 was used while including 95 % of calibrated ranges. From 5000 iterations, two models with age-reversals were removed. As described before, radiocarbon ages entered into the model were first adjusted for an assumed constant old carbon influence to the magnitude of the topmost sample (1415 ^{14}C years) and macrofossil ages were not used for the generation of the final age-depth-model (wood macrofossil in *figure 5* shown only for reference).

The resulting age-depth model of Lake Khamra's core EN18232-3 shows a very uniform sedimentation rate, which is mirrored by the homogenous sediment appearance of the core and the general grain size distribution that only slightly varies between the relatively uniform large silk and smaller clay and sand fractions. The Pb/Cs ages fit exceptionally well with the adjusted ^{14}C ages. The maximum age at 239 cm depth lies between 2039 and 2276 calibrated years BP, corresponding to a mean maximum age of 2114 calibrated years BP. Mean sediment accumulation rate is c. 12.4 years per cm, which translates to a rather high temporal resolution when taking into account the core subsampling scheme consisting of 3 samples per 2 cm increment. On average, one of the continuous samples contains sediment that accumulated within c. 7 years, meaning that this macroscopic charcoal record's resolution is higher than that of most which have been used for fire reconstruction in Siberia until now (see 5.2).

4.2. Charcoal-based fire history

In the following segment, the reconstructed fire history at Lake Khamra is presented, spanning the last c. 2000 years. The main focus lies on the macroscopic charcoal record and the approximation of key fire regime parameters like FRIs. Included are results from correlations between the different charcoal morphotypes and size classes, the SNI, the PCA and the lower-resolution microscopic charcoal record.

Macroscopic charcoal record

First, the absolute charcoal particle counts per volume are presented (charcoal concentration), sorted in a stacked barplot for their size classes (see *figure 6*). Not only could charcoal particles be identified within the sediment of Lake Khamra, but rather almost no samples without any charcoal in them were present. Throughout the last c. 2100 years covered by the core's depth, charcoal was produced and deposited in the lake sediment, with the exception of few short intervals.

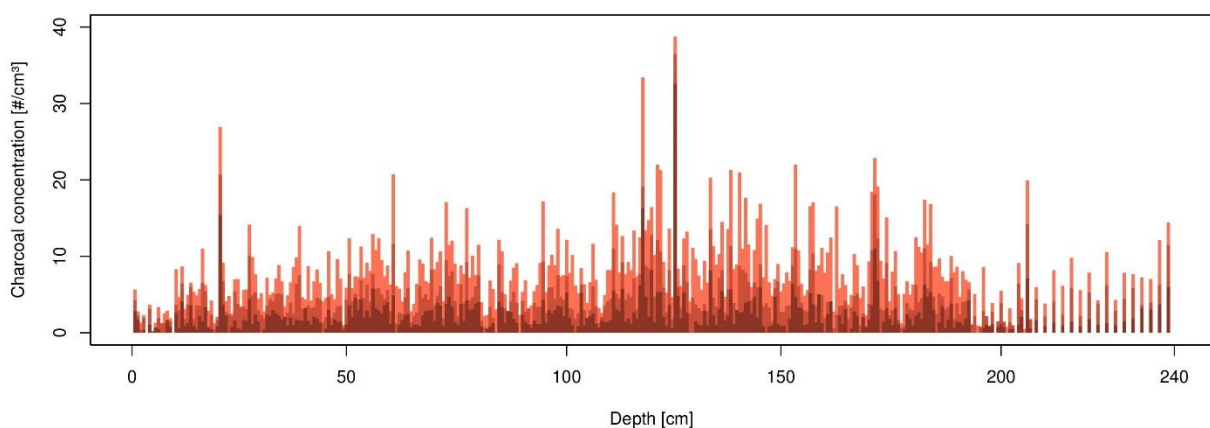


Figure 6: Macroscopic charcoal concentration in of counted samples from Lake Khamra's sediment core EN18232-3. Colour scheme from dark to light red indicates larger to smaller particles, respectively

The prepared and counted samples ($n = 322$) contained a total of 4154 identified macroscopic charcoal particles. Of those, 1802 (43.4 %) belong to the smallest size class $> 150 \mu\text{m}$, 1208 (29.1 %) to the mid-size class $300\text{-}500 \mu\text{m}$ and 1144 (27.5 %) to the large size class $> 500 \mu\text{m}$. On average, one sample contained c. 12 macroscopic charcoal particles, with a highest and lowest individual amount of 56 and zero, respectively. From c. 207 - 239 cm depth, missing values originate from samples that could not be prepared and counted due to an unfortunate shortage of *Lycopodium* spore tablets in early 2020, so these values do not resemble a true charcoal concentration of zero. However, since macroscopic charcoal records should be continuous, the samples deeper than 207 cm are only shown here for additional insight and were not used in most of the following statistical analysis, so they will not be part of any of the other results except for the correlations. This leaves 306 continuous macroscopic charcoal

samples between c. 2018 CE and c. 11 ± 87 BCE. In order to account for some uncertainty from the age-depth model, the range of modelled ages will be added whenever an individual year is referenced instead of a general time period.

The topmost c. 9 cm of the core show smaller amounts of charcoal particles than what is usually found along the rest of the core. Some of the peaks stand out quite conspicuously from the neighboring values (e.g. c. 20 cm, 60 cm, 117 cm, 125 cm). The highest peak at 125 cm depth, with a charcoal concentration of c. 39 particles per cm^3 , is dominated by the biggest size class $> 500 \mu\text{m}$. Together with the peak at c. 20 cm depths, it is also a unique peak within the record, as these consist of predominantly larger, elongated charcoal particles (Type F, more on this will follow). The same record expressed as charcoal accumulation rate (CHAR, see *figure 7*) has a very similar shape and does not change a lot from the distribution of concentrations, due to the quite uniform sedimentation rate within the core derived from the age-depth model.

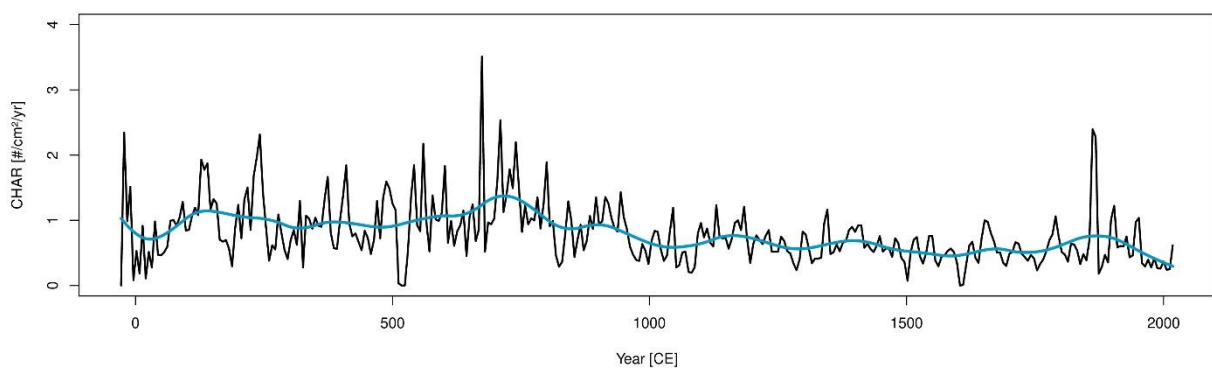


Figure 7: Charcoal accumulation rate (CHAR) of the continuous sequence of counted samples. Blue: Mean CHAR (LOWESS with window width $1/10$ of record length)

Description of CHAR is therefore similar to that of the raw counts. The line graph provides a different look at the data, highlighting other aspects like the increased variance in the older part of the core when compared to the generally lower amplitudes of charcoal peaks in the younger part. LOWESS smoothing makes the general trend of charcoal influx into the lake visible, showing a maximum coinciding with the record's highest individual peaks and a declining trend from around 750 CE towards present time. In general, a higher CHAR resembles higher fire activity, i.e. more burnt biomass in the vicinity of the lake (e.g. CONEDERA et al. 2009, WHITLOCK and LARSEN 2001, MACDONALD 1991). Accordingly, the mean CHAR indicates that generally, a higher fire activity was recorded at Lake Khamra during the first millennium than in the second millennium of the Common Era. After reaching a peak around 750 CE, fire activity decreased up until around 1500 CE. From there, low fire activity lasted until the 18th century. The last decades show rather low CHAR for the most part after gradually decreasing from c. 1900 CE onwards.

The following *figure (8)* represents the reconstruction of fire events using the CharAnalysis method in R (DIETZE et al. 2019). It shows the charcoal accumulation rate (CHAR) of the charcoal particle sum, which is interpolated in equal time intervals, with a LOWESS smoothing at 1/5 of total record length. Triangles with vertical red lines mark fire events as identified by the CharAnalysis script (positive peaks of CHAR exceeding the 99th percentile of the peak component's noise distribution), incorporating the results of SNI calculation (light red: SNI > 3; dark red: SNI < 3).

This provides the foundation to examine not only gradual changes in CHAR, but also identify unique fire events that could be made up by one or more fires within the sampling resolution's time interval. The same graphs created for the different size classes, respectively, show how resulting fire event identification varies depending on the size of charcoal particles analysed (see appendix B). A summary of the main results can be found in *table 4*. The "reduced fire version", limiting the number of fire events identified per peak distribution to one, can be seen in *figure 8B*, whereas *figure 8A* represents the non-adjusted number of identified fire events ("original fire version").

A total of 30 fire events during the last c. 2000 years were identified in the original version, corresponding to a mean fire return interval (FRI_{mean}) of 68.1 years. Between the 14th and 19th century, no fire event was recorded, resulting in the longest FRI of 516 years. With the reduced fire version, 25 fire events were identified, corresponding to $FRI_{mean} = 82.3$ years. It is suggested that the original fire version, which might rather overestimate the number of fire events, constitutes an upper estimate of fires, whereas the reduced fire version, likely tending towards underestimating the total number, constitutes a lower estimate. This results in the mean FRI over the last c. 2100 years being expressed as the range of 68.1 - 82.3 years, incorporating the uncertainty from the two different approaches regarding fire event identification. Mean fire frequency during the last c. 2000 years was about 1.5 fire events per 100 years.

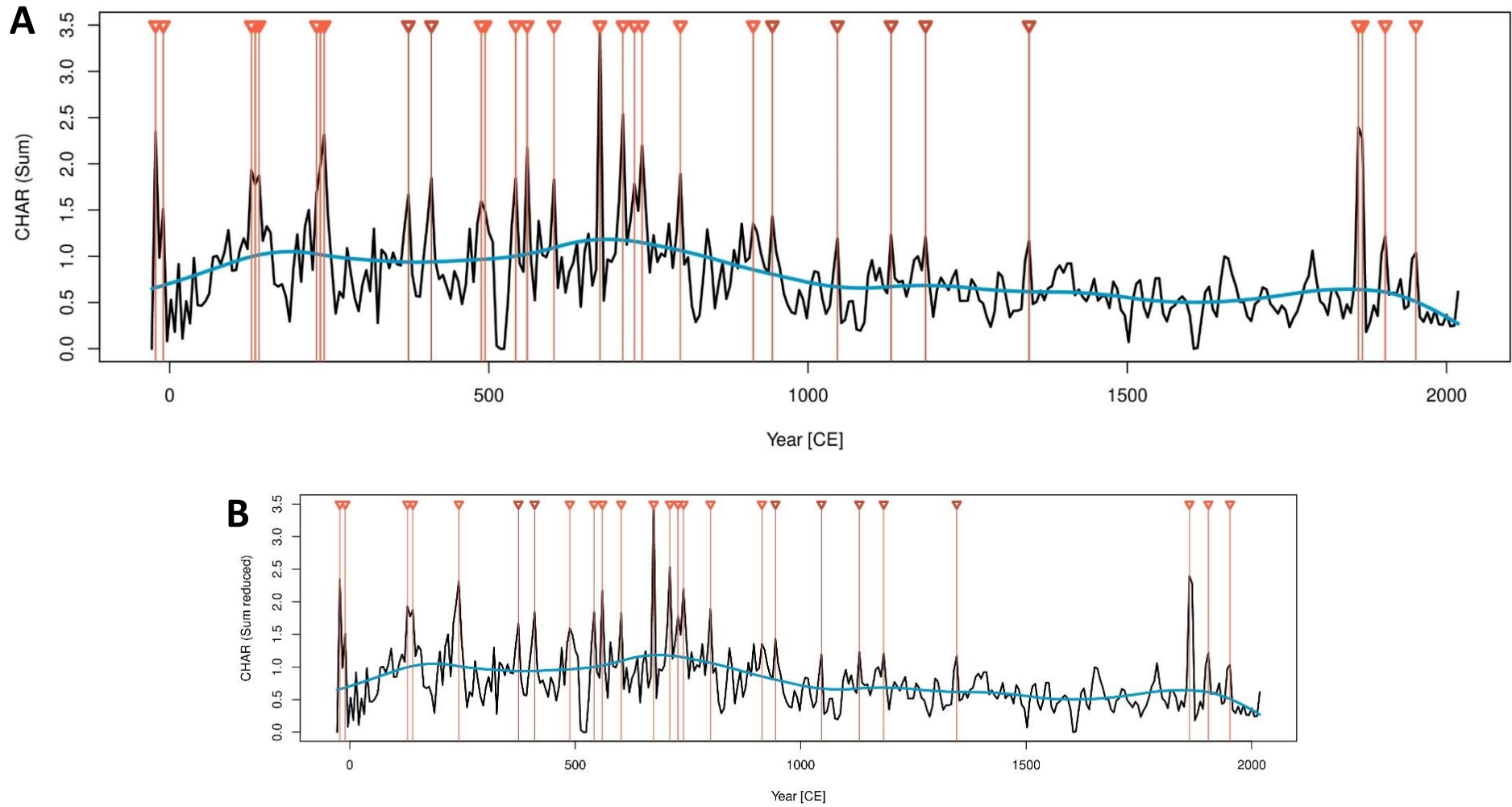


Figure 8: CHAR (black) with LOWESS smoothing (blue) and identified fire events (light red: $SNI > 3$, dark red: $SNI < 3$).

A: All fire events ("original version"), **B:** "reduced fire version"

Two recent fires at Lake Khamra detected with satellite observations recorded by NASA’s MODIS-equipped Terra and Aqua satellites lie only 8 years apart, adding additional evidence for involving the original, non-reduced fire version in the FRI range (more on the remotely sensed fires will follow). Moving from a global FRI_{mean} to a localized one within certain window widths, further differences in reconstructed fire activity can be highlighted (here using the reduced fire version). Around the maximum of CHAR, between c. 650 - 850 CE, 7 fire events were identified. This corresponds to a local $FRI_{\text{mean}} = 42.9$ years. In recent centuries from c. 1700 - 2000 CE, only 3 fire events were identified, leading to a higher local $FRI_{\text{mean}} = 100$ years (incorporating the recent remotely sensed fires, this decreases to 75 years). From the earlier to the recent period examined, FRI_{mean} might therefore have doubled, showing a marked decrease in fire frequency. However, despite generally low levels of CHAR, fire frequency during the last c. 200 years was the highest of the preceding 1000 years. The most recent fire events identified are in the years of 1952 ± 3 , 1904 ± 7 and 1862 ± 11 CE, with 1862 ± 11 CE being among the highest peaks in CHAR within the last c. 2000 years. Previously mentioned remote sensing data reveals two recent wildfires in very close proximity to Lake Khamra (see appendix A), which are likely to leave some trace in terms of heightened charcoal accumulation. They took place in 2014 and 2006 CE – not coinciding with any of the reconstructed events. Reasons for this will be discussed in 5.2.

Looking into results of CharAnalysis being applied to the individual size classes (see appendix B), most fire events were identified for the smallest class ($> 150 \mu\text{m}$, $n = 70$), followed by the medium size class ($300 - 500 \mu\text{m}$, $n = 56$). The largest size class revealed significantly less fire events ($> 500 \mu\text{m}$, $n = 14$). As a consequence of the decreasing amount of identified fire events per increasing size class, FRIs mirror this with their different mean lengths. The shortest FRI is 6 years for every class, including the sum of all particles. This is due to 6 years being the interpolated median resolution of this record after calculation of CHAR using CharAnalysis. In the reduced fire version, no “directly neighboring” fire events exist, increasing FRI_{min} to 12 years. For histograms and boxplots of the FRIs for the original and reduced version of reconstructed fire events, see appendix C.

Table 4: Fire return interval (FRI) length for the macroscopic charcoal record

Particle class	Fire events (#)	FRI_{mean} (yrs)	FRI_{max} (yrs)	FRI_{min} (yrs)
> 150 μm	70	28.6	174	6
300-500 μm	56	35.8	162	6
> 500 μm	14	145.4	966	6
Sum (original)	30	68.1	516	6
Sum (reduced)	25	82.3	516	12

The mean SNI of this charcoal record ($SNI_{\text{mean}} = 3.4$) lies above the cut-off value of $SNI = 3$. According to the authors, a value of $SNI > 3$ is the result of the signal component being relatively distinct to the noise component (i.e. signal values are on average more than three standard deviations above the

mean of the noise component) (KELLY et al. 2011). Therefore, this result indicates very generally how there is a distinct difference between signal and noise for some parts of the record. Of course, due to the variability of CHAR within the record, the SNI is subject to change as well (see *figure 9*), so SNI_{mean} itself is not meaningful enough to evaluate reliability of identified fire events.

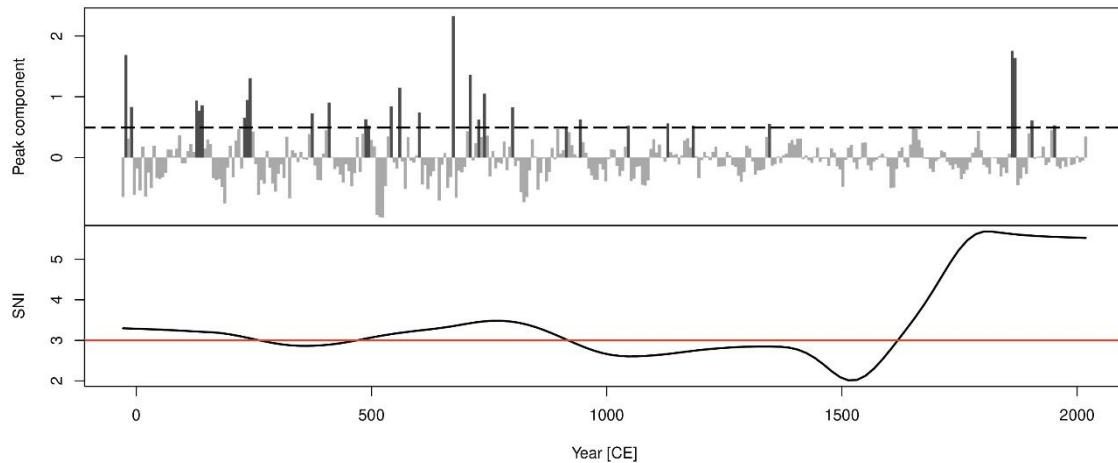


Figure 9: Signal-to-noise index (SNI) with cut-off value of $SNI = 3$ (red line) and the charcoal record's peak component with threshold of 0.492 (black dashed line). Light grey bars are identified as noise, dark grey bars as signal

55.8 % of the macroscopic charcoal record lie above $SNI = 3$, the other 44.2 % lie below, reaching a minimum $SNI_{\text{min}} = 2$ around 1500 CE. The maximum on the other hand reaches $SNI_{\text{max}} = 5.7$. With the exception of the most recent centuries and the pronounced dip around SNI_{min} , index values fluctuate somewhat closely around the cut-off value. Intervals with $SNI > 3$ are located around c. 200 CE, 750 CE, and from c. 1600 CE onwards, integrating 18 of 25 identified fire events for the reduced version. It should be noted that with different window widths in both CharAnalysis and SNI calculation, the percentage of the charcoal record with $SNI > 3$ is subject to change. However, since the CharAnalysis threshold also relies on the choice of window width, they also influence the number of resulting identified fire events. This number varies between 27 (for $w = 204.6$ years) and 36 (for $w = 306.9$ years), while producing lower overall SNIs. For this reason, it was decided to not just use the window width that results in most identified fire events, but rather use one that indicates a preferably large share of $SNI > 3$ (see BARHOUMI et al. 2019), which was found to be at the present window width of 1/5 of record length (i.e. $w = 409.2$ years).

Looking into the different size classes of macroscopic charcoal particle concentrations (*figure 10*, referencing marked grey intervals), it is evident that they have varying degrees of contributing to the total charcoal concentration. Some peaks and intervals are represented best by a specific size class, but not so much by the others. Starting from modern times going backwards, the first major peak of the charcoal sum at $c. 1862 \pm 11$ CE consists mainly of $> 500 \mu\text{m}$ particles and only to less degree those from

the smaller size classes. The charcoal sum peak at $c. 1346 \pm 65$ CE on the other hand mainly consists of the smaller size classes. The distinct peaks of only the $> 150 \mu\text{m}$ class at around 750 CE are overshadowed in the charcoal sum by the highest peak of the record: At $c. 674 \pm 77$ CE the largest size class peaks with a sample of 56 charcoal particles, most of them $> 500 \mu\text{m}$ and of an elongated shape (Type F), as previously described. From here the smallest size class remains on a higher level with higher variance than the other size classes, with some peaks consisting almost completely of $> 150 \mu\text{m}$ particles. In general, the 300 - 500 μm size class shows a lower amplitude than the other two.

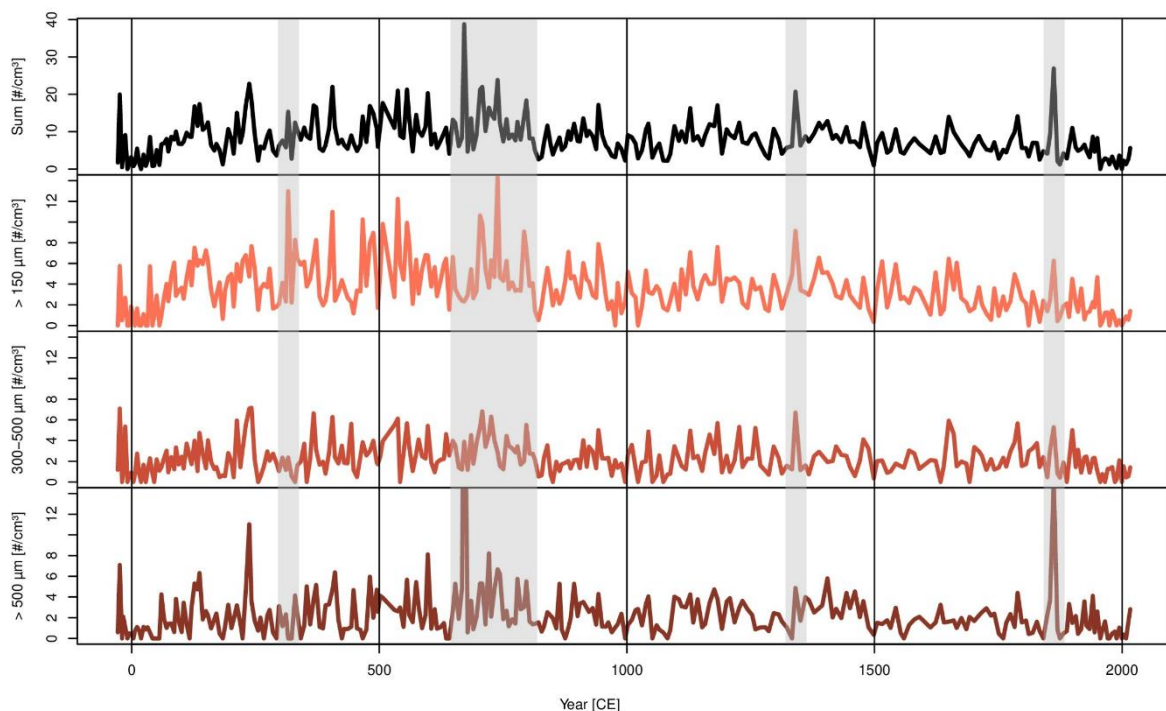


Figure 10: Comparison of contributions of the macroscopic charcoal size classes' concentration to the sum of all particles. Grey bars indicate intervals described in the text

The samples with morphotype identification ($n = 247$) include a total of 3311 categorized charcoal particles and 1950 slightly charred particles (Type Z). Excluding Type Z, these are the different morphotypes in order of total abundance among all those samples: Type F: 1098 (33.2 %), Type M: 970 (29.3 %), Type S: 609 (18.4 %), Type B: 230 (7 %), Type X: 114 (3.4 %), Type C: 102 (3.1 %), Type D: 78 (2.4 %), Type E: 70 (2.1 %) and Type P: 40 (1.2 %). Almost two thirds of all counts are from Types F and M. Types D, E and P received less than 3 % of all counts, respectively. Morphotype distribution was strikingly distinct in the two charcoal samples with the highest number of particles. Although one of the largest and most recent peaks in charcoal concentration at $c. 20$ cm depth, corresponding to the fire event identified in 1862 ± 11 CE, was not classified regarding morphotypes, an unusually high amount of thin, elongated particles was noted during the counting process (equivalent to Type F). The highest peak of charcoal concentration in $c. 123$ cm depth (corresponding to a fire event identified in

674 ± 77 CE, during the phase of heightened fire activity) consists of 50 charcoal particle counts. 80 % of those were classified as Type F, with many also belonging to the largest size class > 500 µm. Such overwhelming shares of just one morphotype were not witnessed in any other samples of higher particle counts. Between c. 105 - 115 cm depth (c. 750 - 850 CE) samples showed notably high amounts of partially charred particles (Type Z) of the largest size class.

A correlation matrix showing the different charcoal morphotypes and size classes can be seen in *figure 11*. Type F is negatively correlated to most other morphotypes and to the smallest size class, but positively to the large size class and the sum of particles. Type M has a similar result, however, it seems to contrast Type F by being stronger associated with smaller than larger particle sizes. The rarer morphotypes X, C, D, E and P, are mostly positively correlated to each other. Varying shares of the three size classes are anticorrelated. When using log-transformed influxes, correlations of morphotypes to size classes and the sum of particles are overwhelmingly positive and significant at $p < 0.05$, which is expected as all of them add to the total amount of particles found in each sample (see appendix D).

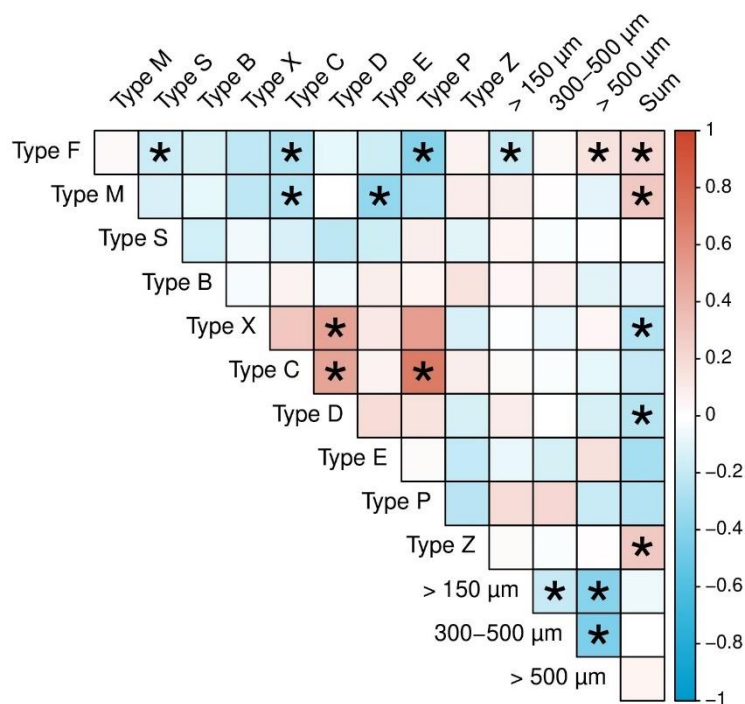


Figure 11: Correlations between macroscopic charcoal morphotypes and size classes (based on 247 samples). Values with $p < 0.05$ are marked with a star

Principle component analysis (PCA) for the charcoal morphotypes and size classes does not seem to be an ideal type of analysis for present data. The variation explained by the different principal components (PCs) decreases rather gradually from the first towards the last PC. This does not permit the explanation of the majority of variation in the dataset by keeping only PC1 and PC2 or potentially even adding PC3. The resulting PCA plot (see *figure 12*) using the two PCs with highest eigenvalues (PC 1 = 13.5 %, PC 2 = 13.2 %) therefore only accounts for < 30 % of variation in the data. However, within the

variables (vectors) of the plot some characteristics of the morphotype/size class distributions are well visualized. The first axis highlights opposing variation between Type F and large particles on the one hand and Type M and small particles on the other. The second axis on the other hand highlights opposing variation in Types X, C, D, E and P, which are more closely correlated to one another as indicated by a narrow angle between vectors, and Types S and B, which have a generally smaller influence on PC2. The PCA variables expectedly mirror the results of the corresponding correlation matrix. The colour scheme of individual samples refers to their depth (blue = top, yellow = bottom). There is no unique clustering of different depths, suggesting a high similarity in many samples and therefore indicating no apparent deposition patterns of morphotypes with increasing depth. Despite this, samples from the top of the analysed core part cluster less densely than others and coincide with trajectories of variables Type E, C and P.

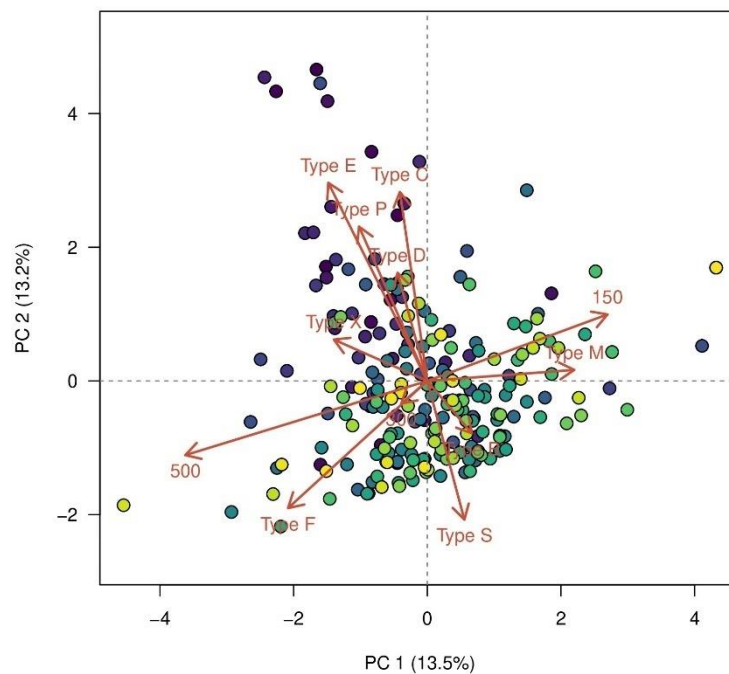


Figure 12: Principal component analysis (PCA) of charcoal morphotypes and size classes (vectors). Samples (points) are coloured depending on depth (blue = core top, yellow = core bottom)

Microscopic charcoal record

From 24 samples spread across the entire length of the core, a total of 6478 microscopic charcoal particles was identified with an average of 270 per individual sample. Together with counts of *Lycopodium* marker grains, this resulted in count sums between 300 - 400 particles as stated in the methods segment (see 3.4). After conversion, mean microscopic charcoal concentration was 53.823 per cm³ with individual highest and lowest values of 95.390 and 32.768 particles per cm³, respectively. The distribution of MIC in counted samples does not correspond very well with the MAC record (see figure 14). It mainly shows two distinct intervals of higher concentrations, first between c. 200 - 700 CE and

from c. 800 - 1300 CE, although none of them directly overlaps with the highest interval of mean macroscopic CHAR at c. 750 CE. MIC concentrations even show a minimum around that time.

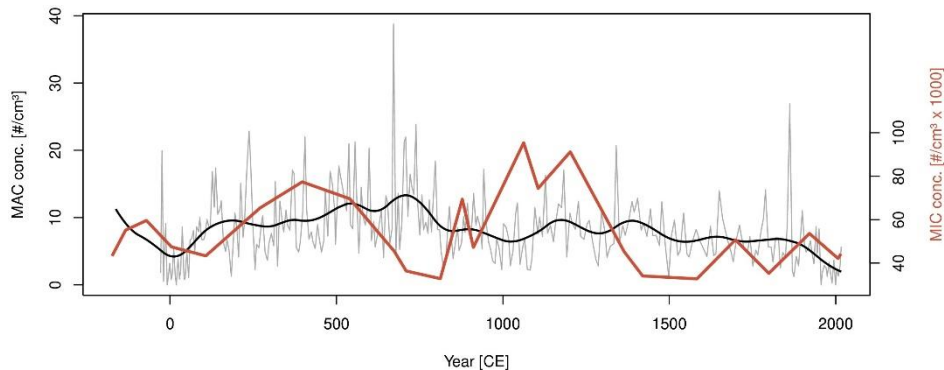


Figure 13: Comparison of macroscopic (grey, black) with microscopic (red) charcoal concentration

Almost all samples contained all different morphotypes, with two exceptions: (1) Type D was only found in few samples and (2) one sample did not contain any particles of Type F. In order of abundance, individual morphotype counts across all samples revealed following values: Type P: 2929 (45.5 %), Type M: 1520 (23.5 %), Type C: 974 (15%), Type B: 547 (8.4 %), Type S: 297 (4.6 %), Type F: 179 (2,8 %) and Type D: 12 (0.2 %). More than two thirds of all counts are made up of Types P and M, whereas F and D contribute only c. 3 %.

Charcoal reflectance test

For the charcoal reflectance test measurements, resulting estimated charring temperatures during charcoal formation can be seen in *table 5* (results provided by Dr. Alicja Bonk).

Table 5: Reconstructed charring temperature from charcoal reflectance measurements

Sample ID	Mean depth [cm]	Charring temperature [°C]
KCh 14-13 Char	13.5 cm	600.0
KCh 21-19 Char	20 cm	480.0
KCh 25-23 Char	24 cm	705.0
KCh 34-33 Char	33.5 cm	490.0
KCh 39-37 Char	38 cm	500.0

The reconstructed charring temperature for these samples ranges between 480 - 705 °C, showing that the calculation of such temperatures is generally possible even for smaller particles as found in Lake

Khamra. Mean charring temperature of the five successfully analyzed samples is 555 °C. These temperatures are discussed in 5.2.

4.3. Reconstructed vegetation

Counted pollen and non-pollen palynomorph types with an abundance of at least 10 % are shown in *figure 14* (a graph featuring all counts can be found in appendix E). As revealed by the results of palynomorph identification by Dr. Andrei Andreev, there is little variation in the pollen spectrum. However, that is according to expectations, as other studies from Yakutia also did not show notable shifts in larger-scale vegetation composition during these most recent millenniums (e.g. NAZAROVA et al. 2013, KATAMURA et al. 2009b)

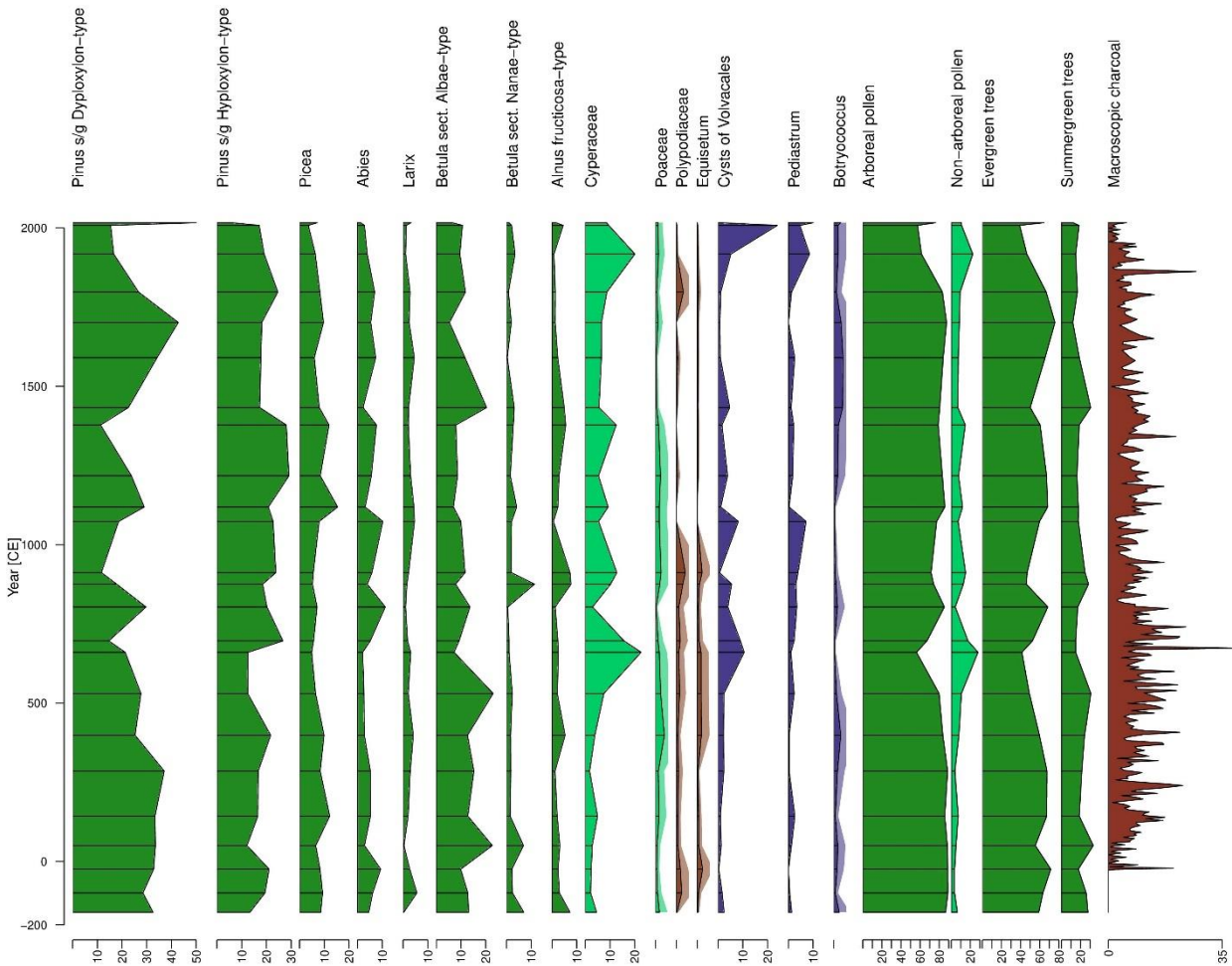


Figure 14: Pollen and non-pollen palynomorph record. Pollen types and classes are based on percentages of concentrations, macroscopic charcoal is shown as concentration [$\#/cm^3$]

The pollen diagram shows a rather uniform distribution of total pollen and spore abundances throughout the last c. 2200 years. Most pollen counts derive from arboreal pollen and within this class mainly

from *Pinus*, followed by *Betula*, *Picea*, *Abies* and *Larix*. Some few counts were made for *Alnus*, *Salix*, *Juniperus* and *Populus*. *Pinus* s/g *Dyploxylon*-type and *Pinus* s/g *Haploxylon*-type show somewhat opposing abundances – in samples with high counts of one type, the other often shows a lower amount. In the herbs class, only Cyperaceae have more abundant counts when compared to most other types. Poaceae are also found in most samples. *Artemisia* and Ericales are the only other herb vegetation types found on multiple occasions throughout the core. Most prevalent fungi include Polypodiaceae, *Equisetum* and *Sphagnum*. Non-pollen palynomorphs belonging to green algae were present in most samples and included cysts of Volvocales, with some counts of *Pediastrum* and *Botryococcus*. Additionally, few Tardigrada eggs and Chironomid remains were found. Comparisons with macroscopic CHAR as a proxy for fire activity are limited by the low temporal resolution of the reconstructed vegetation history. However, a shift towards more herb and less arboreal pollen coincides with peak fire activity around c. 750 CE. The increasing share of herb pollen around this time is mainly reflected by Cyperaceae. A second instance of increasing herb and decreasing arboreal pollen happened after the latest peak in charcoal influx at c. 1862 ± 11 CE.

Correlating the most abundant pollen types with charcoal morphotypes yields only few statistically significant results of $p < 0.05$ (see *figure 15*), however, from a look into the scatterplots of these correlations, it should be noted that none of them look very obviously correlated. For this reason, none of the correlations should be treated as if they were certainly indicating some association between the pairs. Instead, they might rather only show hints that could be tested in future studies in more detail. Further interpretation of the correlation results is especially focussed on more prevalent morphotypes (e.g. Types F, M, S, B), since some of the highest correlation coefficients were achieved for pollen types and/or morphotypes with low abundance. This somewhat misleading effect was especially pronounced with Type P, which was excluded from correlations since it only includes two samples with counts out of the 18 used for correlation here (this mirrors results by ENACHE and CUMMING 2007). Significant correlations include Types M and C with cysts of Volvocales, Type X with *Pediastrum* and Type C with *Equisetum*. Aside from the significant correlations, some of the results show weaker, but differing contrary distributions of morphotypes to pollen types. These are indicated by red outlines in the correlation matrix. For example, there is a slightly negative correlation of Types F and M (elongated and irregular shape, respectively) to Cyperaceae, whereas S and B (which appear more angular/geometric) correlate weakly positive. Regarding arboreal pollen, Types F and M correlate slightly positive with *Abies*, but negatively with *Larix*. Type S on the other hand is negatively correlated to all of the arboreal pollen types except for *Alnus* and rather shows aforementioned weak positive correlation with Cyperaceae. Pollen types from conifers generally have positive correlations with small to medium charcoal sizes, whereas those from broad-leaved trees seem to cluster more around medium to large

charcoal sizes. Keeping in mind the generally low correlation coefficients, the validity of these results will be discussed in 5.3.

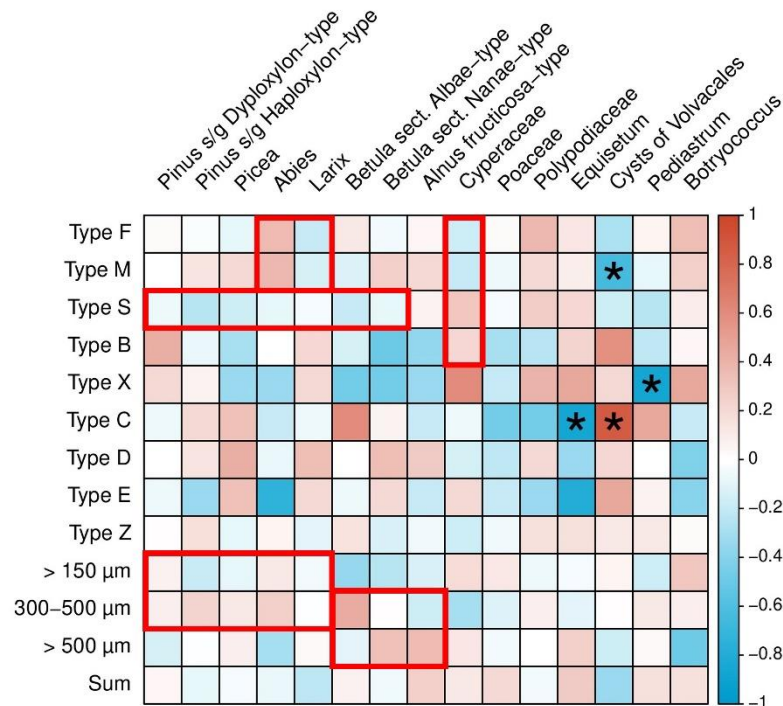


Figure 15: Correlations of macroscopic charcoal classes and pollen types (based on 18 samples). Values with $p < 0.05$ are marked with a star. Red outlines show patterns described in the text

In order to see the correlation of charcoal morphotypes to more general classifications of the reconstructed vegetation, they were correlated with grouped pollen types (see figure 16). Results show no statistically significant result. Again, a look into the scatterplots was used to aid classification of these correlations. Despite not being significant at the level of $p < 0.05$, the distribution of correlations might hint at a very basic level of associations through contrasting patterns. These are again indicated by the red outlines in the correlation matrix. Types F, M, D and Z have similar patterns, being weakly positively correlated to arboreal pollen (AP) and all classes among those, but negatively to non-arboreal pollen (NAP). Contrary to that, Types S, B and X have positive correlations with NAP, but negative correlations with AP. Types S, X and E have a contrasting pattern to those of F, M, D and Z mentioned above. Type B is weakly negatively correlated to AP, but this seems to primarily be the influence of summergreen and not evergreen tree pollen types. Type C contrasts Type B in that it is positively correlated to summergreen tree pollen types. This pattern doesn't change with the inclusion of *Larix* in either the summergreen or the conifer class. In the matrix with pollen types, Type C has the highest coefficient among AP with *Betula* sect *Albae*-type and Type B with *Pinus* s/g *Dyploxylon*-type, mirroring the pattern observed in the matrix with pollen classes.

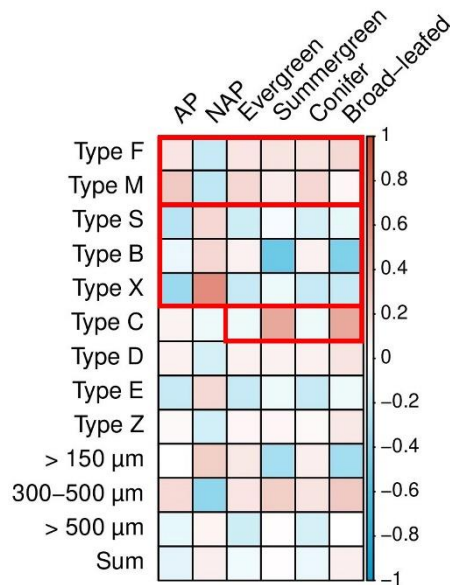


Figure 16: Correlations of macroscopic charcoal classes and grouped pollen types (based on 18 samples). Red outlines show patterns described in the text

Further increasing the generalization of specific morphotypes or vegetation types, the grouped pollen types were also correlated to morphotype classes (see figure 17). These classes based on comparable appearances between charcoal particles do incorporate some of the slight contrasting patterns mentioned above (e.g. Type B and C both in the “angular” class), which likely leads to smaller correlation coefficients and adds to the reason for why there are no significant pairs. However, even within the weak correlations there is a pronounced pattern that differentiates between irregular (Types M, P, X) and angular or geometric appearance (Types S, B, C). Irregular morphotypes, which are often found to be planar with a grid-like structure, show weak positive associations with all arboreal pollen types. In contrast, angular or geometric morphotypes, which often have a somewhat rectangular silhouette and can be both flat and of a brick-like structure, show the exact opposite, with the only weak positive correlation coefficient appearing for NAP (i.e. herbs, grasses).

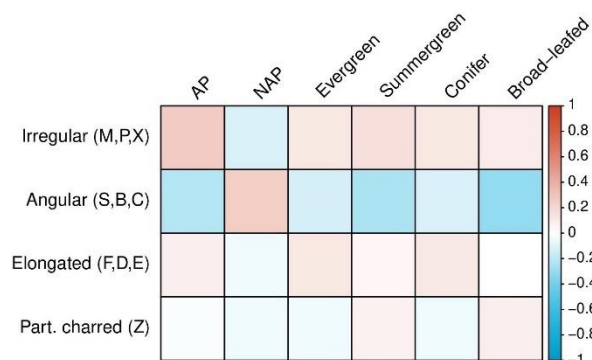


Figure 17: Correlations of grouped macroscopic morphotypes and pollen classes (based on 18 samples)

4.4. Impacts on soil geochemistry

Elements chosen for closer analysis with the SEA (“fire elements” including Ti, Ca, K, Al, P, S and Si) partially show very similar distributions within the sediment core, with S and P being the exception (see appendix G). From c. 200 BCE to 550 CE, mean changes in Ti, Ca, K, Al and Si distributions are oscillating in somewhat regular intervals of c. 200 years. After that, they reach a minimum and continually increase until reaching two maxima at c. 1050 and 1250 CE, followed by another minimum at c. 1500 CE. From there, their abundance gradually increases towards present time, with a mostly pronounced trough at c. 1750 CE. S and P on the other hand show higher variability and often also more counts than the other elements, not matching the general distribution of the other elements for the most part.

The SEA applied to existing XRF data and the reconstructed fire history from Lake Khamra yielded more inexpressive results than what was found by the authors of studies this approach was based upon. *Figure 18* shows exemplary how SEA output for Ti did not show a clear effect of fires on the geochemical sediment properties, which is similar for all of the analysed elements (all corresponding graphs can be found in appendix F). This is especially clear when focussing on the grey lines, indicating the individual “cut-outs” of the Ti-timeseries around every identified fire event. However, as indicated by the similar distribution of Si throughout the core, SEA using Si leads to similar results to using Ti or Ca. This contrasts the results from the original study where Si response differed markedly from that of other elements (LEYS et al. 2016).

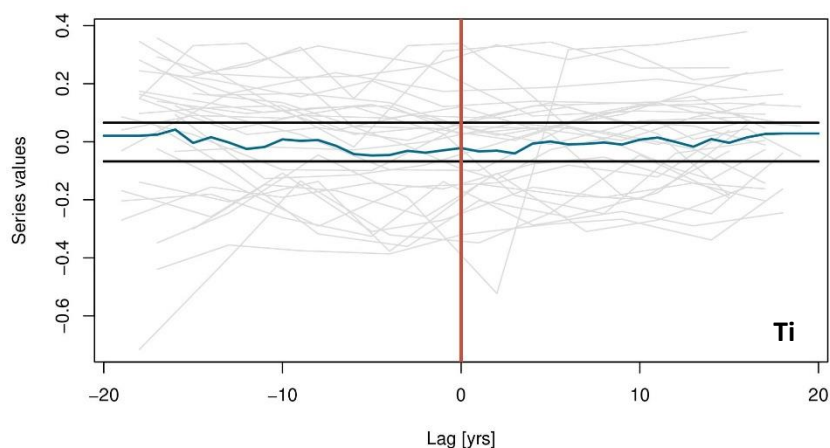


Figure 18: SEA for titanium using all identified fire events. Red bar: Fire event, grey lines: individual “cut-outs” of the Ti-timeseries, blue line: average of Ti-timeseries response to fire events input, black bars: confidence interval

In order to see if this might create clearer results, the reduced fire version was used as an input to the SEA (see 3.3 and 4.2). By restricting the number identified fire events to one per peak in charcoal accumulation rate, overlapping and therefore potential cancellation of element timeseries cut-outs

might be reduced. This indeed leads to a slightly different result (see *figure 19*), still not indicating a significant impact of identified fire events on the geochemical elements as measured by the XRF scanner, but potentially reducing noise within the SEA and therefore leading to a slightly clearer output. This is visible in the grey lines of the different timeseries overlapping more uniformly in many cases.

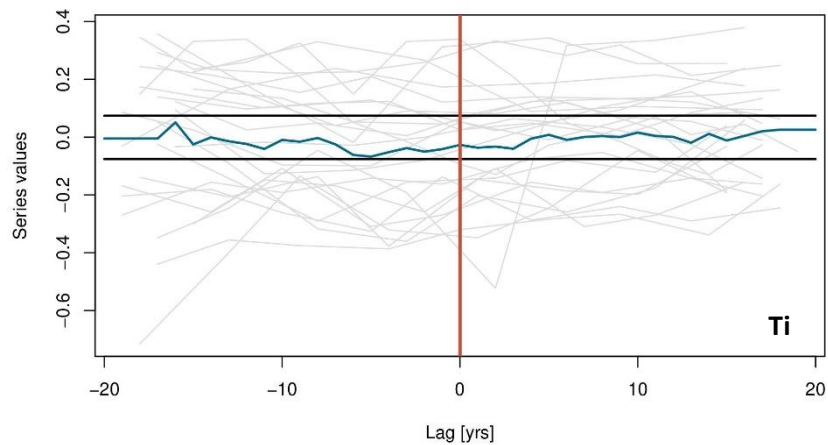


Figure 19: SEA for titanium using the reduced version of identified fire events. Red bar: Fire event, grey lines: individual “cut-outs” of the Ti-timeseries for every fire event, blue line: average of Ti-timeseries response to fire events input, black bars: confidence interval

Other inputs into the SEA were tried to test if they created different results. For example, only fire events identified by the largest size class thought to represent fires closest to the lake (to see if geochemical impact might be clearer if source area was more restricted) or using only fire events corresponding with SNI > 3 (to further minimize potential noise within the analysis). However, these inputs did not lead to a different overall outcome.

5. Discussion

In the following segment, the results gathered in this research project and their implications will be discussed in more detail. The various proxies and the practical and statistical methods applied will be evaluated, and the different results will be put together to create a synthesis regarding the charcoal-based fire history at Lake Khamra. Additionally, special emphasis is placed on presenting the issues encountered in this study and how they might point out improvements to make future research both more robust and efficient.

5.1. Approach to age-depth modelling

Establishing a reliable age-depth model has proven to be one of the most important tasks in this study and at the same time seems to not uncommonly present a challenge for paleoecological studies in permafrost regions.

The uncalibrated radiocarbon bulk sediment ages covered a shorter time interval than what was expected beforehand. However, this proves to be very beneficial for the charcoal method, where higher temporal resolution of a record leads to a more precise analysis of fire history (less temporal averaging through subsequent fire events). The major challenge for the age-depth model lies within the radiocarbon bulk sediment dating results showing an age of 1415 ¹⁴C years BP in the topmost centimeter of the core, being almost equivalent to a surface sample. It should be very unlikely that no sedimentation took place during the last c. 1500 years at Lake Khamra. As a mere hypothesis, more likely would potentially be a mistake during core drilling on site, leading to a loss of the topmost sediment material. There is no report on any occurrence like this and correspondence with expedition members confirmed that. If a loss of sediment were to be true and if then also the sedimentation rate of the safely obtained part between 1415 - 3551 ¹⁴C years BP was somewhat comparable to that of the part younger than 1415 ¹⁴C years BP that would have been lost, this would mean that over 1 m of core length would have gone missing without notice. All this validates that the topmost core centimeter is indeed from at least close to the lake sediment surface. Sediment mixing during core extraction or from bioturbation is hardly an option to explain this large of an offset in radiocarbon age and there is no evidence for large-scale sediment upheaval processes at Lake Khamra – which would have shown in the Pb/Cs ages as well, indicating a rather constant rate of ²¹⁰Pb deposition from the atmosphere. Since there is no reason to suspect any malfunctions or influences during the MICADAS radiocarbon dating process, the reason for this old dated age can only lie within the sediment itself. Bulk sediment samples are generally regarded as one of the more imprecise dating methods, because a lake's sediment is made up of

many different components. Some of them originate from within the lake (e.g. organic material from aquatic plants and animals), some of them are washed in from the outside through inflows or along slopes surrounding the lake's shore (e.g. mineral grains, plant structures or – as is very welcomed in this study – charcoal particles) or transported in the air and deposited on the water surface before eventually descending. Accumulating on the lake's bottom, surface sediment might be mixed and disturbed by water currents or animals (bioturbation) for some time before it is conserved under new layers of material. All that leads to the radiocarbon dating result of a bulk sediment sample representing a mean age of all included components (GRIMM et al. 2009). However, when confronted with only few and mostly small plant macrofossils of rather unknown origin in non-laminated sediments, there is hardly another option than to rely on bulk sediment dating.

With the Pb/Cs ages showing a recent age of the topmost sediment sample (as would be expected), this leads to the conclusion that some components within the topmost radiocarbon bulk sediment sample must be older than their surrounding material. This in turn influences radiocarbon dating results by increasing the measured ^{14}C age, leading to an offset or over-estimation. With the Pb/Cs ages apparently not being affected, this only leaves the origin of the bulk sample's carbon as the main suspect. The most likely explanation for the age of the topmost sample therefore comes from the interaction of the lake with its environment.

Old carbon can be introduced to a lake as carbonate from sources like karst areas to result in subsequent overestimation of radiocarbon ages (hard-water effect, DEEVEY et al. 1954), however, there is no indication of either abundant carbonate in Lake Khamra, nor of areas rich in limestone within its catchment. However, there is discontinuous and sporadic permafrost consisting of frozen and conserved organic material, i.e. carbon. This constitutes by far the most likely source of old carbon and simultaneously explains why the issue of potentially overestimated radiocarbon ages comes up in other paleoecological studies set in Yakutia's permafrost regions, showing that this issue is indeed not a new one. While sometimes only the age offset of the topmost radiocarbon sample is adjusted (e.g. BISKABORN et al. 2012), other studies do not have age dating results from the sediment core's top and therefore assume recent surface age (e.g. NAZAROVA et al. 2013, KATAMURA et al. 2009a).

This conclusion naturally leads to attributing the difference between radiocarbon and Pb/Cs age (1415 + 68 years) to old carbon input and therefore an adjustment of the topmost radiocarbon age by subtracting this difference, setting it to a recent age as well. The resulting age-depth model (see 4.1, *figure 5A*) shows an unusually sudden change in sedimentation rates between the Pb/Cs ages and the deeper ^{14}C ages, which cannot be recognized in the very homogenous and uniform material throughout the sediment core or the grain size distribution. This is interpreted here to be evidence that the old carbon

influence was not only happening during recent years, but rather is a constant factor in sediment deposition throughout the whole core. And herein lies the main difficulty in constructing a robust age-depth model: While for the topmost radiocarbon age there is good evidence for the magnitude of influence of old carbon from the difference between radiocarbon age to Pb/Cs or simply recent age, this is not true for the other radiocarbon ages. It should be conceivable that the input of older organic material did not just start recently but rather happens frequently as a natural process applying to lake systems in permafrost regions. The logical consequence of that is an adjustment of not only the topmost radiocarbon age, but all radiocarbon ages. For this thesis it was not possible to infer the magnitude of this assumed age-offset for other samples than the surface sample, leaving only the option to assume a constant magnitude of 1415 ± 68 years for all radiocarbon ages. In fact, there does not seem to be a safe way to approach difficulties like that in existing literature. The assumption of a constant input of old carbon to the lake must by all means be seen as an approximation, however, in this case it is an approximation that can indeed be argued for and that is also able to create an age-depth model that fits the physical appearance of the sediment core itself (see 4.1, *figure 5B*).

The macrofossil dating results also present some evidence for the influence of old carbon. It is important to note that macrofossils can potentially be a very precise source of age information, however, under the circumstances of a lake within permafrost regions, they too present the difficulty of potentially originating from old carbon storages. This might especially be true for the sort of macrofossils used for age dating here, being very small seeds and fragile organic strings without a certain origin. If only the topmost radiocarbon age would be adjusted to recent age, some of the macrofossils would be dated younger than their surrounding sediment matrix. As previously mentioned, there is no evidence for some sort of large-scale sediment upheaval processes at Lake Khamra, which makes this result unlikely. However, comparing this to the final age-depth model with all radiocarbon ages adjusted, all of the macrofossil samples are dated older than the model, which is a more likely scenario. This might also indicate first-hand how old organic material leads to an overestimation of radiocarbon age when distributed across bulk sediment samples. Furthermore, in this approach the one larger and known terrestrial macrofossil, being a piece of wood at c. 85 cm depth (dated at 1244 ± 29 ^{14}C years BP) suspected to present a more reliable age than the other, smaller macrofossils, lies closer to the modelled age of the same depth (914 ± 83 calibrated years BP). On the contrary, when adjusting only the topmost radiocarbon age, this piece of wood dates over 1000 years younger than the modelled surrounding sediment matrix (see 4.1, *figure 5A*). This is further evidence that the assumption of the constant influence of old carbon throughout time does manage to approximate a realistic scenario at Lake Khamra.

Finally, to conclude this part on the age-depth model, it is noted that the assumption of a constant magnitude in age-offset seems to be a common procedure in other studies found to be influenced by

the hard-water effect. Usually a living shell or plant is dated to subtract that age from all other dated sediment ages (LOCKOT et al. 2014). A somewhat worrisome aspect that came up during the work on the age-depth model of this study is an apparent lack of a robust way to deal with this issue among the geoscientific community. Studies focussing on unravelling and adjusting the influence of allochthonous carbon throughout time for lakes affected by carbonate input from limestone sources manage to only roughly approximate the magnitude of this effect (LOCKOT et al. 2015). Sometimes the potential influence of an old carbon effect is not even mentioned or discussed in publications. Studies with sediment cores for which no surface ages exist do not even seem to have the possibility to approximate the magnitude of age-offset, therefore left with no other option than using unadjusted age results and assuming a recent surface age (e.g. KATAMURA et al. 2009a).

Whether using adjusted or non-adjusted ages for age-depth modelling, resulting sedimentation rates have the potential to significantly alter the distribution of any proxy when calculating an influx. Therefore, choices made for the age-depth model can alter not only the attributed ages of any subsequent research results, but also the result itself. Because this is an ongoing problem and will likely also affect future studies, it seems to be of major importance to conduct more research on the different ways old carbon can influence lake sediment radiocarbon dating in permafrost regions. For example, it would be a more than welcomed improvement for all future studies if a way is found to quantify the magnitude of this old carbon effect not only on the surface, but throughout a sediment core, or at least approximate the uncertainty that arises for all following analysis by not being able to do so and having to assume constant magnitude.

5.2. Significance of the charcoal record

The following discussion of the reconstructed fire history at Lake Khamra will start with remarks about the preparation process and the general suitability of the location for this sort of analysis and then continue to highlight various important parameters of a fire regime, from the overall CHAR variation and its potential drivers, reconstructed FRIs and how they compare to other studies, to the influence of different size classes, the SNI and the distribution of morphotypes.

Charcoal preparation and reflectance measurement

Beginning with the sampling scheme of the EN18232-3 sediment core, uneven sampling widths (1 cm for pollen samples, c. 0.5 cm for charcoal samples) turned out to be somewhat inefficient for further analysis and data handling. Additionally, the usage of syringes for the middle sample of one increment and knives to extract the remaining material to both ends might lead to a slight overlap of sediment material between subsequent samples, due to the resulting round shape, adding a (probably rather minor, but non-quantifiable) averaging aspect to the data. Future studies might benefit from the more usual uniform sampling scheme, if sediment quantity allows for that. Using the combined pollen and charcoal extraction method presented in this study, it should be possible to sample in evenly spaced intervals for all proxies. Simultaneously, sampling itself (i.e. the extraction of the sediment material from the core) should always be volumetric and as precise as possible, unlike the dedicated charcoal samples in this study. This would make the interpolation of sediment densities unnecessary, taking away another (probably also minor) component of uncertainty. The use of syringes for pollen samples in this study did provide volumes, however, depending on the consistency/water content of sediment material, a different tool (e.g. a volumetric cube-shaped spoon, as used for volume determination in this study as well) might be able to achieve more precise results.

Preparation of both macroscopic charcoal and pollen samples from the same sediment material with the method established for this thesis provides an effective way to reduce the amount of sediment needed, therefore potentially enabling additional analyses for a given sediment core. However, even though sieving the sediment worked fine in this instance, some samples still contained small lumps of sediment during the charcoal counting step. Although it is unlikely that this influenced the outcome of this research project, it might still be beneficial to add a chemical dispersant anyways. Since this will probably only impact outcome in a positive way, keeping the method as uniform as possible across multiple records helps eliminate additional sources of unknown influences, thus increasing comparability. The sieving step is especially important here, considering that smaller fractions that are not thoroughly sieved through the mesh will be missing in the pollen sample. Any possibility to reduce the likelihood of such a potentially distorting effect on the pollen samples should be implemented, therefore the use of a dispersant (see different approaches in 3.3) is recommended for future studies.

Charring temperatures of charcoal particles found in Lake Khamra's upper sediment were estimated to lie between 480 - 705 °C from the explorative test of the reflectance measurement method (see 3.3 and 4.2). This lies within, although also exceeding, the temperature range of charcoal formation from c. 200 - 600 °C as summarized by CONEDERA et al. (2009). WHITLOCK and LARSEN (2001) provide a narrower range of 280 - 500 °C. The mean formation temperature of 555 °C places these results at the upper end of the temperature range, implying rather high fire intensity. This contrasts the description of the

prevalent Siberian fire regime as generally having a lower intensity (DE GROOT et al. 2013), although any occurrence of higher intensity fires is not ruled out by that assertion. Also, high intensity fires might be more likely to produce larger charcoal particles (WARD and HARDY 1991). The rather high reconstructed charring temperatures and the generally smaller particles sizes at Lake Khamra, likely produced by lower intensity wildfires, might point towards an uncertainty within the reflectance measurement of small particles. If there is evidence for the validity of this method's application to smaller charcoal particles with a limited number of possible random point measurements, it could provide a powerful new insight. An application to a greater number of samples across the record, especially to samples being statistically identified as prominent fire events, could potentially add an important component to the evaluation of past fire regimes. However, due to the nature of the measurement, these samples are no longer useful for another round of counting or other applications with the charcoal particles afterwards, so it is very important to strategically plan all methods to be applied to charcoal samples beforehand.

Choice of location

The Lake Khamra macroscopic charcoal record can serve as a highly resolved reconstruction of fire activity and seems to be unique within central and eastern Siberia. Few other studies seem to exist that reach the point of determining FRIs from sedimentary charcoal in Siberia. Other macroscopic charcoal records seem to be either not sampled continuously (EICHLER et al. 2011, KATAMURA et al. 2009b, VÄLIRANTA et al. 2003) or originate from lakes that do not permit evaluation of a fire signal to that level, either because sedimentation rate is too low leading to lower temporal resolution (KATAMURA et al. 2009b) or because thermokarst processes likely impacted the taphonomy of charcoal particles (KATAMURA et al. 2009a).

With a high average temporal resolution of c. 7 years per sample, Lake Khamra is exceptionally well suited for fire reconstruction in that regard, with CONEDERA et al. (2009) recommending deposition times of 10 - 30 years or less. The mean temporal resolution is also considerably shorter than the expected FRI, a pre-requisite to confidently assess fire events throughout time (WHITLOCK and LARSEN 2001). Although varved sediments would be able to provide even higher resolution and superior chronology (WHITLOCK and LARSEN 2001), they seem to be rare in Arctic and Subarctic boreal forest lakes. This might be due to various reasons, from the last glaciation preventing the formation of long sediment sequences to sediment accumulation processes in permafrost areas (REGNÉLL et al. 2018). In the newly available Varved Sediments Database (VARDA, RAMISCH et al. 2020 [Preprint]) collecting paleoclimatic proxies from varved sediment records, only one of 189 sites is located in Siberia (Lake Teletskoye, not too far from the southern border to Kazakhstan, China and Mongolia and not located

within the boreal forest; see RUDAYA et al. 2016). Although VARDA will likely be expanded with more records, this underpins the perceived scarcity in varved sediment records in Siberia. Tying in with the discussion of the age-depth model, this might indicate that the challenge of establishing robust chronologies from potentially old carbon-affected bulk sediment will continue to come up in future studies.

Lake Khamra's surface area (c. 4.6 km²) and the estimated catchment area of c. 107 km² (Bettina Winkler, AWI Potsdam, High-latitude Vegetation Change working group, personal correspondence) lead to a relatively large ratio of catchment per lake area (c. 23). That implies both the advantage of potentially having more charcoal from the catchment be transported to the lake (therefore increasing the regional fire signal), as well as the disadvantage of potentially also incorporating more "background-charcoal". The balance between the two input sources is unknown, however it is assumed that a large catchment per lake area ratio will generally increase signal when compared to lakes with a low ratio (WHITLOCK and LARSEN 2001).

Overall CHAR variation

A somewhat unexpected result from the fire reconstruction is the pronounced decrease in CHAR following a period of high fire activity around 750 CE. Except for the heightened fire activity during the late 19th century, recent CHAR is among the lowest of the record, indicating fire activity at a minimum unmatched throughout most of the last c. 2000 years. Especially considering how boreal forests, guided by supposedly increasing fire activity, are thought to pose a tipping point contributing to the warming of the global climate (see 1.2), this result seems to be at odds with the general understanding of changes happening in the boreal zone. In fact, it does contrast the results of other studies that found FRIs and overall fire activity in Siberia to be increasing in recent centuries and decades (e.g. BARHOUMI et al. 2019, KHARUK et al. 2016, CHERSOV et al. 2010). However, some studies also report the opposite for the boreal zone: a decrease of fire activity in recent decades and centuries, mirroring the results of this study (e.g. WALLENIOUS et al. 2011a, b). Both an increase and decrease of fire activity are commonly attributed to varying anthropogenic influence. Some studies find humans responsible for decreasing fire frequency through the rise of fire suppression measures in the 20th century and a shift from traditional and rural towards industrial and more centralized livelihoods and modern agriculture (WALLENIOUS et al. 2011a). Other studies find humans responsible for increasing fire activity through their growing impact on the environment, land-use changes and deliberate raising of fires (e.g. slash-and-burn agriculture, BARHOUMI et al. 2019, DROBYSHEV et al. 2004). CHERSOV et al. (2010) attribute higher average fire activity in Yakutia during the last decades to a decrease in funding for firefighting institutions. Humans might well be held accountable for both of those outcomes depending on time and/or place.

This is highlighted by studies incorporating both possible anthropogenic impacts on fire activity (e.g. DIETZE et al. 2018).

MARLON et al. (2008) synthesized charcoal records from the GCD for a global fire history of the last c. 2000 years. Keeping in mind that Siberia is poorly represented in studies of this kind due to the limited number of charcoal records available, the reconstructed global trend of CHAR shows a distinct decrease from c. 1 CE onwards, reaching its absolute minimum in the 17th century before sharply increasing until c. 1850 CE. After that, CHAR decreases during the last century. In a follow-up study MARLON et al. (2013) expanded upon this global reconstruction by applying it to records spanning the complete Holocene. The authors note how it is difficult to disentangle the complex interactions between fire activity, climate and human impact, and that at different spatiotemporal scales, the main fire cause is subject to change (MARLON et al. 2013, 2008). In general terms, before c. 1850 CE increases in fire activity are often thought to happen because of human activity, whereas a decrease in fire activity afterwards is thought to have happened despite growing human activity (i.e. through fire suppression).

Thinking human involvement in a vast perceived wilderness of Siberia might be neglectable could potentially be an erroneous prejudgment. For Siberian circumstances at least, many areas of Yakutia tend to be rather densely populated (CHERSOV et al. 2010). This is highlighted by the c. 5000 people living in Peledui, not far from Lake Khamra, and remote sensing imagery indicating large-scale logging c. 10 km from the lake's catchment. The fact that Lake Khamra's low overall CHAR during the last decades is recorded despite a higher fire frequency from c. 1850 CE onwards could potentially hint at some recent involvement of humans as fire suppressors, however, this must stand as a mere hypothesis for now. Humans seem to have transitioned from deliberately raising fires towards fire suppression in many places, not allowing for the generalization that less human population necessarily translates into less anthropogenic fires (DIETZE et al. 2018). Due to most contributing factors to fire activity (vegetation, climate, humans) varying depending on time and place, searching for more detailed reasons behind a changing fire history should benefit from being restricted to a local to regional scale at first.

Reconstructed fire events and FRIs

As mentioned, before, few other studies in Siberia involving charcoal as a fire proxy manage to reconstruct fire events for various reasons. A recent study by BARHOUMI et al. (2019) established the first continuous macroscopic charcoal record for the northern Ural region that was suitable for determining fire events and therefore FRIs. Examined peat sequences revealed a general decrease in FRIs over the course of the Holocene, with long FRIs ranging between 200 - 600 years in its first half. During the second half of the Holocene, a prolonged decrease in FRIs towards 40 - 200 years was observed. Since 1500 CE, FRIs ranging from 40 - 100 years belong to the shortest of the entire Holocene. The authors

attribute this mainly to increasing human influence (BARHOUMI et al. 2019). In contrast to macroscopic charcoal, microscopic charcoal is usually never continuously sampled, since it is counted on pollen slides and counting is more time-consuming. Also, the likely large area of origin, which has been defined as including continental and even global scales (CLARK 1988), makes it impossible to deduce fire events (and therefore FRIs) from a microscopic charcoal record. However, other fire proxies did allow for FRI establishment in central and eastern Siberia. Northwest of Lake Khamra, at 60 - 65 °N and c. 100 °E, studies with tree stand ages and fire scars revealed recent FRIs of 80 - 90 years (KHARUK et al. 2008, SOFRONOV et al. 1998, VAGANOV and ARBATSKAYA 1996). Further East, FRI was found to have increased from 52 years in the 18th to 164 years in the 20th century. This lower frequency of fires was attributed to suppression measures and less human-caused fires (WALLENIOUS et al. 2011b). FRIs seem to increase with latitude in most studies, for example from 77 years at 61 °N to 320 years at 71 °N, close the current northern boundary of the boreal forest. This is attributed to lower incoming solar radiation at higher latitudes, leading to shorter fire seasons and lower general flammability of moist biomass (KHARUK et al. 2016, 2011). In NE Siberian larch-dominated boreal forest, FRI was estimated to lie between 50 - 80 and 80 - 120 years at different sites (KHARUK et al. 2011, after SCHEPASCHENKO et al. 2008).

This study estimates a mean FRI based on the macroscopic charcoal record from Lake Khamra (c. 60 °N and 112 °E) of 68.1 years during the last 2000 years. With the reduced fire version, mean FRI increases to 82.3 years. Using these values as lower and upper boundaries (as mentioned in 4.2), the mean FRI for the last c. 2000 years in SW Yakutia is expressed as the range of 68.1 - 82.3 years. This range sits at the lower average of previously reported FRI lengths in central and eastern Siberia, fitting well within their general scope. Lake Khamra's location at a lower latitude might also play a role in slightly lower FRIs, since a stronger continental climate usually results in stronger seasonal extremes (i.e. drier and warmer summers, DUCKSON 1987). Additionally, reconstructions using fire scars on trees or within tree ring chronologies might naturally lead to higher FRIs than the charcoal method, since they only include fires that happened exactly at the location of research. With the charcoal method on the other hand, fires from directly around the lake, within and possibly from outside the catchment are mixed into the record. Of course, there is the statistical approach of using the signal of the charcoal record's peak component to better reflect fire events that directly impacted the lake's catchment. However, this probably still includes charcoal originating from a larger source area than with dendrochronological methods, thus having a higher probability of recording more fires and resulting in lower overall FRIs.

Addressing the most recent identified fire events from the reduced fire version (1952 ± 3 CE, 1904 ± 7 CE, 1862 ± 11 CE) provides an opportunity to discuss what insight these individual "events" can or cannot provide. None of the years directly coincide with recent recorded fires close to the lake shore in 2014 and 2006. It is a confident assumption that these events must have produced charcoal that

accumulated in the lake. However, a precise representation of these years might not even be expected in a charcoal record of this kind. Although this upper core part is supported by relatively precise Pb/Cs age dating, a sample still consists of bulk material that is likely to have experienced some averaging influence before depositing. Looking at all charcoal particles deposited in a 1 cm increment of core depth only reveals the average charcoal influx to the lake during c. 12.4 years (using the mean sedimentation rate of the whole sediment core). That is why fire “event” is still a somewhat misleading term, as it does not necessarily describe a single wildfire, but rather episodes of wildfires producing a collective charcoal peak (“fire episodes” being a term for fire events used by DIETZE et al. 2019). This is also reason for WHITLOCK and LARSEN (2001) to recommend that a charcoal record’s temporal sampling resolution should be significantly higher than the expected mean FRI. It would be expected that two wildfires in a time interval about as short as the maximum resolution of the charcoal record might well add to the same fire event, which might just be the case here (2014 and 2006 being represented by the increase in CHAR in the topmost sample, which does not reach above the threshold for fire identification). Also, as previously stated, the top few millimeters of the sediment core might not show in the CHAR record due to limited analytical precision. The lag time between fire and charcoal deposition in the lake’s sediment, together with the analytical effects in the topmost few millimeters of sediment from core drilling and preparation, might lead to a loss of signal from those most recent fires. This circumstance highlights the need for longer fire reconstructions, e.g. from tree fire scars, to sufficiently calibrate a charcoal record from non-varved lake sediment. A calibration of this sort was successfully achieved in other studies and generally results in a more robust fire reconstruction (e.g. MAGNE et al. 2020, HIGUERA et al. 2005).

SNI and fire event identification

The SNI of the macroscopic charcoal record provides an efficient, quantified method to evaluate the reliability of fire event identification. Potential reasons for $SNI < 3$ are discussed by the authors of the method to be either a “lack of signal and/or the addition of noise”. Noise might be increased if a lake is subject to a lot of sediment mixing, gradually leveling out the charcoal concentration during deposition. Another possibility is low-severity fire regimes producing smaller amounts of charcoal, leading to a less distinct signal. If then secondary charcoal input to the lake is at a sufficient level, the signal will be even harder to distinguish from noise. Additionally, the authors stress how $SNI < 3$ does not necessarily equal no signal, and $SNI > 3$ doesn’t necessarily equal fire event (KELLY et al. 2011). The SNI should in that sense not be used to verify or falsify identified fire events. However, the method provides an interpretation frame for charcoal records and makes visible intervals where identification of fire events

might probably be less reliable. For the macroscopic charcoal record of Lake Khamra, there is one distinct minimum in SNI around 1500 CE. No peak reached above threshold around that time, so in this case the minimum SNI resembles the indicated lack of signal, i.e. no to only low fire activity around Lake Khamra. Apart from that instance and the most recent centuries, the SNI of present macroscopic charcoal record remains close to $SNI = 3$ even when dropping below this proposed cut-off value. Together with the inclusion of both an upper and lower estimation of reconstructed fire events (by using the original and reduced fire versions, respectively), this was reason to also include fire events with $SNI < 3$ in the determination of mean FRI length.

KELLY et al. (2011) proposed the usage of a changing local threshold instead of a constant global one, arguing that changes in noise distribution within the record should lead to constant adjustment of the threshold. In this study, a global (i.e. constant) threshold is used for the whole record. Going forward, the implementation of a local threshold could be a next step with this sort of analysis, using the Gaussian mixture model to identify the 99th percentile of modeled noise distribution within a moving window (KELLY et al. 2011: 14) instead of applying it to the whole record at once. Additionally, the CharAnalysis R script by DIETZE et al. (2019) used in this thesis might benefit from being expanded with the inclusion of the SNI method by KELLY et al. (2011). Furthermore, in the CharAnalysis application by HIGUERA et al. (2009) a Poisson distribution test is used as a statistically rooted method to reduce multiple fire events being identified in one peak distribution. This would be an analogue to the reduced fire version manually created in this thesis, without relying on the visual inspection of fire peaks. Applying the statistical method instead would ensure that different studies come to the same conclusion on which peaks to keep, and which not to. As noted in the R script by DIETZE et al. (2019), this might be another useful expansion going forward. Bundling all these resources into a single R script accessible to the paleofire community might help further standardizing studies and increase overall comparability.

BLARQUEZ et al. (2013) point out how most fire reconstructions derive fire events from a set of statistical operations that require an input of certain variables, therefore making discrete assumptions (e.g. choosing the window-width of the LOWESS resembling the background component of CHAR). Different inputs likely lead to differences in the identification of fire events, which can be witnessed by changes of SNI depending on the chosen window-width. The authors managed to quantify the uncertainty arising from those choices by incorporating the results of the whole span of potential inputs in an ensemble-member approach (BLARQUEZ et al. 2018, 2013). This approach was also applied to a varved sediment core by DIETZE et al. (2019). Going forward, the potential application of this method to the present charcoal record could be evaluated. BLARQUEZ et al. (2013: 2671) note, however, that it should only be applied to records featuring a “[...] good chronology, little sediment mixing, [from] small lakes with a strong local source and small watersheds [...]” and a distinct separation of signal and noise in the peak component (i.e. high SNI). So to use the ensemble-member approach in this case might first make it

necessary to obtain an estimate of uncertainty arising from the underlying assumptions behind the age-depth model and find ways to potentially improve the SNI or otherwise incorporate uncertainty from including intervals of SNI < 3 as well.

Particle sizes and source area

Based on the previous research (see 1.3), macroscopic charcoal > 150 µm as used in this thesis is thought to resemble primarily local sources (within the catchment area). This is especially true for the large size class (> 500 µm), which has been observed to deposit right at fire sites in boreal forest burning experiments (OHLSON and TRYTERUD 2000). Using the CharAnalysis method on each size class individually leads to significantly less identified fire events for large particles than for medium or small ones (> 150 µm: 70; 300 - 500 µm: 56; > 500 µm: 14). The difference between the small and medium classes is not as striking but fits in this pattern of smaller particles recording increasingly more fire events. This is an expected result if smaller particles are suspected to originate from a larger source area, thereby naturally incorporating more potential fires into their signal. Based on the previous observations and experiments, it could be suspected that large particles are more likely to derive from fires close to Lake Khamra's shore. Small and medium-sized particles on the other hand might rather originate from fires within the catchment area, more distant to the lake itself. Using this categorization, it is possible to attribute the varying degree of the size classes' contribution to overall CHAR to the proximity of fire activity to the lake. Periods where small particles have a higher share (e.g. around c. 500 CE) might indicate fire activity towards the boundaries of the catchment area, whereas peaks prominently consisting of large particles, like those in 674 ± 77 and 1862 ± 11 CE, could indicate fire events right next to the lake (see 4.2, *figure 11*).

Morphotype distribution

The morphotype classification scheme used in this thesis was adapted from ENACHE and CUMMING (2007, 2006). It is thought that different types of biomass burning (fuel) might lead to different appearances of produced charcoal particles. However, as has been briefly stated in 1.3, these studies did not use morphotypes to infer fuel types, but rather to reconstruct charcoal taphonomy and sedimentation processes. Morphotypes were correlated to the total burnt area around a lake, precipitation and temperature. Results showed how fragile, irregular particles (Type M) might represent burned area most precisely, because they might originate from primary input through the air rather than secondary input along the ground, which might favor the fragmentation of fragile particles specifically. More robust particles on the other hand (e.g. Type C) correlated to precipitation but not fire and were therefore thought to represent secondary deposition. The authors also proposed that Type F likely originates from breakage of fragile particles like Type S (ENACHE and CUMMING 2007). Based on these findings,

some subsequent studies were mainly basing their key findings about fire history on the prevalence of Type M charcoal particles (see MOOS and CUMMING 2012). Judging from the vastly diverse appearances of charcoal morphologies at Lake Khamra, it seems unlikely that these are only results from particle taphonomy.

Different types of fuel load have shown to produce different types of charcoal morphologies in experimental studies (MUSTAPHI and PISARIC 2014, JENSEN et al. 2007), so there might rather be a multitude of structure-shaping factors at play. The prevalence of fragile morphotypes at Lake Khamra, with significantly fewer morphotypes deemed more stable, contrasts the assumption by ENACHE and CUMMING (2007, 2006) that a large catchment to lake area-ratio favors more stable types through increased secondary input (i.e. more reworking on the ground leading to more breakage of fragile morphotypes). The corresponding ratio of Lake Khamra (c. 23) is almost double the size from the largest ratio among the lakes studied by ENACHE and CUMMING (2007) (c. 12.3), yet around 80 % of all particles counted belong to fragile morphotypes (Types F, M and S). This is evidence for suspecting a stronger impact of fuel types and fire attributes on charcoal morphology rather than taphonomy – at least when comparing study sites situated in different ecological environments (here: subboreal western Canada and boreal central Siberia).

The two charcoal samples with some of the highest concentration of charcoal particles, the fire events identified in 674 ± 77 and 1862 ± 11 CE, consisted of a strikingly big share of large Type F particles. This might be evidence for a specific type of vegetation burning. From the similarity of Type F to experimentally burnt *Picea* needles (MUSTAPHI and PISARIC 2014, see 5.3), it might have been primarily conifer trees, suggesting a higher than usual fire intensity. Together with the large share of $> 500 \mu\text{m}$ particle sizes, it could also point towards very close and/or very high intensity fires. It could be suspected that these events represent rare high-intensity wildfires affecting trees right next to the lake's shore. However, the reconstructed charring temperature of c. 480°C belonging to the fire event of 1862 ± 11 CE is at the lower end of the reflectance measurement results. While this value alone would stand as a rather high charring temperature corresponding well to the assumed higher fire intensity, it remains uncertain if the overall range of the very high reconstructed charring temperatures is representative (see 3.3). Ways in which methods could be improved to have results like this be more robustly interpreted will be discussed in the following paragraphs as well. Both correlations and the PCA furthermore indicate an association of both Type F and large particles and Type M and small particles.

In general, the explorative approach of morphotype identification in this thesis following the scheme of ENACHE and CUMMING (2007) revealed the need for morphological classes adapted specifically to the environment a record is located in. Many particles at Lake Khamra appeared different from any of the classes proposed by ENACHE and CUMMING (2007), which resulted in the slight expansion of their

scheme (Types E, X and Z, see 3.3). However, this did not fully eradicate a degree of ambiguity in classification. This ambiguity likely leads to a decrease of useful signal within morphotype abundances and also hinders reproducibility. The expanded classification by MUSTAPHI and PISARIC (2014) is for this reason explicitly open for adaptation to the wealth of morphotype shapes encountered at a given study site. This approach might benefit from explorative particle counts to establish the basic classification scheme before starting more thorough evaluation. Additionally, results by MUSTAPHI and PISARIC (2014) indicate the high value of burning experiments using prevalent local vegetation.

Microscopic charcoal record

The general lack of comparability between the microscopic (MIC) and macroscopic charcoal (MAC) concentrations could be a consequence of the significantly lower resolution of the MIC part. Counted MIC sample density along the core depth is less than 10 % that of MAC samples. Other studies involving both types of charcoal proxy can serve both as examples for higher (OLSSON et al. 2010) and lower (LARSEN and MACDONALD 1998, MACDONALD et al. 1991) comparability between the two. FROYD (2005) analyzed both MAC and MIC in four lakes in Scotland with resulting records showing great comparability of the two proxies in three of them, but a lack thereof in the fourth. Studies like these confirm that this outcome is not necessarily unique to this thesis and that factors influencing the accumulation of MAC and MIC might vary stronger between sites than suspected.

It is also generally more difficult to estimate source area and transport processes for MIC particles (WHITLOCK and LARSEN 2001), making the reasons behind the apparent inconsistency with the MAC record harder to pin down. As previously described, MIC particles are thought to originate anywhere from extra-local to continental or even global sources, depending on their size. That is why some studies chose to exclude MIC particles < 10 µm from counts (CONEDERA et al. 2009, WHITLOCK and LARSEN 2001), something that was not done while counting the samples for this thesis. The MIC record could therefore be disproportionately influenced by large-scale variations in Siberian fire activity rather than by fires within Lake Khamra's catchment, leading to a different signal. However, if the MIC signal really does integrate fire activity over such huge areas, reconstructions should probably show some similarities on regional to continental scales. That does not seem to be the case, judging from variability in MIC records in the Lake Baikal region alone (comparing GCD sites 580 - 584: SHICHI et al. 2009, AKIRA et al. (unpubl.), TAKAHARA and KRIVOGONOV (unpubl.)).

All of this leads to suspect that the higher amount of unknown factors leading to the deposition of MIC particles, their likely larger area of origin and the inclusion of very small and more ambiguous particles in counts of this thesis are equally responsible for the outcome. Additionally, the shown comparison

(see 4.2, *figure 13*) visually exaggerates the variation within the MIC record by using the lowest concentration as the lowest value on the y-axis instead of using zero. Actual variability is lower than it appears from this graph, suggesting that the responsible factors mentioned before influence a record that could mirror the lower variability of the pollen record, as it is often expected for MIC particles (WHITLOCK and LARSEN 2001).

Morphotypes of microscopic and macroscopic charcoal show partially contrasting distributions and overall weak and inconclusive correlations, which probably lies within the nature of each method. Whereas Type F is the most common in MAC samples, it is second rarest in MIC samples. The exact opposite is true for Type P, which accounts for only 1.2 % of MAC morphotypes, but 45.5 % of MIC morphotypes. This difference is likely due to two reasons: (1) More fragile charcoal particles like the elongated Type F are subject to break during the pollen preparation process, with their fragments' resulting shape more closely resembling angular/geometric particles like Type C. (2) Morphotypes without structure (Types P and C) are rarer among MAC particles, where it is easier to identify common charred patterns because of the larger particle size. On the other hand, with small MIC particles, a structure is harder to make out and often less pronounced when viewed with a transmitted-light microscope. This also explains the significantly higher amount of Type S particles among MAC samples. Basically, looking at MIC particles might be thought of as looking at fragments of the individual structures that make up the charred patterns of MAC particles. Not only are the MIC morphotype distributions expected to differ from those of MAC morphotypes, but the additional overall difference in concentrations between the two proxies is reflected in the weak correlations as well. It remains to be seen whether a higher resolution of counted MIC samples can improve this generally inconclusive outcome.

5.3. Impact on the environment

This segment discusses the secondary goals of this thesis: The evaluation of potential fire impacts on vegetation and soil geochemistry. Both approaches revealed useful hints for further research but were hampered by rather low expressiveness. However, this outcome is constructively used to assess potential reasons and solutions in order to create stronger results going forward.

Vegetation history and fire impact

Vegetation history as inferred from pollen type abundance within Lake Khamra's sediment core indicates generally that both conifers and broad-leafed trees can be found in the region, although conifers

show higher overall pollen counts. *Larix* pollen are present throughout the record, which is to be expected with the lake lying in the transition zone towards summergreen (i.e. larch-dominated) boreal forest. The share of *Larix* pollen is generally rather low, however. These counts cannot be directly translated into a detailed species composition, since different Taxa may release different amounts of pollen grains, leading to over- or underrepresentation in the pollen diagram (see SUGITA 2007). It is evident that throughout the last c. 2100 years, the vegetation composition surrounding Lake Khamra has been quite stable. Peaks in Cyperaceae, coinciding with fire events or heightened overall fire activity as inferred from the macroscopic charcoal record, might be a consequence of effective succession of grasses on recently burnt areas. These peaks might also just be the consequence of the lower share of arboreal pollen types, which could in turn be viewed as potential fire impact as well.

It would not be expected to find patterns of fire activity at higher temporal resolution within the pollen record. Assessing pre- and post-fire vegetation compositions requires very high temporal resolution of densely sampled pollen samples, which is not achieved by the counted 24 samples representing c. 2100 years in this study. It is difficult to estimate how far a fire would have to spread in order to leave behind a striking mark in the pollen record, since the pollen source area is generally not constricted to local sources (PRENTICE 1985). Any estimation requires (among other factors) knowledge of the source area of deposited pollen grains and the time needed before any burnt area will produce pollen grains at pre-fire quantities. It might well be that the generally low-intensity surface fire regime prevalent in Siberia does not impact overall pollen production long enough to have that signal withstand averaging factors of pollen taphonomy (e.g. collection on the lake's water surface before sinking to the ground and being reworked towards deeper positions under the influence of bioturbation) and the averaging nature of a sediment sample.

Correlations of macroscopic charcoal morphotypes and vegetation history resulted in some non-significant, but quite apparent contrasting patterns. The most abundant Type F particles found at Lake Khamra appeared very similar to what MUSTAPHI and PISARIC (2014) showed to be burnt *Picea* needles, although generally smaller in size, while Type S particles on the other hand seem often resemble their burnt Poaceae leaves. Correlations with pollen types revealed weak positive coefficients for Type F with *Abies* and Type S with Cyperaceae. It might be suspected that different types of burnt needles or grasses could lead to similar appearance of needle- or grass-like morphotypes. Looking at the very basic shape and structure of charcoal particles might therefore most effectively be used only for more general classification of burnt vegetation (i.e. pollen classes used in this thesis or similar approaches). The contrasting pattern between angular morphotypes and non-arboreal pollen types versus irregular particles and arboreal pollen types could have the potential to infer some basic fire attributes, e.g. fuel types, from peaks in the charcoal record. For example, a peak consisting almost completely of angular

morphotypes might indicate lower severity surface fire activity than a peak consisting of irregular morphotypes, since the latter would have had the ability to affect trees instead of predominantly herbs. This could potentially be expanded with particle size distribution, i.e. angular morphotypes and smaller particle sizes indicating low-severity surface fires more distant to the lake. However, that creates the necessity of first disentangling the different potential factors behind charcoal particle size distribution first and reliably correlate morphotypes to vegetation.

The correlation patterns of morphotypes could be experimentally tested (and potentially calibrated) by burning collected vegetation samples from the field sites in Siberia and examining the resulting charcoal particle structures (see MUSTAPHI and PISARIC 2014). This would also benefit the conception of a morphotype classification scheme specific for the setting within Siberia's boreal zone and has the potential to greatly improve interpretation of the morphotype distribution. A combination of these refinements, appropriate research sites and high resolution of the pollen record are likely to improve the robustness of future studies' correlations, increasing the possible level of detail in interpretation.

Fire impact on soil geochemistry

The lack of a more pronounced response of examined elements to identified fire events in the SEA could have multiple reasons: (1) There is no comparable association between fire events and soil geochemistry. (2) There is an association, but it is not recorded sufficiently enough within the lake sediment to appear clearly. Or (3), any association present is obscured by analytical methods applied in this thesis.

Reason (1) is rather self-explanatory, although it has got to be stressed that the original study by LEYS et al. (2016) was conducted in a very different environment (subalpine forest in the Rocky Mountains, Colorado, US), with geochemical processes potentially being not completely comparable to the sub-arctic Siberian boreal forest. By applying the general methods by LEYS et al. (2016) within this study and directly comparing results, the assumption is made that similar results might be expected. At least regarding the ratio of catchment to lake area, both sites are indeed comparable (20.7 for the original and c. 23 for this study). However, the cold climate of Yakutia was also suspected to slow down biogeochemical processes (CHERSOV et al. 2010). This might stretch any fire response in soil geochemistry over longer periods of time, decreasing their initial amplitude.

For reason (2), two explanations might be that either elements are prevented from depositing in the lake sediment (e.g. by vegetation along the shoreline obstructing potential input) or that smaller-scale sediment mixing processes during deposition lead to an averaging of signal, that might have already been weaker by default due to the expected lower intensity fire regime at Lake Khamra.

This leads to reason (3), which might be the most substantial. There are several factors in the analytical approach of this thesis likely to negatively impact any geochemical signal. In the original studies by LEYS et al. (2016) and DUNNETTE et al. (2014), a differentiation was made between high and low-severity fires with help of measurements of the sediment's magnetic susceptibility (MS). MS is commonly used to tell autochthonous from allochthonous sediment input, thereby serving as a proxy for the magnitude of erosion around a lake (WHITLOCK and LARSEN 2001). Fire peaks coinciding with peaks of MS were deemed high severity, because of their potential to increase allochthonous sediment input through erosion. In this study, due to a lack of MS measurement, this step cannot be replicated. This might indeed explain part of the inexpressiveness of present analysis, since the authors of the original study mention how "no significant geochemical changes were observed after low-severity / extra-local fires" (LEYS et al. 2016: 6). Also, in contrast to the original study, no quantification of XRF-derived element concentrations was done in this thesis. Instead, transformed counts per second were used. Adding to this might be the well constrained age-depth model of the original study and the probably less certain age-depth model presented in this thesis, which is the foundation of the reconstructed fire events. Uncertainty in fire event position within the XRF elements' timeseries likely leads to further decrease of signal derived from the subsequent timeseries "cut-outs" around each event during SEA.

A combination of various factors behind all reasons (1), (2) and (3) might be at play and lead to the rather inexpressive results. With the emphasis of this thesis on the fire reconstruction and the application of SEA on the available XRF data having a rather explorative character, a more detailed analysis of geochemistry and soil nutrient processes at Lake Khamra will have to be postponed. By addressing the potential negative impacts on the XRF signal found within this thesis, future studies might be able to improve their outcome and show whether previously reported geochemical impacts of wildfires do or do not exist in Siberia as well. Within this project, no evidence for similar associations to those of LEYS et al. (2016) could be found.

6. Conclusion

Within the research project of this thesis, it was possible to create a unique high-resolution record of macroscopic charcoal particles from lake sediments and infer fire history around Lake Khamra, SW Yakutia, for the last c. 2000 years. This adds valuable data for a region where long-term fire regimes, although being an influential ecological variable, remain poorly understood.

The newly established preparation protocol of extracting both macroscopic charcoal and the fossil pollen spectrum from a single sediment sample efficiently decreases the amount of sediment material needed for different proxy analyses. In the age-depth model, an assumed constant age-offset of radiocarbon ages by old, allochthonous carbon, as indicated by the Pb/Cs age dating results, was manually adjusted. This potentially adds a non-quantifiable uncertainty to the resulting chronology, although it mirrors the homogenous physical appearance of the sediment core. The fire reconstruction at Lake Khamra must be viewed while keeping this approach towards the sediment core's chronology in mind.

Based on this age-depth model and an evaluation of 306 continuous macroscopic charcoal samples, fire history for the last c. 2000 years was reconstructed. A high average temporal resolution of c. 7 years per sample is thought to make this reconstruction the first of its kind in central and eastern Siberia, attempting to fill a pronounced gap of charcoal records in the Russian boreal forest. Peaks in CHAR identified as fire events indicate an average FRI ranging between c. 70 - 80 years. This includes an extent of uncertainty from fire peaks found in periods of a lower signal-to-noise ratio, although more than 70 % of identified fire events were distinctly separated from the noise component. During peak fire activity around c. 750 CE, fire events happened about twice as often as within recent centuries. After multiple centuries of decreasing and generally low CHAR and following a pronounced fire event in 1862 ± 11 CE, fire activity during the 20th century was among the lowest of the record. Charcoal particle size classes are thought to enable an approximation of fire distance to the lake, with larger particles > 500 μm originating right next to the shore and smaller particles from within the more distant catchment. Charcoal morphotypes are primarily suspected to resemble types of vegetation burned and not so much differences in charcoal taphonomy. The low-resolution microscopic charcoal record did not compare well with the macroscopic counterpart, likely a result of both the analytical process and differing information expressed by the two proxies. Higher than usual reconstructed charring temperatures could potentially indicate that the reflectance measurement of very small charcoal particles might not yield valid results when compared to the usually larger particle sizes used for this method.

Vegetation history from the fossil pollen spectrum reveals an overall consistent composition during the last c. 2100 years. Although classification of charcoal morphotypes was hampered by some ambi-

guity, correlations with the pollen spectrum hint at some contrasting patterns. Generally low correlation coefficients indicate weak associations between some morphotypes and pollen types. Irregularly shaped charcoal particles might be associated with arboreal pollen, whereas angular particles correlate with non-arboreal pollen. This outcome could be improved by further adapting the morphotype classification scheme to charcoal particles found specifically at the location of research and conducting charring experiments of local vegetation. In contrast to previous research, no clear impact of fire events on soil geochemistry was found. This might be most likely due a slower rate of geochemical processes in cold continental climates when compared to temperate forests and a weakening of any remaining signal during the analytical procedure.

Despite a decreasing trend in charcoal accumulation during recent decades, contrasting both other studies from NE Siberia and the notion of increasing fire activity with global warming, the frequency of identified fire events since c. 1850 CE seems to be higher than during the preceding millennial. This disparity of more frequent fires before a pronounced minimum in charcoal accumulation might potentially indicate anthropogenic fire suppression, although this remains just a hypothesis as humans pose just one of multiple factors influencing fire activity. These partially differing results highlight two important aspects: First, by comparing it to other studies the present fire reconstruction at Lake Khamra indicates a pronounced degree of regional heterogeneity in fire regimes of Siberia. And second, in order to disentangle climatic from anthropogenic forcing on a fire regime, a better understanding of local human fire management and usage throughout time is urgently needed.

Reconstructions of fire history can potentially be of great use for non-scientists involved with ecosystem management. For example, they can enable the evaluation of a “safe fire-operating space”, i.e. assess the attributes of fires and fire frequency that human society has been proven to successfully co-exist with (see LESTIENNE et al. 2018). Learning from fire history, potential boundaries of that safe operating space could be compared with the forecast global changes and their regional consequences. However, in order to use fire reconstructions for the ambitious purpose of extrapolating into the future, they should be reliable and cross-validated. In addition to a robust chronology, the charcoal method might greatly benefit from being calibrated using other proxies like fire scars on trees. Together with other potential improvements discussed in this thesis, robust fire reconstructions might become one of the most useful tools for understanding the multitude of changes happening in the boreal zone, many of them involving wildfires as key ecological disturbances.

VI. References

- AKIRA O., S.K. KRIVONOGOV and H. TAKAHARA (unpublished). Institute of Geology and Mineralogy, Siberian Branch of Russian Academy of Sciences, Novosibirsk, Russia
- APPLEBY P.G., N. RICHARDSON and P.J. NOLAN (1992): Self-absorption corrections for well-type germanium detectors. In: *Nuclear Instruments and Methods B* Vol. 71: 228–233
- APPLEBY P.G., P.J. NOLAN, D.W. GIFFORD, M.J. GODFREY, F. OLDFIELD, N.J. ANDERSON and R.W. BATTARBEE (1986): ^{210}Pb dating by low background gamma counting. In: *Hydrobiologia* Vol. 141: 21–27
- BARHOUMI C., O. PEYRON, S. JOANNIN, D. SUBETTO, A. KRYSHEN, I. DROBYSHEV, M.P. GIRARDIN, B. BROSSIER, L. PARADIS, T. PASTOR, S. ALLEAUME and A.A. ALI (2019): Gradually increasing forest fire activity during the Holocene in the northern Ural region (Komi Republic, Russia). In: *The Holocene* Vol. 29 (12): 1906–1920.
- BISKABORN B.K., U. HERZSCHUH, D. BOLSHIYANOV, L. SAVELIEVA and B. DIEKMANN (2012): Environmental variability in northeastern Siberia during the last 13,300 yr inferred from lake diatoms and sediment-geochemical parameters. In: *Palaeogeography Palaeoclimatology Palaeoecology* Vol. 329: 22–36
- BLAAUW M. (2010): Methods and code for ‘classical’ age-modelling of radiocarbon sequences. In: *Quaternary Geochronology* Vol. 5 (5): 512–518
- BLARQUEZ O., J. TALBOT, J. PAILLARD, L. LAPOINTE-ELMRABTI, N. PELLETIER and C.G. ST-PIERRE (2018): Late Holocene influence of societies on the fire regime in southern Québec temperate forests In: *Quaternary Science Reviews* Vol. 180: 63–74
- BLARQUEZ O., B. VANNIÈRE, J. MARLON, A.-L. DANIAU, J. POWER, S. BREWER and P. BARTLEIN (2014): paleofire: An R package to analyse sedimentary charcoal records from the Global Charcoal Database to reconstruct past biomass burning. In: *Computers & Geosciences* Vol. 72: 255–261
- BLARQUEZ O., M.P. GIRARDIN, B. LEYS, A.A. ALI, J.C. ALEMAN, Y. BERGERON and C. CARCAILLET (2013): Paleofire reconstruction based on an ensemble-member strategy applied to sedimentary charcoal. In: *Geophysical Research Letters* Vol. 40: 2667–2672
- BOLLHÖFER A., A. MANGINI, A. LENHARD, M. WESSELS, F. GIOVANOLI and SCHWARZ B. (1994): High-resolution ^{210}Pb dating of Lake Constance sediments: Stable lead in Lake Constance. In: *Environmental Geology* Vol. 24: 267–274
- BOUCHARD F., A. LAUREN, L.A. MACDONALD, K.W. TURNER, J.R. THIENPONT, A.S. MEDEIROS, B.K. BISKABORN, J. KOROSI, R.I. HALL, R. PIENITZ and B.B. WOLFE (2016): Paleolimnology of thermokarst lakes: a window into permafrost landscape evolution. In: *Arctic Science* Vol. 3: 91–11
- BRUNELLE A. and S. ANDERSON (2003): Sedimentary charcoal as an indicator of late-Holocene drought in the Sierra Nevada, California, and its relevance to the future. In: *The Holocene* Vol. 13 (1): 21–28
- CHAMBERS F., B. GEEL and L. MARJOLEIN (2011): Considerations for the preparation of peat samples for palynology, and for the counting of pollen and non-pollen palynomorphs. In: *Mires and Peat* Vol. 7 (11)

- CHEROSOV M.M., A.P. ISAEV, S.I. MIRONOVA, L.P. LYTKINA, L.D. GAVRILYEVA, R.R. SOFRONOV, A.P. ARZHAKOVA, N.V. BARASHKOVA, I.A. IVANOV, I.F. SHURDUK, A.P. EFIMOVA, N.S. KARPOV, P.A. TIMOFEYEV, and L.V. KUZNETSOVA (2010): Chapter 4. Vegetation and Human Activity. In: TROEVA E.I., A.P. ISAEV, M.M. CHEROSOV and N.S. KARPOV (eds., 2010): *The Far North: Plant Biodiversity and Ecology of Yakutia*, Springer, Dordrecht, The Netherlands
- CLARK J.S. (1988): Particle Motion and the Theory of Charcoal Analysis: Source Area, Transport, Deposition, and Sampling. In: *Quaternary Research* Vol. 30 (1): 67–80
- CONARD S.G., A.I. SUKHININ, B.J. STOCKS, D.R. CAHOON, E.P. DAVIDENKO and G.A. IVANOVA (2002): Determining Effects of Area Burned and Fire Severity on Carbon Cycling and Emissions in Siberia. *Climatic Change* Vol. 55: 197–211
- CONEDERA M., W. TINNER, C. NEFF, M. MEURER, A. DICKENS and P. KREBS (2009): Reconstructing past fire regimes: methods, applications, and relevance to fire management and conservation. In: *Quaternary Science Reviews* Vol. 28: 435–456
- DAVIDENKO E.P., V.V. FURYAEV, A.I. SUKHININ and J.G. GOLDAMMER (2003): Fire Management Needs in Russia's Boreal Forest Zone. Conference Paper, Intl. Wildland Fire Conference 2003, Sydney
- DEEVEY E.S., M.S. GROSS, G.E. HUTCHINSON and H.L. KRAYBILL (1954): The Natural C Contents of Materials from Hard-Water Lakes. In: *Proceedings of the National Academy of Sciences of the United States of America* Vol. 40 (5): 285–288
- DIETZE E., D. BRYKAŁA, L.T. SCHREUDER, K. JAŻDŻEWSKI, O. BLARQUEZ, A. BRAUER, M. DIETZE, M. OBREMSKA, F. OTT, A. PIEŃCZEWSKA, S. SCHOUTEN, E.C. HOPMANS and M. SŁOWIŃSKI (2019): Human-induced fire regime shifts during 19th century industrialization: A robust fire regime reconstruction using northern Polish lake sediments. In: *PLoS one* Vol. 14 (9)
- DIETZE E., M. THEUERKAUF, K. BLOOM, A. BRAUER, W. DÖRFLER, I. FEESER, A. FEURDEAN, L. GEDMINIENÉ, T. GIESECKE, S. JAHNS, M. KARPIŃSKA-KOŁACZEK, P. KOŁACZEK, M. LAMENTOWICZ, M. LATAŁOWA, K. MARCISZ, M. OBREMSKA, A. PĘDZISZEWSKA, A. POSKA, K. REHFELD, M. STANČIKAITĖ, N. STIVRINS, J. ŚWIĘTA-MUSZ-NICKA, M. SZAL, J. VASSILJEV, S. VESKI, A. WACNIK, D. WEISBRODT, J. WIETHOLD, B. VANNIÈRE and M. SŁOWIŃSKI (2018): Holocene fire activity during low-natural flammability periods reveals scale-dependent cultural human-fire relationships in Europe. In: *Quaternary Science Reviews* Vol. 201: 44–56
- DROBYSHEV I., M. NIKLASSON, P. ANGELSTAM and P. MAJEWSKI (2004) Testing for anthropogenic influence on fire regime for a 600-year period in the Jaksha area, Komi Republic, East European Russia. In: *Canadian Journal of Forest Research* Vol. 34: 2027–2036
- DUCKSON D.W. (1987): Continental climate. In: *Climatology. Encyclopedia of Earth Science*. Springer, Boston, Massachusetts, United States of America
- DUNNETTE P., P.E. HIGUERA, K. MCLAUCHLAN, K. DERR, C. BRILES and M. KEEFE (2014): Biogeochemical impacts of wildfires over four millennia in a Rocky Mountain subalpine watershed. In: *New Phytologist* Vol. 203: 900–912
- EICHLER A., W. TINNER, S. BRÜTSCH, S. OLIVIER, T. PAPINAE and M. SCHWIKOWSKI (2011): An ice-core based history of Siberian forest fires since AD 1250. In: *Quaternary Science Reviews* Vol. 30 (9–10): 1027–1034

- ENACHE M. and B. CUMMING (2007): Charcoal morphotypes in lake sediments from British Columbia (Canada): an assessment of their utility for the reconstruction of past fire and precipitation. In: *Journal of Paleolimnology* Vol. 38: 347–363
- ENACHE M. and B. CUMMING (2006): Tracking recorded fires using charcoal morphology from the sedimentary sequence of Prosser Lake, British Columbia (Canada). In: *Quaternary Research* Vol. 65 (2): 282–292
- Esri (2020): “World Imagery” (Basemap). Scale Not Given. Esri, DigitalGlobe, GeoEye, i-cubed, USDA, USGS, AEX, Getmapping, Aerogrid, IGN, IGP, swisstopo, and the GIS User Community. Internet: <https://www.arcgis.com/home/item.html?id=10df2279f9684e4a9f6a7f08febac2a9> (18.04.2020)
- FEDOROV A.N., N.F. VASILYEV, Y.I. TORGOVKIN, A.A. SHESTAKOVA, S.P. VARLAMOV, M.N. ZHELEZNYAK, V.V. SHEPELEV, P.Y. KONSTANTINOV, S.S. KALINICHEVA, N.I. BASHARIN, V.S. MAKAROV, I.S. UGAROV, P.V. EFREMOV, R.N. ARGUNOV, L.S. EGOROVA, V.V. SAMSONOVA, A.G. SHEPELEV, A.I. VASILIEV, R.N. IVANOVA, A.A. GALANIN, V.M. LYTKIN, G.P. KUZMIN and V.V. KUNITSKY (2018): Permafrost-Landscape Map of the Republic of Sakha (Yakutia) on a Scale 1:1,500,000. In: *Geosciences* Vol. 8: 465
- FINSINGER W. and W. TINNER (2005): Minimum count sums for charcoal-concentration estimates in pollen slides: accuracy and potential errors. In: *The Holocene* Vol. 15 (2): 293–297
- FROYD C.A. (2006): Holocene fire in the Scottish Highlands: evidence from macroscopic charcoal records. *The Holocene* Vol. 16 (2): 235–249
- GARNIER S. (2018): viridis: Default Color Maps from 'matplotlib'. R package version 0.5.1. Internet: <https://CRAN.R-project.org/package=viridis> (12.04.2020)
- GAVIN D. (2018): Quantitative Methods in Paleoecology. Working with stratigraphical data. University of Oregon course material. Internet: https://pages.uoregon.edu/dgavin/courses/Geog607/sea_example.html (17.04.2020)
- GIGLIO L., C. JUSTICE, L. BOSCHETTI and D. ROY (2015): MCD64A1 MODIS/Terra+Aqua Burned Area Monthly L3 Global 500m SIN Grid V006 [Data set]. NASA EOSDIS Land Processes DAAC. Internet: <https://doi.org/10.5067/MODIS/MCD64A1.006> (20.04.2020)
- GORELICK N., M. HANCHER, M. DIXON, S. ILYUSHCHENKO, D. THAU and R. MOORE (2017): Google Earth Engine: Planetary-scale geospatial analysis for everyone. In: *Remote Sensing of Environment*
- GRIMM E., L. MAHER and D. NELSON (2009): The magnitude of error in conventional bulk-sediment radiocarbon dates from central North America. In: *Quaternary Research* Vol. 72 (2): 301–308
- GROSSE G., B. JONES and C. ARP (2013): Thermokarst lakes, drainage, and drained basins. In: SHRODER J.F. (ed.): *Treatise on geomorphology*. Academic Press, San Diego: 325–353
- HALSALL K.M., V.M. ELLINGSEN, J. ASPLUND, R.H. BRADSHAW and M. OHLSON (2018): Fossil charcoal quantification using manual and image analysis approaches. In: *The Holocene* Vol. 28 (8): 1345–1353
- HAWTHORNE D., C. MUSTAPHI, J. ALEMAN, O. BLARQUEZ, D. COLOMBAROLI, A. DANIAU, J. MARLON, M. POWER, B. VANNIÈRE, Y. HAN, S. HANTSON, N. KEHRWALD, B. MAGI, X. YUE, C. CARCAILLET, R. MARCHANT, A. OGUNKOYA, E. GITHUMBI and R. MURIUKI (2018): Global Modern Charcoal Dataset (GMCD): A tool for exploring proxy-fire linkages and spatial patterns of biomass burning. In: *Quaternary International* Vol. 488: 3–17

- HERZSCHUH U., H. BIRKS, T. LAEPPEL, A. ANDREEV, M. MELLES and J. BRIGHAM-GRETTE (2016): Glacial legacies on interglacial vegetation at the Pliocene-Pleistocene transition in NE Asia. In: *Nature Communications* Vol. 7
- HIGUERA P.E., D.G. GAVIN, P.J. BARTLEIN and D.J. HALLETT (2010): Peak detection in sediment-charcoal records: impacts of alternative data analysis methods on fire-history interpretations. In: *International Journal of Wildland Fire* Vol. 19: 996–1014
- HIGUERA P.E., L.E. BRUBAKER, P.M. ANDERSON, F.S. HU and T.A. BROWN (2009): Vegetation mediated the impacts of postglacial climate change on fire regimes in the south-central Brooks Range, Alaska. In: *Ecological Monographs* Vol. 79 (2): 201–219
- HIGUERA P.E., M.E. PETERS, L.B. BRUBAKER and D.G. GAVIN (2007): Understanding the origin and analysis of sediment-charcoal records with a simulation model. In: *Quaternary Science Reviews* Vol. 26 (13–14): 1790–1809
- HIGUERA P.E., D.G. SPRUGEL and L.B. BRUBAKER (2005): Reconstructing fire regimes with charcoal from small-hollow sediments: a calibration with tree-ring records of fire. In: *The Holocene* Vol. 15 (2): 238–251
- HODGES G. (n.d.): Russian Smokejumpers. In: *National Geographic Magazine*. Internet: <https://www.nationalgeographic.com/environment/natural-disasters/russian-smokejumpers/> (17.04.2020)
- HUDSPITH V., C. BELCHER, R. KELLY and F. HU (2015): Charcoal Reflectance Reveals Early Holocene Boreal Deciduous Forests Burned at High Intensities. In: *PLoS ONE* Vol. 10 (4)
- IPCC (2018): Global warming of 1.5°C. An IPCC Special Report on the impacts of global warming of 1.5°C above pre-industrial levels and related global greenhouse gas emission pathways, in the context of strengthening the global response to the threat of climate change, sustainable development, and efforts to eradicate poverty [V. MASSON-DELMOTTE, P. ZHAI, H.O. PÖRTNER, D. ROBERTS, J. SKEA, P.R. SHUKLA, A. PIRANI, W. MOUFUOMA-OKIA, C. PÉAN, R. PIDCOCK, S. CONNORS, J.B.R. MATTHEWS, Y. CHEN, X. ZHOU, M.I. GOMIS, E. LONNOY, T. MAYCOCK, M. TIGNOR and T. WATERFIELD (eds.)]
- IVERSEN J. (1941): Land occupation in Denmark's Stone Age. In: *Danmarks Geologiske Forendlinger* Vol. 2 (66)
- JENSEN K., E. LYNCH, R. CALCOTE and S. HOTCHKISS (2007): Interpretation of charcoal morphotypes in sediments from Ferry Lake, Wisconsin, USA: do different plant fuel sources produce distinctive charcoal morphotypes? In: *The Holocene* Vol. 17 (7): 907–915
- JUGGINS S. (2017) rioja: Analysis of Quaternary Science Data, R package version (0.9-21). Internet: <http://cran.r-project.org/package=rioja> (06.04.2020)
- KATAMURA F., M. FUKADA, N. BOSIKOV and R. DESYATKIN (2009a): Charcoal records from thermokarst deposits in central Yakutia, eastern Siberia: Implications for forest fire history and thermokarst development. In: *Quaternary Research* Vol. 71: 36–40
- KATAMURA F., M. FUKUDA, N. BOSIKOV and R. DESYATKIN (2009b): Forest fires and vegetation during the Holocene in central Yakutia, eastern Siberia. In: *Journal of Forest Research* Vol. 14 (1): 30–36
- KELLY R., P.E. HIGUERA, C. BARRETT and F. HU (2011): A signal-to-noise index to quantify the potential for peak detection in sediment-charcoal records. In: *Quaternary Research* Vol. 75 (1): 11–17

- KHARUK V.I., M.L. DVINSKAYA, I.A. PETROV, S.T. IM and K.J. RANSON (2016): Larch forests of Middle Siberia: long-term trends in fire return intervals. In: *Regional Environmental Change* Vol. 16: 2389–2397
- KHARUK V.I., K.J. RANSON, M.L. DVINSKAYA and S.T. IM (2011): Wildfires in northern Siberian larch dominated communities. In: *Environmental Research Letters* Vol. 6
- KHARUK V.I., K.J. RANSON and M.L. DVINSKAYA (2008): Wildfires dynamic in the larch dominance zone. In: *Geophysical Research Letters* Vol. 35
- KLINK H.-J. (⁴2008): *Vegetationsgeographie. Das Geographische Seminar*. Westermann, Braunschweig
- KREEB K.-H. (¹1983): *Vegetationskunde*. Verlag Eugen Ulmer GmbH & Co., Stuttgart
- KRUSE S., D. BOLSHIYANOV, M. GRIGORIEV, A. MORGENSTERN, L. PESTRYAKOVA, L. TSIBIZOV and A. UDK (eds., 2019): *Reports on Polar and Marine Research. Russian-German Cooperation: Expeditions to Siberia in 2018*. Internet: https://doi.org/10.2312/BzPM_0734_2019 (17.04.2020)
- KRUSE S., M. WIECZOREK, F. JELTSCH and U. HERZSCHUH (2016): Treeline dynamics in Siberia under changing climates as inferred from an individual-based model for *Larix*. In: *Ecological Modelling* Vol. 338: 101–121
- KUULUVAINEN T. and S. GAUTHIER (2018): Young and old forest in the boreal: critical stages of ecosystem dynamics and management under global change. In: *Forest Ecosystems* Vol. 5
- LARSEN C. and G. MACDONALD (1998): Fire and vegetation dynamics in a jack pine and black spruce forest reconstructed using fossil pollen and charcoal. In: *Journal of Ecology* Vol. 86: 815–828
- LENTON T.M., J. ROCKSTRÖM, O. GAFFNEY, S. RAHMSTORF, K. RICHARDSON, W. STEFFEN and H.J. SCHELLNHUBER (2019): Climate tipping points - too risky to bet against. Comment. In: *Nature* Vol. 575: 592–595
- LENTON T.M. (2012): Arctic Tipping Points. In: *Ambio* Vol. 41: 10–22
- LESTIENNE M., J. ALEMAN and D. COLOMBAROLI (2018): How paleofire research can better inform ecosystem management. In: *Eos* Vol. 99. Internet: <https://doi.org/10.1029/2018EO096613> (19.04.2020)
- LEYS B., P.E. HIGUERA, K.K. MCLAUCHLAN and P.V. DUNNETTE (2016): Wildfires and geochemical change in a subalpine forest over the past six millennia. In: *Environmental Research Letters* Vol. 11 (12)
- LOCKOT G., A. RAMISCH, B. WÜNNEMANN, K. HARTMANN, T. HABERZETTL, H. CHEN and B. DIEKMANN (2015): A Process- and Provenance-Based Attempt to Unravel Inconsistent Radiocarbon Chronologies In Lake Sediments: An Example From Lake Heihai, North Tibetan Plateau (China). In: *Radiocarbon* Vol. 57 (5): 1003–1019
- LOCKOT G., K. HARTMANN, B. WÜNNEMANN, A. RAMISCH and B. DIEKMANN (2014): Hard-water dynamics and their reservoir effects on radiocarbon dating of Lake Heihai sediments (NE Tibetan Plateau, Qinghai, China). In: *Geophysical Research Abstracts* Vol. 16, EGU 2014
- MACDONALD G., C. LARSEN, J. SZEICZ and K. MOSER (1991): The reconstruction of boreal forest fire history from lake sediments: A comparison of charcoal, pollen, sedimentological, and geochemical indices. In: *Quaternary Science Reviews* Vol. 10 (1): 53–71

- MAGNE G., B. BROSSIER, E. GANDOUIN, L. PARADIS, I. DROBYSHEV, A. KRYSHEN, C. HÉLY, S. ALLEAUME and A. ALI (2020): Lacustrine charcoal peaks provide an accurate record of surface wildfires in a North European boreal forest. In: *The Holocene* Vol. 30 (3): 380–388
- MARLON J., R. KELLY, A.-L. DANIAU, B. VANNIÉRE, M. POWER, P. BARTLEIN, P.E. HIGUERA, O. BLARQUEZ, S. BREWER, T. BRÜCHER, A. FEURDEAN, G. GIL-ROMERA, V. IGLESIAS, S. MAEZUMI, B. MAGI, C. MUSTAPHI and T. ZHAI (2016): Reconstructions of biomass burning from sediment charcoal records to improve data-model comparisons. In: *Biogeosciences* Vol. 13: 3225–3244
- MARLON J., P. BARTLEIN, C. CARCAILLET, D. GAVIN, S. HARRISON., P. HIGUERA, F. JOOS, M. POWER and I. PRENTICE (2008): Climate and human influences on global biomass burning over the past two millennia. In: *Nature Geoscience* Vol. 1: 697–702
- MARLON J., P. BARTLEIN, A.-L. DANIAU, S. HARRISON, S. MAEZUMI, M. POWER, W. TINNER and B. VANNIÉRE (2013): Global biomass burning: a synthesis and review of Holocene paleofire records and their controls. In: *Quaternary Science Reviews* Vol. 65: 5–25
- MOONEY S. and W. TINNER (2011): The analysis of charcoal in peat and organic sediments. In: *Mires and Peat* Vol. 7: 1–18
- MOONEY S. and K. RADFORD (2001): A simple and fast method for the quantification of macroscopic charcoal from sediments. In: *Quaternary Australasia* Vol. 19 (1): 43–46
- MOOS M. and B. CUMMING (2012): Climate–fire interactions during the Holocene: a test of the utility of charcoal morphotypes in a sediment core from the boreal region of north-western Ontario (Canada). In: *International Journal of Wildland Fire* Vol. 21 (6): 640–652
- MUSTAPHI C. and M. PISARIC (2014): A classification for macroscopic charcoal morphologies found in Holocene lacustrine sediments. In: *Progress in Physical Geography* Vol. 38 (6): 734–754
- NAZAROVA L., H. LÜPFERT, D. SUBETTO, L. PESTRYAKOVA and B. DIEKMANN (2013): Holocene climate conditions in central Yakutia (Eastern Siberia) inferred from sediment composition and fossil chironomids of Lake Temje. In: *Quaternary International* Vol. 290/291: 264–274
- OHLSON M. and E. TRYTERUD (2000): Interpretation of the charcoal record in forest soils: forest fires and their production and deposition of macroscopic charcoal. In: *The Holocene* Vol. 10 (4): 519–525
- OLSON D.M., E. DINERSTEIN, E.D. WIKRAMANAYAKE, N.D. BURGESS, G.V.N. POWELL, E.C. UNDERWOOD, J.A. D'AMICO, I. ITOUA, H.E. STRAND, J.C. MORRISON, C.J. LOUCKS, T.F. ALLNUTT, T.H. RICKETTS, Y. KURA, J.F. LAMOREUX, W.W. WETTENGEL, P. HEDAO and K.R. KASSEM (2001): Terrestrial Ecoregions of the World: A New Map of Life on Earth: A new global map of terrestrial ecoregions provides an innovative tool for conserving biodiversity. In: *BioScience* Vol. 51 (11): 933–938
- OLSSON F., M.-J. GAILLARD, G. LEMDAHL, A. GREISMAN, P. LANOS, D. MARGUERIE, N. MARCOUX, P. SKOGLUND and J. WÄGLIND (2010): A continuous record of fire covering the last 10,500 calendar years from southern Sweden - The role of climate and human activities. In: *Palaeogeography, Palaeoclimatology, Palaeoecology* Vol. 291 (1–2): 128–141
- PISARIC M.F. (2002): Long-distance transport of terrestrial plant material by convection resulting from forest fires. In: *Journal of Paleolimnology* Vol. 28: 349–354

- POWER M.J., J.R. MARLON, P.J. BARTLEIN and S.P. HARRISON (2011): Fire history and the Global Charcoal Database: A new tool for hypothesis testing and data exploration. *Palaeogeography, Palaeoclimatology, Palaeoecology* Vol. 291 (1–2): 52–59
- PUTH M.-T., M. NEUHÄUSER and G. RUXTON (2015): Effective use of Spearman's and Kendall's correlation coefficients for association between two measured traits. In: *Animal Behaviour* Vol. 102: 77–84
- RAMISCH A., A. BRAUSER, M. DORN, C. BLANCHET, B. BRADEMANN, M. KÖPPL, J. MINGRAM, I. NEUGEBAUER, N. NOWACZYK, F. OTT, S. PINKERNEIL, B. PLESSEN, M.J. SCHWAB, R. TJALLINGII and A. BRAUER (2020): VARDA (VARved sediments DAtabase) - providing and connecting proxy data from annually laminated lake sediments. In: *Earth System Science Data* [Preprint]
- R Core Team (2020). R: A language and environment for statistical computing. R Foundation for Statistical Computing, Vienna, Austria. Internet: <https://www.R-project.org/> (25.02.2020)
- REGNÉLL C., H. HAFLIDASON, J. MANGERUD and J. SVENDSEN (2019): Glacial and climate history of the last 24 000 years in the Polar Ural Mountains, Arctic Russia, inferred from partly varved lake sediments. In: *Boreas* Vol. 48: 432–443
- REIMER P.J., E. BARD, A. BAYLISS, J.W. BECK, P.G. BLACKWELL, C. BRONK RAMSEY, C.E. BUCK, R.L. EDWARDS, M. FRIEDRICH, P.M. GROOTES, T.P. GUILDERSON, H. HAFLIDASON, I. HAJDAS, C. HATTÉ, T.J. HEATON, D.L. HOFFMANN, A.G. HOGG, K.A. HUGHEN, K.F. KAISER, B. KROMER, S.W. MANNING, M. NIU, R.W. REIMER, D.A. RICHARDS, E.M. SCOTT, J.R. SOUTHON, C.S.M. TURNEY and J. VAN DER PLICHT (2013): IntCal13 and Marine13 radiocarbon age calibration curves, 0-50,000 years cal BP. In: *Radiocarbon* Vol. 55: 1869–1887
- REVELLE W. (2019): psych: Procedures for Personality and Psychological Research, Northwestern University, Evanston, Illinois, USA. Internet: <https://CRAN.R-project.org/package=psych> Version = 1.9.12. (15.04.2020)
- RHODES T. and R. DAVIS (1995): Effects of Late Holocene Forest Disturbance and Vegetation Change on Acidic Mud Pond, Maine, USA. In: *Ecology* Vol. 76 (3): 734–746
- RUDAYA N., L. NAZAROVA, E. NOVENKO, A. ANDREEV, I. KALUGIN, A. DARYIN, V. BABICH, H.-C. LI and P. SHILOV (2016): Quantitative reconstructions of mid- to late holocene climate and vegetation in the north-eastern altai mountains recorded in lake teletskoye. In: *Global and Planetary Change* Vol. 141: 12–24
- SCHEFFER M., M. HIROTA, M. HOLMGREN, E. VAN NES and F.S. CHAPIN III (2012): Thresholds for boreal biome transitions. In: *PNAS* Vol. 109 (52): 21384-21389
- SCHEPASCHENKO D.G., A.Z. SHVIDENKO and V.S. SHALAEV (2008): Biological Productivity and Carbon Budget of Larch Forests of Northern-East Russia. Moscow State Forest University
- SCOTT A. (2010): Charcoal recognition, taphonomy and uses in palaeoenvironmental analysis. In: *Palaeogeography, Palaeoclimatology, Palaeoecology* Vol. 291 (1–2): 11–39
- SCOTT A. and I. GLASSPOOL (2005): Charcoal reflectance as a proxy for the emplacement temperature of pyroclastic flow deposits. In: *Geology* Vol. 33 (7): 589–592
- SEIDL R., D. THOM, M. KAUTZ, D. MARTIN-BENITO, M. PELTONIEMI, G. VACCHIANO, J. WILD, D. ASCOLI, M. PETR, J. HONKANIEMI, M. LEXER, V. TROTSIUK, P. MAIROTA, M. SVOBODA, M. FABRIKA, T. NAGEL and C. REYER (2017): Forest disturbances under climate change. In: *Nature Climate Change* Vol. 7: 395–402

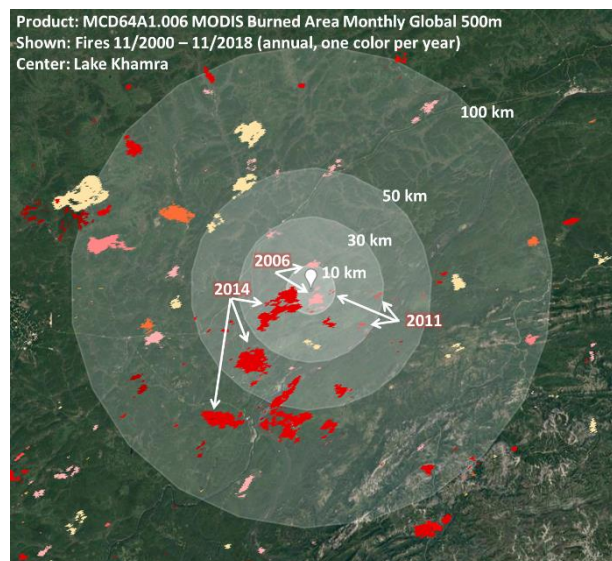
- SÉJOURNÉ A., F. COSTARD, A. FEDOROV, J. GARGANI, J. SKORVE, M. MASSÉ and D. MÈGE (2015): Evolution of the banks of thermokarst lakes in Central Yakutia (Central Siberia) due to retrogressive thaw slump activity controlled by insolation. In: *Geomorphology* Vol. 241: 31–404
- SHICHI K., H. TAKAHARA, S. KRIVONOGOV, E. BEZRUKOVA, K. KASHIWAYA, A. TAKEHARA and T. NAKAMURA (2009): Late Pleistocene and Holocene vegetation and climate records from Lake Kotokel, central Baikal region. In: *Quaternary International* Vol. 205 (1–2): 98–110
- SOFRONOV M., A. VOLOKITINA and A. SHVIDENKO (1998): Wildland fires in the north of Central Siberia. In: *Commonw For Rev* Vol. 77: 211–218
- STOCKMARR J. (1971): Tablets with spores used in absolute pollen analysis. In: *Pollen et Spores* Vol. 13: 615–621
- SUGITA S. (2007): Theory of quantitative reconstruction of vegetation I: pollen from large sites REVEALS regional vegetation composition. In: *The Holocene* Vol. 17 (2): 229–241
- SWAIN A. (1973): A History of Fire and Vegetation in Northeastern Minnesota as Recorded in Lake Sediments. In: *Quaternary Research* Vol. 3 (3): 383–396
- SWARZENSKI P. (2014): ²¹⁰Pb Dating. In: *Encyclopedia of Scientific Dating Methods*. Springer, Dordrecht
- TAKAHARA H. and S. KRIVONOGOV (unpublished data). Institute of Geology and Mineralogy, Siberian Branch of Russian Academy of Sciences, Novosibirsk, Russia
- TINNER W., S. HOFSTETTER, F. ZEUGIN, M. CONEDERA, T. WOHLGEMUTH, L. ZIMMERMANN and R. ZWEIFEL (2006): Long-distance transport of macroscopic charcoal by an intensive crown fire in the Swiss Alps - implications for fire history reconstruction. In: *The Holocene* Vol. 16 (2): 287–292
- TOLONEN K. (1986): Charred particle analysis. In: BERGLUND B. (ed.): *Handbook of Holocene Palaeoecology and Palaeolimnology*. John Wiley & Sons Ltd.
- VAGANOV E.A. and M.K. ARBATSKAYA (1996): Climate history and wildfire frequency in the central part of Krasnoyarsky krai. I. Climatic conditions in growing season and seasonal wildfires distribution. In: *Siberian Journal of Ecology* Vol. 3: 9–18.
- VÄLIRANTA M., A. KAAKINEN and P. KUHRÝ (2003): Holocene climate and landscape evolution East of the Pechora Delta, East-European Russian Arctic. In: *Quaternary Research* Vol. 59 (3): 335–344
- VAN DEN BOOGAART K.G., R. TOLOSANA-DELGADO and M. BREM (2020): compositions: Compositional Data Analysis. R package version 1.40-4. Internet: <https://CRAN.R-project.org/package=compositions> (13.04.2020)
- VENKATARAMAN S., X. MENG, F. CHEUNG and The Apache Software Foundation (2020): SparkR: R Front End for 'Apache Spark'. R package version 2.4.5. Internet: <https://CRAN.R-project.org/package=SparkR> (15.04.2020)
- WALKER X., J. BALTZER, S. CUMMING, N. DAY, C. EBERT, S. GOETZ, J. JOHNSTONE, S. POTTER, B. ROGERS, E. SCHUUR, M. TURETSKY and M. MACK (2019): Increasing wildfires threaten historic carbon sink of boreal forest soils. In: *Nature* Vol. 572: 520–523
- WALLENIUS T. (2011a): Major decline in fires in coniferous forests – reconstructing the phenomenon and seeking for the cause. In: *Silva Fennica* Vol. 45 (1): 139–155

- WALLENIOUS T., M. LARJAVAARA, J. HEIKKINEN, and O. SHIBISTOVA (2011b): Declining fires in Larix-dominated forests in northern Irkutsk district. In: International Journal of Wildland Fire Vol. 20 (2): 248–254
- WARD D. and C. HARDY (1991): Smoke emissions from wildland fires. In: Environment International Vol. 17: 117–134
- WASSERSTEIN R.L., A.L. SCHIRM and N.A. LAZAR (2019): Moving to a World Beyond “ $p < 0.05$ ”. In: The American Statistician Vol. 73 (1): 1–19
- WEI T. and V. SIMKO (2017). R package "corrplot": Visualization of a Correlation Matrix (Version 0.84). Internet: <https://github.com/taiyun/corrplot> (12.04.2020)
- WEST J.J. and L.J. PLUG (2008): Time-dependent morphology of thaw lakes and taliks in deep and shallow ground ice. In: Journal of Geophysical Research Vol. 113
- WHITLOCK C. and C. LARSEN (2001): Charcoal as a fire proxy. In: SMOL J., H. BIRKS AND W. LAST (eds.) (2001): Tracking Environmental Change Using Lake Sediments. Volume 3: Terrestrial, Algal, and Siliceous Indicators. Kluwer Academic Publishers, Dordrecht, The Netherlands

VII. Appendix

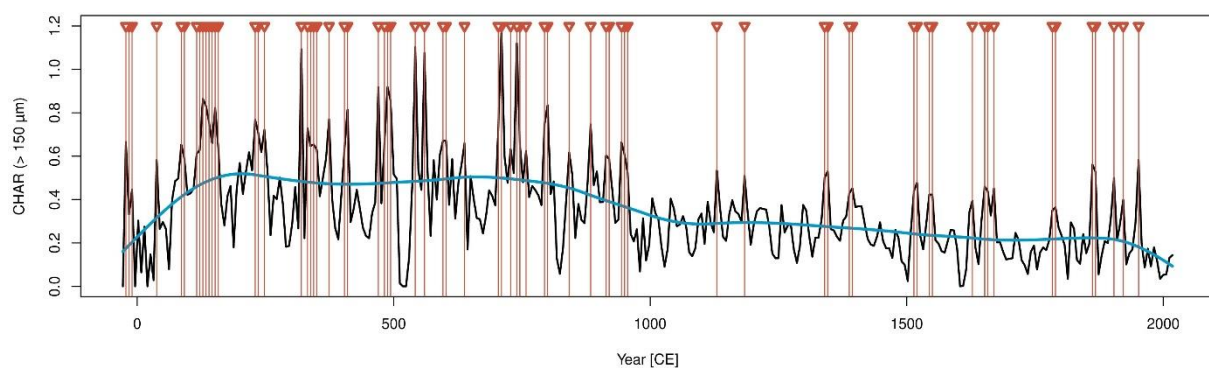
A. Remotely sensed fires at Lake Khamra

This map draft was created in 12/2018 as a test using Google Earth Engine (GORELICK et al. 2017), with colored areas showing remotely sensed fires (GIGLIO et al. 2015) around Lake Khamra between 11/2000 - 11/2018. It indicates fires in 2006 and 2014 affecting large areas near the lake

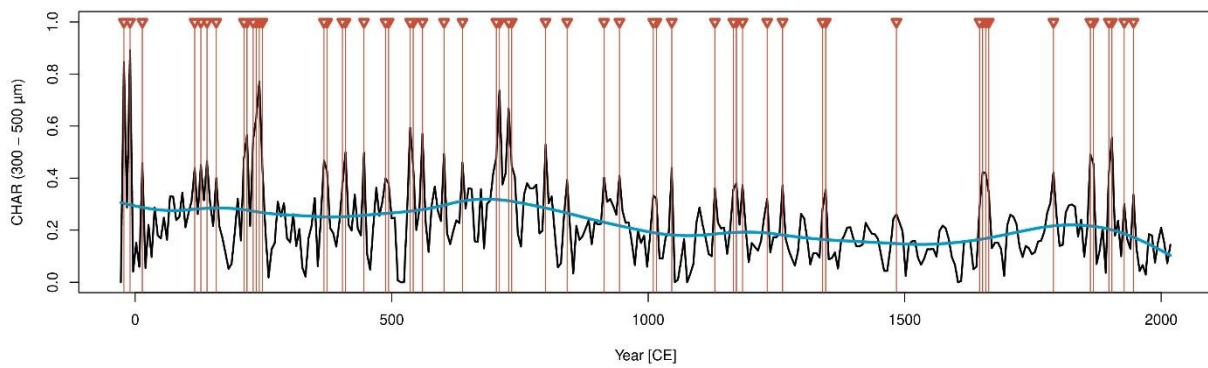


B. Results of fire event identification using the CharAnalysis method (DIETZE et al. 2019, HIGUERA et al. 2009) with the individual size classes (all non-reduced versions)

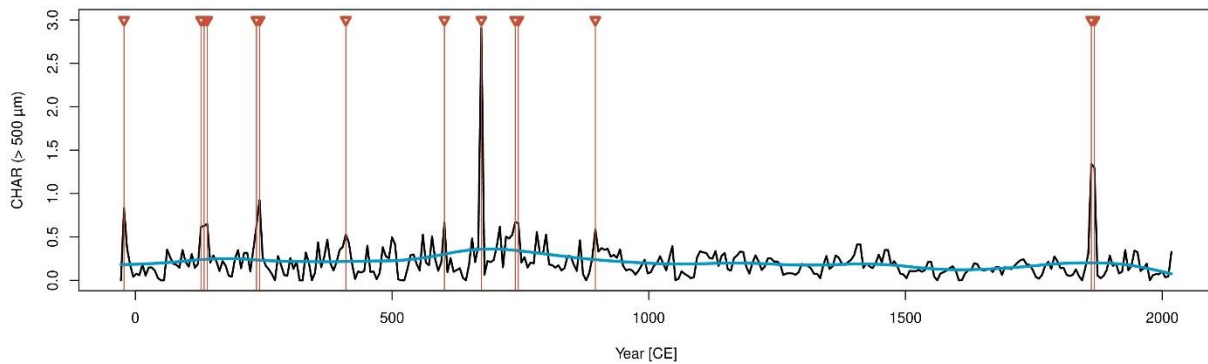
1. Fires events identified with the **small** charcoal size class (n = 70):



2. Fires events identified with the **medium** charcoal size class (n = 56):

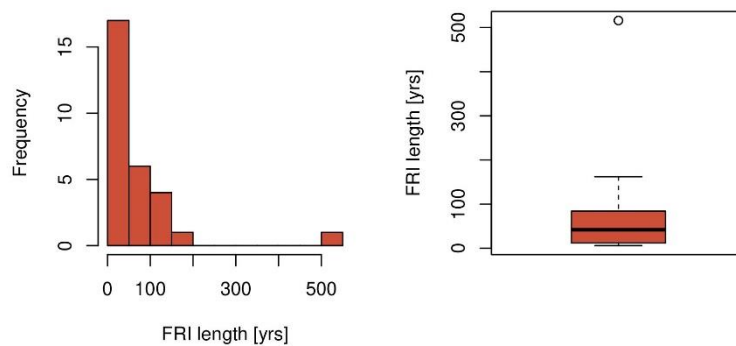


3. Fire events identified with the **large** charcoal size class: (n = 14)

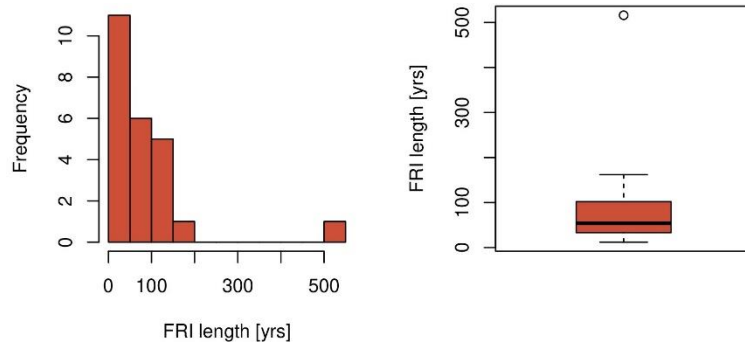


C. Histograms and boxplots for original and reduced versions of identified fire return intervals

1. Histogram and boxplot indicating FRI length for the **original** version of identified fire events:

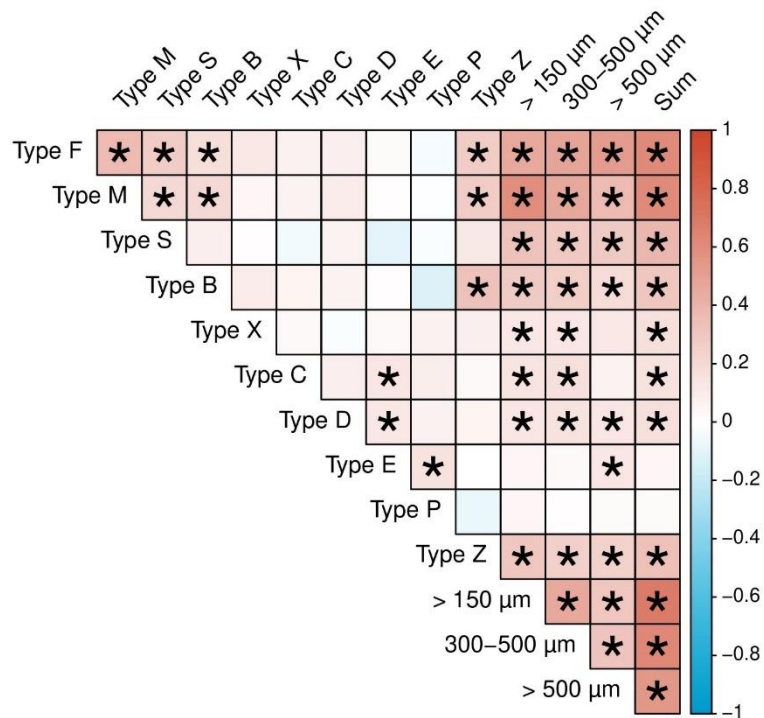


2. Histogram and boxplot indicating FRI length for the **reduced** version of identified fire events:



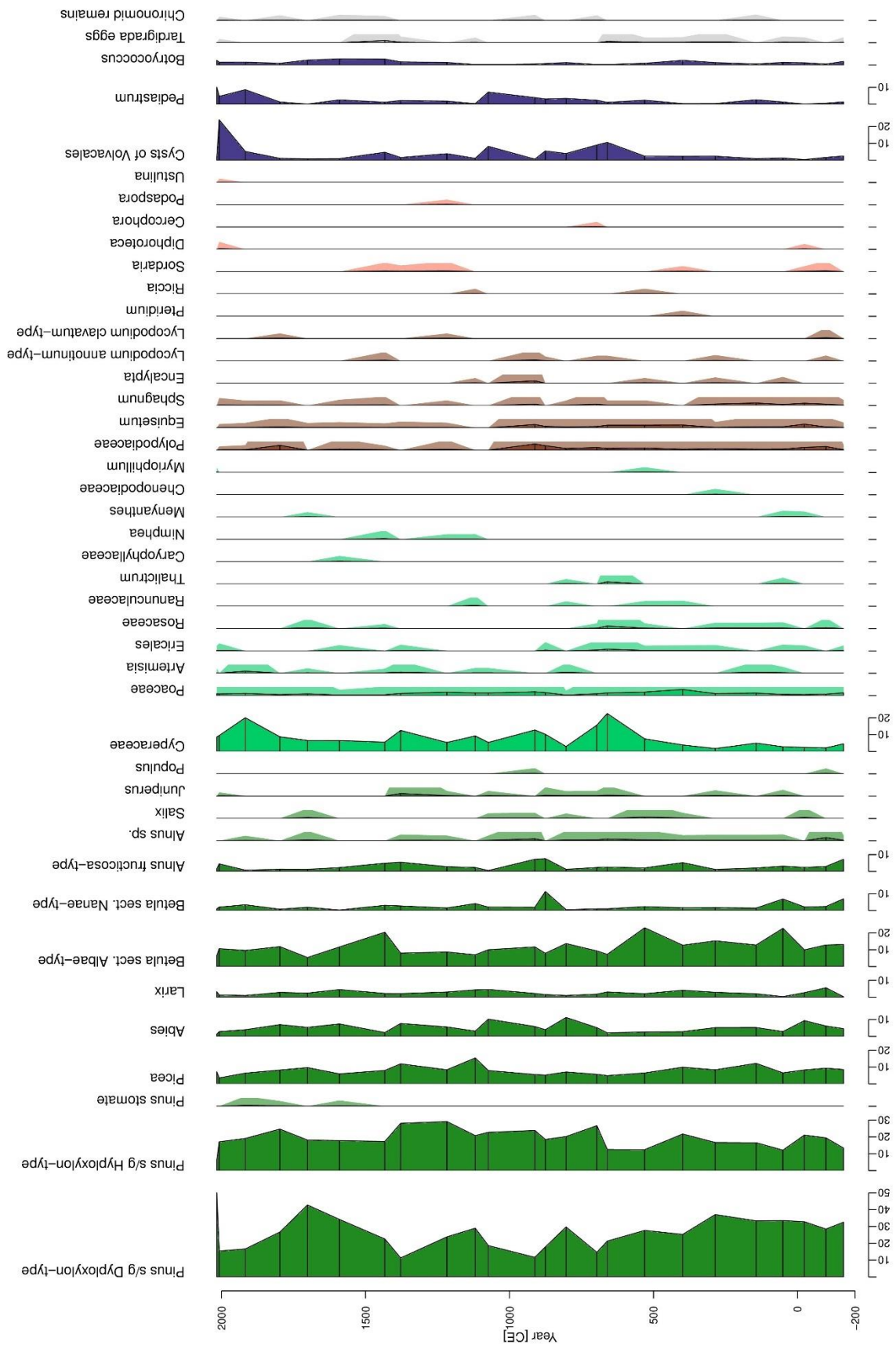
D. Correlation of macroscopic charcoal classes using influxes instead of percentages

Correlation matrix of macroscopic charcoal classes (morphotypes and size classes) using Kendall's tau with log-transformed influxes, based on 247 samples (stars mark values with $p < 0.05$)



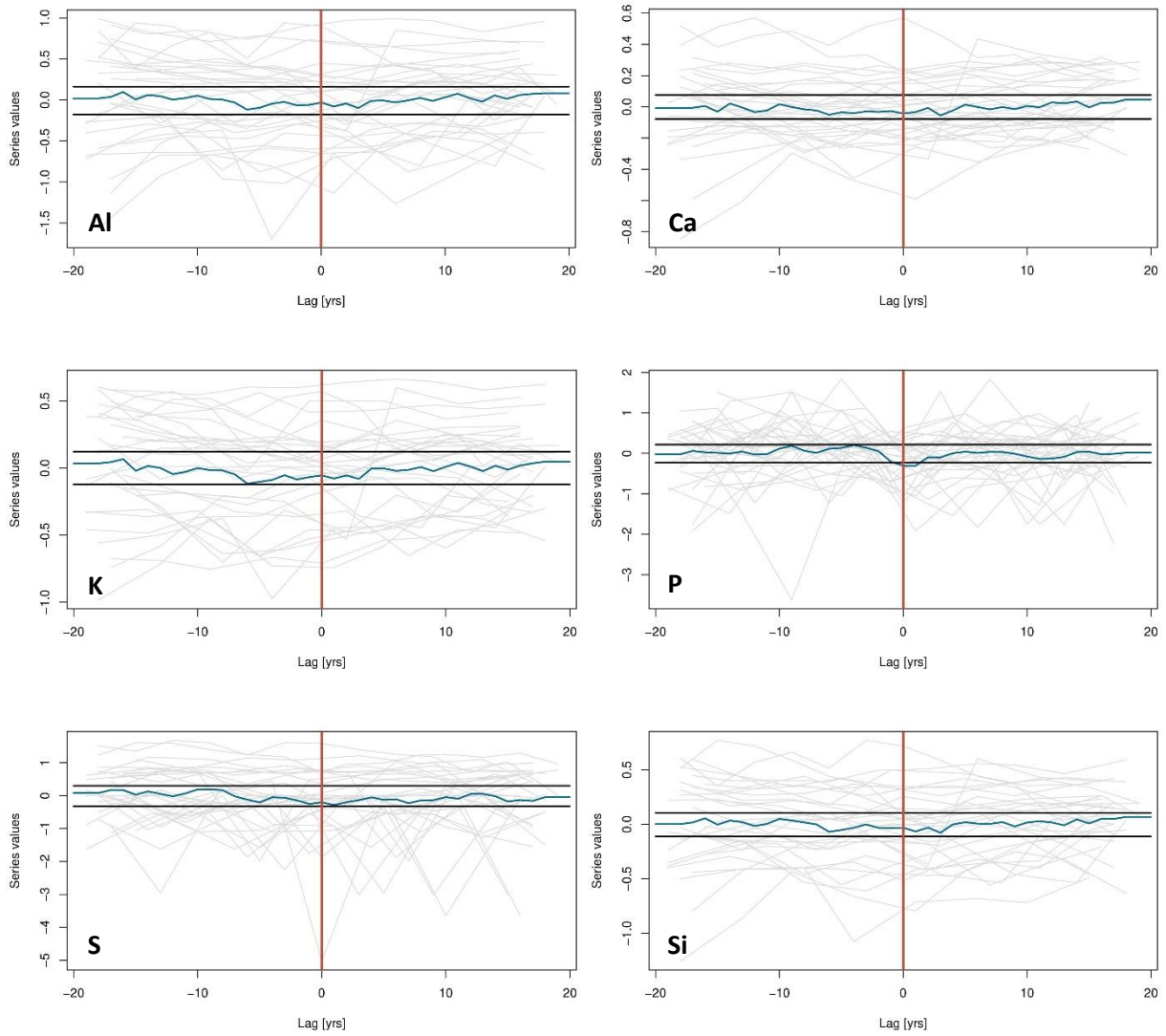
E. Complete pollen and non-pollen palynomorph record (counts by Dr. Andrei Andreev)

Percentages of concentrations, types with few counts are visually exaggerated

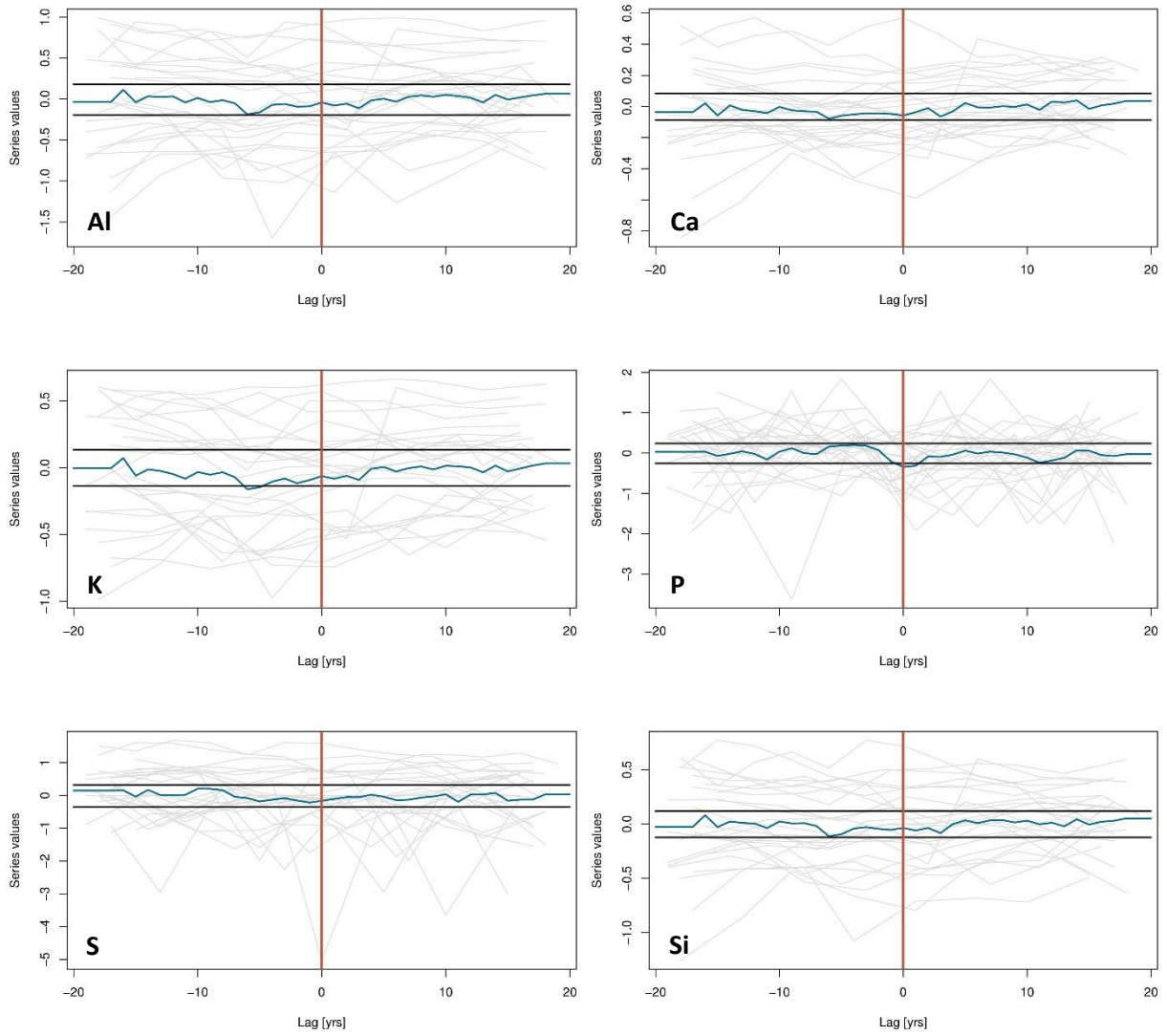


F. Superposed epoch analysis results for all “fire elements”, using the original and the reduced fire events

1. Results based on **all** identified fire events (“original fire version”):

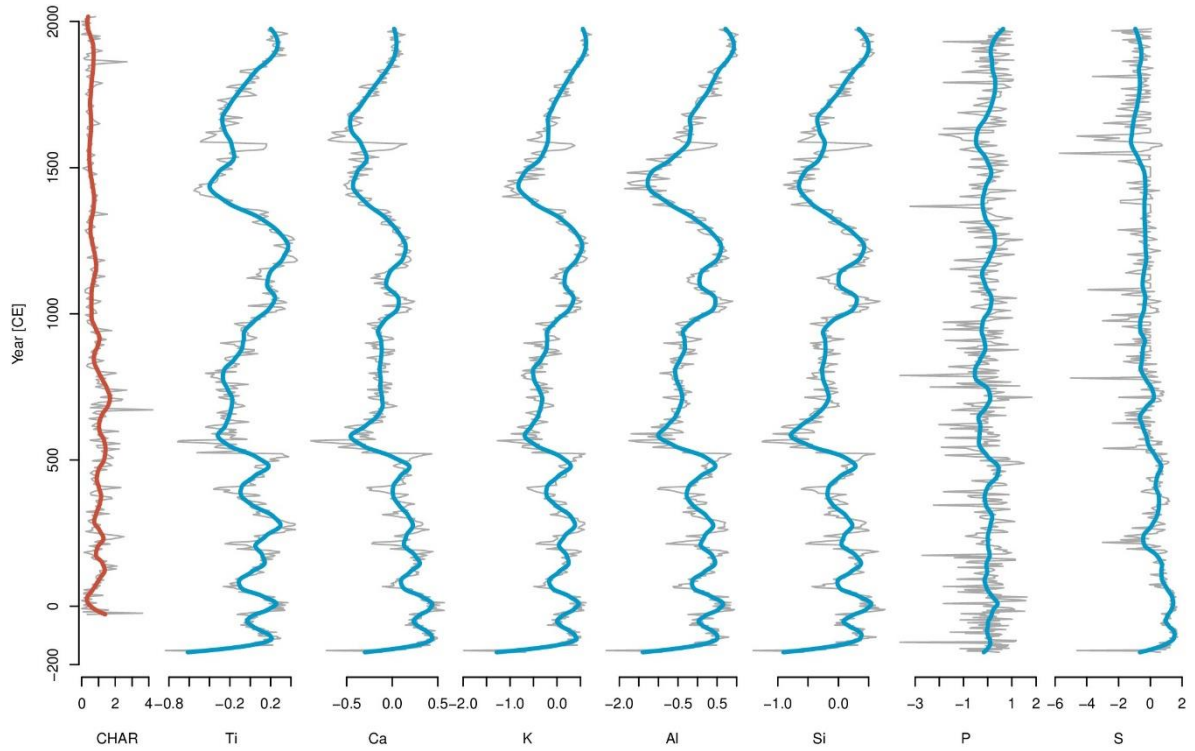


2. Results based on the **reduced** fire version:



G. Distribution of XRF counts of “fire elements” throughout the EN18232-3 sediment core

All elements centered log-ratio transformed. CHAR in [$\#/cm^2/yr$]. Colored lines represent LOWESS at a window width of 1/10 of the respective timeseries length



H. Preparation protocol for macroscopic charcoal created for this research project

1. **Prearrangement**

1. Put sample container on scale (full and with cap) → note "weight full"
2. Transfer sediment material to labelled falcon tube (50 ml) using a spatula and a demineralized (DM) water lab bottle, do not use too much water
3. Put empty sample container on scale (with cap) → note "weight empty"

2. **Dispersing (skip this step if no dispersing is done)**

1. Fill sample tubes with DM water (c. 30 ml)
2. Add small amount of $\text{Na}_4\text{P}_2\text{O}_7$ (sodium pyrophosphate) to each tube (amount depends on type of sediment, might benefit from doing some tests beforehand)
3. Gently rotate the closed falcon tubes to have the pyrophosphate come into contact with all sediment material
4. Leave samples to soak overnight (longer is also possible, e.g. over the weekend)

3. **Adding *Lycopodium* (skip this step if no or other marker grains are added)**

1. Add *Lycopodium* tablet to empty 50 ml falcon tubes → note batch number and quantity of tablets per sample
2. Add c. 10 ml of 10 % HCl (hydrochloric acid) to each sample
3. Let *Lycopodium* tablets soak in HCl for c. 10 - 15 min until fully dissolved
4. Add the HCl suspension to the falcon tubes of the charcoal samples (make sure to transfer all *Lycopodium* spores by using the DM water bottle for rinsing as well)

4. **Sieving and condensing smaller fractions**

1. Sample material is transferred into a sieve (150 μm) resting over a flat bowl
2. Material is gently washed through the sieve using the DM water bottle
 1. Break down any sediment lumps with DM water bottle squirts
 2. Add some DM water to the sieve and gently stir it within the bowl below
 3. When only large fractions remain, rinse them with the DM water bottle one more time and rinse the part of the sieve standing in the bowl and coming into contact with the suspended smaller fractions
3. Suspension of smaller fractions < 150 μm in bowl are transferred to a labelled beaker
4. Suspension from beaker is iteratively added to a new labelled falcon tube, centrifuged (4 min at 3200 rpm) and subsequently decanted (repeat until beaker is empty and all smaller fractions are condensed in the new falcon tube)
5. Remaining larger fractions > 150 μm are rinsed together on side of the sieve under a gentle stream of tap water before transferring them to their respective charcoal sample tube using a funnel and the DM water bottle
6. Wash sieve, funnel and bowls with tap and DM water after every sample
7. Leave charcoal samples until all particles accumulated on the tube's bottom

5. **Bleaching**

1. Water from charcoal sample falcons is carefully decanted
2. About 15 - 20 ml of undiluted household bleach (NaClO) is added to each charcoal falcon (if previously treated with HCl, any traces might react to chlorine gas - work at a fume hood)
3. Samples are left to soak in bleach overnight (if previously treated with HCl: do not close the tubes all the way, leave fume hood active)
4. Fill tubes until c. 30 ml with DM water. Once all particles are settled, carefully decant bleach into a beaker, dispose accordingly. Macroscopic charcoal samples can now be counted.

Erklärung

gemäß § 19 Abs. 3 + 5 der Ordnung für die Prüfung im Masterstudiengang Klima- und Umweltwandel an der Johannes Gutenberg-Universität Mainz.

Hiermit erkläre ich, _____ (Matr.-Nr.: _____),
dass ich die vorliegende Arbeit selbstständig verfasst und keine anderen als die angegebenen Quellen
oder Hilfsmittel (einschließlich elektronischer Medien und Online-Quellen) benutzt habe. Mir ist bewusst,
dass ein Täuschungsversuch oder ein Ordnungsverstoß vorliegt, wenn sich diese Erklärung als unwahr
erweist. §19 Absatz 3 und 5 gilt in diesem Fall entsprechend.

Ort, Datum

Unterschrift

Auszug aus § 19 PO (3) + (5) M.Sc. Klima- und Umweltwandel: Versäumnis, Rücktritt, Täuschung, Ordnungsverstoß

(3) Versucht die Kandidatin oder der Kandidat das Ergebnis einer Prüfung durch Täuschung oder Benutzung nicht zugelassener Hilfsmittel zu beeinflussen, oder erweist sich eine Erklärung gemäß § 13 Absatz 2 Satz 5 als unwahr, gilt die betreffende Prüfungsleistung als mit „nicht ausreichend“ (5,0) absolviert. (...).

(5) Die Bestimmungen der Absätze 1-4 gelten für Studienleistungen entsprechend.